NATALIA ZIĘBACZ

Dynamics of nano and micro objects in complex liquids

Supervisor: Professor Robert Holyst

Ph.D. dissertation

prepared within the International Ph.D. in Chemistry Studies

at the Institute of Physical Chemistry of the Polish Academy of Sciences

Warsaw 2011

First and foremost, I wish to express my deepest gratitude to my supervisor Professor Robert Hołyst for his guidance, valuable comments, long discussions and patience, without whom, this research could not have been developed.

Moreover, I would like to sincerely thank Dr. Stefan Wieczorek who has also played a significant part in this work. His willingness to support contributed tremendously to the project.

I also would like to convey special thanks to all colleagues from Department III who have been very helpful and accommodating during my Ph. D. studies. In particular I would like to thank Professor Marcin Fiałkowski for developing *Two scale diffusion model*.

Most especially, I would like to acknowledge my parents, sister and grandmother for being my constant support and motivation.

I dedicate this thesis to my husband.

Acknowledgements

The thesis was supported by the project operated within the Foundation for Polish Science Team Programme co-financed by the EU European Regional Development Fund TEAM/2008-2/2. The thesis has been also supported by the President of the Polish Academy of Sciences through Ph. D. scholarship.

List of publications

10. **N. Ziębacz**, S. A. Wieczorek, T. Kalwarczyk, M. Fiałkowski, R. Hołyst. *Crossover regime for diffusion of nanoparticles in polyethylene glycol solutions: influence of depletion layer.*

    Soft Matter **2011, DOI:**10.1039/C0SM01357A

9. S. Hou, **N. Ziębacz**, S. A. Wieczorek, E. Kalwarczyk, V. Sashuk, T. Kalwarczyk, T. S. Kaminski, R. Hołyst, *Formation and Structure of PEI/DNA Complexes: Quantitative Analysis.*

    Soft Matter **2011**, *7*, 6967 – 6972.

8. T. Kalwarczyk, **N. Ziębacz**, A. Bielejewska, E. Zaboklicka, K. Koynov, J. Szymański, A. Wilk, A. Patkowski, J. Gapiński, H.-J. Butt, R. Hołyst, *Comparative analysis of viscosity of complex liquids and cytoplasm of mammalian cells at the nano scale.*

    Nano Letters **2011,** *11*, 2157 – 2163.

7. S. Hou, **N. Ziębacz**, T. Kalwarczyk, T. Kamiński, S. A. Wieczorek, R. Hołyst, *Influence of Nano-viscosity and Depletion Interactions on Cleavage of DNA by Enzymes in Glycerol and Poly(ethylene) Glycol Solutions: Qualitative Analysis.*

    Soft Matter **2011**, *7*, 3092 – 3099.

6. X. Xin, H. Li, S.A. Wieczorek, T. Szymborski, E. Kalwarczyk, **N. Ziębacz**, E. Górecka, D. Pociecha, R. Hołyst, *Incorporation of carbon nanotubes into a lyotropic liquid crystal by phase separation in the presence of a hydrophilic polymer*.

    Langmuir **2010**, *26*, 3562 – 3568.

5. H. Li, S.A. Wieczorek, X. Xin, T. Kalwarczyk, **N. Ziębacz**, T. Szymborski, R. Hołyst, J. Hao, E. Górecka, D. Pociecha, *Phase transition in salt-free catanionic surfactant mixtures induced by temperature*.

    Langmuir **2010**, *26*, 34 – 40.

4. **N. Ziębacz**, S. A. Wieczorek, T. Szymborski, P. Garstecki, R. Hołyst, *Thousand-fold acceleration of phase decomposition in polymer / liquid crystal blends.*
   ChemPhysChem **2009**, *10*, 2620 – 2622.
3. R. Hołyst, A. Bielejewska, J. Szymański, A. Wilk, A. Patkowski, J. Gapiński, A. Żywociński, T. Kalwarczyk, E. Kalwarczyk, M. Tabaka, **N. Ziębacz**, S. A. Wieczorek, *Scaling form of viscosity at all length-scales in poly(ethylene glycol) solutions studied by fluorescence correlation spectroscopy and capillary electrophoresis.*
   Physical Chemistry Chemical Physics **2009**, *11*, 9025 – 9032.
2. T. Kalwarczyk, **N. Ziębacz**, M. Fiałkowski, R. Hołyst**,** *Late Stage of Phase Separation Process: Coalescence-Induced Coalescence, Gravitational Sedimentation, and Collective Evaporation Mechanisms.*
   Langmuir **2008**, *24*, 6433 – 6440.
1. T. Kalwarczyk, **N. Ziębacz,** S.A. Wieczorek, R. Hołyst, *Kinetics and Dynamics of Dissolution/Mixing of a High – Viscosity Liquid Phase in a Low – Viscosity Solvent Phase.*
   Journal of Physical Chemistry B **2007**, *111*, 11907 – 11914.

List of patent applications

1. R. Hołyst, **N. Ziębacz,** S. A. Wieczorek, T. Szymborski, P. Garstecki „*Sposób przyspieszania separacji faz w układach niejednorodnych, zwłaszcza w układach polimer/ciekły kryształ i polimer/polimer*”. Patent application number: P-385743.
   Biuletyn Urzędu Patentowego **2010**, *3*, 13.

List of abbreviations and symbols

Abbreviation	Meaning
5CB	4-cyano-4’-n-pentylbiphenyl
8CB	4-cyano-4’-n-octylbiphenyl
AC EF	alternating current electric field
DC EF	direct current electric field
DLS	dynamic light scattering
dyCHASE	dynamic charge separation
EF	electric field
ELS	elastic light scattering
GPC	gel permeation chromatography
I	isotropic phase
IELS	inelastic light scattering
ITO	indium thin oxide
L	size of domains
LC	liquid crystal
N	nematic phase
NA	numerical aperture
OEF	oscillating electric field
OM	optical microscope
PEG	poly(ethylene glycol)
PMPS	poly(methylphenylsiloxane)
PS	polystyrene
SLS	static light scattering
Sm	smectic phase
QELS	quasi-elastic light scattering

Symbol	Meaning
c^*	overlap concentration
d	diameter
D	diffusion coefficient
d_{min}	space between two adjacent particles
f	frequency
$g_1(q,\tau)$	autocorrelation function
$I(q)$	scattering intensity
k_B	Boltzmann constant
M_W	weight average molecular weight
M_n	number average molecular weight
n	refractive index
$P(q)$	particle form factor
R	radius of the probe particle
R_g	radius of gyration
$S(q)$	structure factor
$S(q,t)$	scattering intensity
t	time
T	temperature
q	wavevector

Greek symbol	Meaning
ξ	blob size
θ	scattering angle
λ	wavelength
η	viscosity
Γ	decay rate

Contents

1. Introduction and purposes of the Ph. D. dissertation

The main purpose of the Ph. D. thesis is to analyze dynamics of nano and micro objects in complex liquids. The experimental results are described in three main Chapters: **3.1** *Diffusion of nano-particles in polymer solutions,* **3.2** *Diffusion of plasmid DNA in polymer solutions* and **3.3** *Ions motion in liquid crystal/polymer mixtures.*

The Chapter **3.1** is devoted to the important issue of translational diffusion of nanoparticles in nanostructured media represented by solutions of water soluble polymers. I address this problem experimentally by determining diffusion coefficients of nanoparticles in aqueous polyethylene glycol solutions for a wide range of molecular weights and concentrations of the polymer. I study the problem using the Dynamic Light Scattering technique. The observations are explained on the basis of the concept of scale-dependent diffusion coefficient and strong spatial variations of the viscosity as a function of a distance from the nanoparticle. Such variations of viscosity is due to the presence of the depletion layer around the particles. The quantitative studies carried out for a wide range of polymer viscosities and ratios of the particle size to the polymer gyration radius provide deeper insight into the physics of this complex phenomenon at the micro- and nanoscales.

The main goal of the researches contained in the Chapter **3.2**, is a qualitative study of diffusion of biomolecules in polymer and in low molecular mass agent solutions. It is known, that biochemical reactions in living systems take place in an environment crowded by various macromolecules and ligands. Such environment strongly affects the dynamics of biomolecules in living cells, but not in an evident way. Hence, careful analysis of influence of complex liquids (glycerol, PEG 6000 and PEG 8 M solutions) on the dynamics of biomolecules (DNA and restriction enzyme HindIII) is a very important topic. I show that PEG 6000 solution decreases the diffusion coefficient of DNA and HindIII more efficiently

than glycerol solution of the same concentration or PEG 8 M solution of the same macro-viscosity. I explain the DNA cleavage in PEG and glycerol solution by the concept of size dependent nano-viscosity. I also compare the size of DNA obtained by Dynamic Light Scattering measurement with that obtained by theoretical analysis to demonstrate formation of aggregates of plasmid DNA in PEG 6000 solution due to depletion interactions.

The main purpose of the Chapter **3.3** is to demonstrate the industrial applications of the study of motion of nano and micro objects in complex liquids. Free ions (ionic impurities) inevitably contaminate liquid crystal and polymer systems. All experiments, which I present in this section, prove that such ions are responsible for the acceleration of the phase separation process in the liquid crystal/polymer mixtures. In this part, I demonstrate experimentally, that alternating current electric field can be used to accelerate the rate of phase separation in the liquid crystal/polymer mixtures by orders of magnitude.

2. Literature review

2.1. Molecules in motion

Brownian (random) motion of nanoparticles is most common in solutions. In the Chapter 2.1.1, I will concentrate on the Brownian motion and diffusion of molecules in liquids.

Another simple type of motion is uniform motion of particles in solution under influence of an external field. In the Chapter 2.1.2, I will focus on electrophoresis, which describes a migration of a charged particle relative to the surrounding liquids under the influence of the external electric field.

2.1.1. Brownian motion and diffusion

In 1827, Robert Brown, Scottish botanist, noticed pollen grains jiggling in a water solution. Velocity of such particles undergoing Brownian motion, constantly changed in magnitude and direction, thus its trajectory represented a complicated random zigzag (see Figure 1).

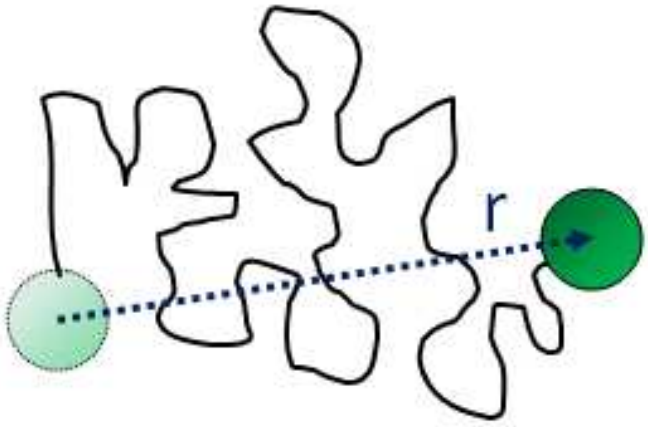

Figure 1. Brownian motion of a particle results from molecular collisions, leading to a path that is a random walk.

Although Robert Brown was the first scientist who observed such motion, he could not explain this phenomenon. The first one, who finally came up with the explanation, was Albert Einstein[1] in 1905 and independently Marian Smoluchowski[2] in 1906. Einstein developed thermodynamic theory of Brownian motion based on osmotic pressure and Navier – Stokes equation. Smoluchowski realized that the random motion of pollen grains was due to presence of molecules of water, hitting the pollen grains from all directions. Because of chaotic motion of the molecules, these collisions from different directions never equalized each other. Therefore the collisions resulted in random motion of pollen grains. By treating the Brownian motion as a random walk, Smoluchowski showed that the mean-square displacement $\langle r^2 \rangle$ of particles at time t, is given by:

$$\left\langle r^2 \right\rangle = 2dD_0 t \tag{1}$$

where D_0 is the diffusion coefficient at infinite dilution and d is the dimensionality of space. The mean-square displacement accordingly grows linearly in time and can be described as a measure of the spread of particles when they diffuse in all directions from the origin.[3]

In normal diffusion, the mean-square displacement $\langle r^2 \rangle$ is proportional to time and the diffusion coefficient is constant. Several other types of motion can also be distinguished. Table 1 shows mathematical forms for the $\langle r^2 \rangle$ a function of time t for different types of random or directed motion.

Table 1. Types of motion which are used in the analysis of single-particle tracking data. Here $\langle r^2 \rangle$ is the mean-square displacement, t is time, d is dimensionality, D_0 is the diffusion coefficient at infinite dilution, D is the diffusion coefficient, Γ is a constant, α is the anomalous subdiffusion exponent, v is velocity, $\langle r^2 \rangle_0$ is the square of the radius of a cage, and τ is a time constant.

Normal diffusion	$\langle r^2 \rangle = 2dD_0 t$
Hindered normal diffusion	$\langle r^2 \rangle = 2dDt,\ D < D_0$
Anomalous diffusion	$\langle r^2 \rangle = \Gamma t^{\alpha},\ \alpha < 1$
Directed + normal diffusion	$\langle r^2 \rangle = 2dDt + v^2 t^2$
Confined diffusion	$\langle r^2 \rangle = \langle r^2 \rangle_0 [1 - \exp(-t / \tau)]$

Figure 2 shows the shape of the curves of mean-square displacement versus time and an example of trajectories for different types of motion, mentioned in Table 1.

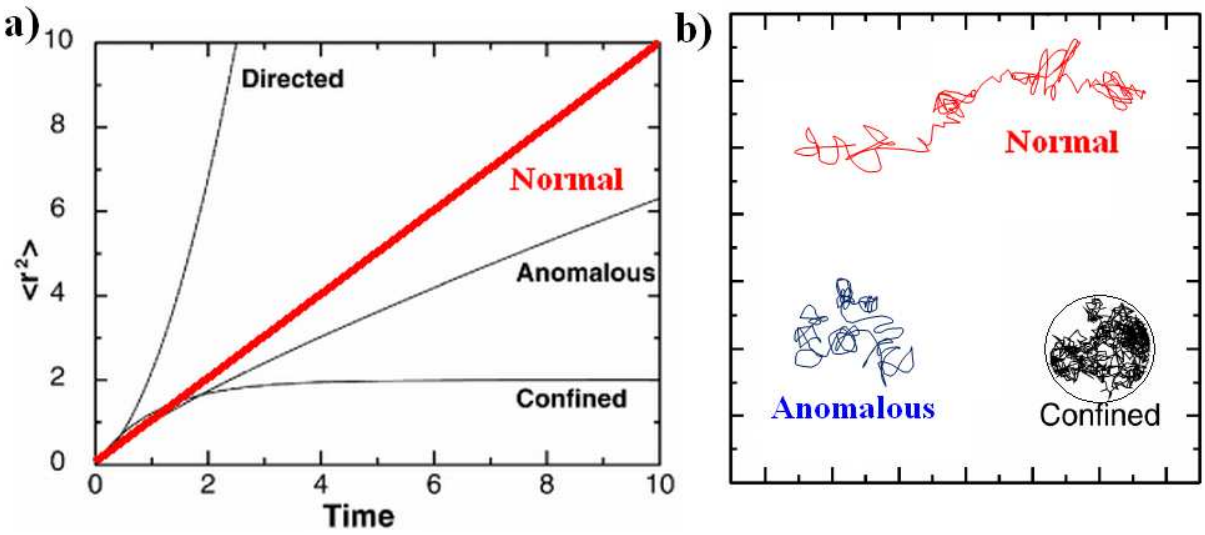

Figure 2. a) Mean-square displacement $<r^2>$ as a function of time for directed motion plus diffusion, normal diffusion, anomalous diffusion with α = 0.8 and confined diffusion. **b)** Typical trajectories for a random walk for normal diffusion, anomalous subdiffusion with α = 0.8, and confined motion in a circular cage.

In hindered normal diffusion mean-square displacement is still proportional to time, but the diffusion coefficient is reduced. In three dimensional systems it may be found, for example, in moderately concentrated solution of proteins. In anomalous subdiffusion (Figure 2), the motion is extremely hindered, and the mean-square displacement is proportional to some power of time less than 1. It is known,[4,5] that anomalous diffusion may result from traps or obstacles at the percolation threshold in concentrated solutions. The diffusion coefficient is therefore time-dependent, $D(t) = \Gamma / t^{1-\alpha}$, and goes to zero at large times. Today, an increasing number of processes can be described by anomalous diffusion (motion of protein in the living cell[6] or foraging behaviour of animals[7]).

We can also distinguish confined diffusion, which is normal at short times, but at long times mean-square displacement approaches constant i.e. the square of the radius of the cage (Table 1 and Figure 2b). An additional type is diffusion within a diffusing region (walking

confined diffusion[8]), which might be observed for a mobile particle within a mobile lipid domain.

The diffusion coefficient D is a constant for a single particle in an unbounded fluid, and is related to the frictional coefficient f by the Stokes – Sutherland – Einstein[9] (SSE) relation:

$$D = \frac{k_B T}{f} \tag{2}$$

where $k_B T$ is an estimate of the translational energy per particle. k_B is the Boltzmann constant and T the temperature. The frictional coefficient f for a spherical particle is given by the Stokes law:

$$f = 6\pi\eta R \tag{3}$$

where R is the hydrodynamic radius of the particle and η is the solvent viscosity. Above-mentioned equations lead to the SSE equation for the diffusion of a spherical particle:

$$D = \frac{k_B T}{6\pi\eta R} \tag{4}$$

2.1.2. Electrophoresis

Electrophoresis is defined as a motion of charged objects (ions, proteins, colloids) relative to a fluid phase under the influence of an external electric field. When an electric field is applied to the solution, such objects experience a force attracting them towards the oppositely charged electrode.[10] The scheme of electrophoresis is presented in Figure 3. The electrophoresis was first observed by Reuss[11] in 1807, who noticed that the application of a constant electric field caused migration of clay particles dispersed in water. This phenomenon is generated by the presence of a charged interface between the particle surface and the surrounding fluid.

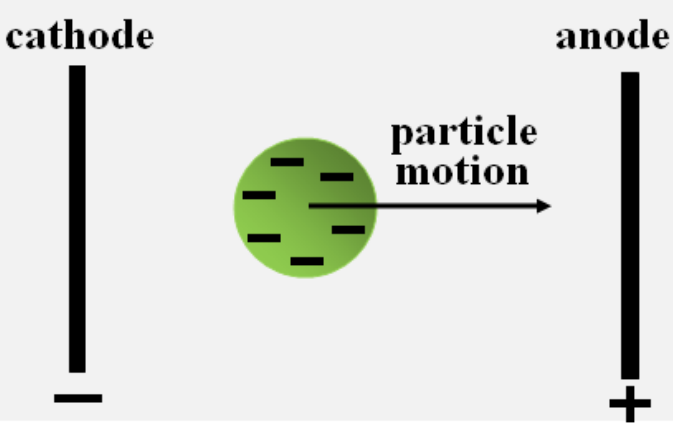

Figure 3. Electrophoresis. Colloid particle with a negative charge on the surface is moving to a oppositely charged electrode.

The force, *F*, which is experienced by a charged object (of charge *q*) in an external electric field, *E*, can be described as follows:

$$F = q \cdot E \tag{5}$$

This force accelerates the particle in a fluid till a steady state is reached (usually very fast). In the steady state the frictional force, *f*, is equal and opposite to the applied force. *v* is the steady state velocity and

$$f \cdot v = q \cdot E \Rightarrow v = \frac{q \cdot E}{f} \tag{6}$$

For a spherical particle of radius *R* in a solvent of viscosity η, the frictional force is given by $f=6\pi\eta R$, so we can obtain the following relation:

$$v = \frac{q \cdot E}{6\pi\eta R} \tag{7}$$

The electrophoretic mobility, μ, is defined as the velocity per unit electric field.

$$\mu = \frac{v}{E} = \frac{q}{6\pi\eta R} \tag{8}$$

Thus the electrophoretic mobility is directly proportional to the magnitude of the charge on the particle, and is inversely proportional to the size of the particle.[12]

During my Ph. D. studies, I investigated motion of ions under the influence of external electric fields in binary mixtures. In such mixtures, each of the two phases possesses different conductivity, thus free ions can accumulate at the interface after reaching it. Applying the external electric field caused motion of interface, and as a result, accelerate the phase separation process. Experimental details are described in Chapter 3.3 entitled *Ions motion in liquid crystal/polymer mixtures.*

2.2. Characterization of nano and micro objects

In this chapter I will focus on three types of nano and micro objects, which were used to probe the properties of complex liquids. I will describe in more details: (i) nanoparticles – as a typical spherical monodisperse probes; (ii) plasmid DNA – as biomolecule of shape approximated by an equivalent rigid cylinder; and (iii) free ions – as nanoobjects, which move under influence of an external electric field.

2.2.1. Nanoparticles

Nanoparticles can be defined as particles with size in the range of 1 to 100 nm at least in one of three dimensions. Size of nanoparticles is between the size of atoms (0.1 nm) and macroscopic objects 1 ~ 1000nm. In this size range, the physical, chemical and biological properties of the nanoparticle change in fundamental ways from the properties of both individual atoms and bulk material.[13]

Nanoparticles usually consist of 10 to 10^6 atoms. Their structure is schematically presented in Figure 4. Such nanoparticles have special stability because they consist of a "magic number" of metal atoms. Only well defined number of metal atoms allow to complete closure of successive shells in a cubic close packed arrangement. The "magic numbers" as 13, 55 or 147 correspond to the closure of 1, 2, and 3 shells respectively.[14]

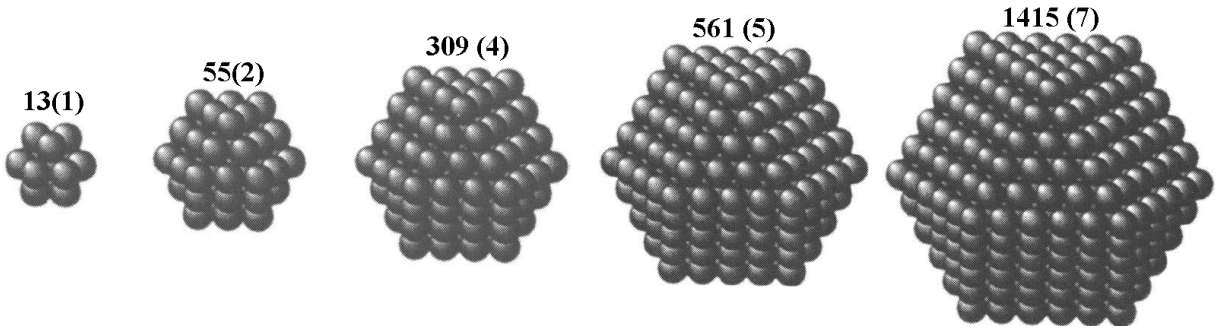

Figure 4. Atomic structure of nanoparticles. First number corresponds to number of atoms, second number in bracket corresponds to number of shells. Figure is based on figure from reference 14.

Nanoparticles can be composed of semiconductive, pure metallic, metal oxide, organic, biological and polymeric components. They also exhibit great morphological diversity with shapes such as sphere, prism, cube, tetrapod, triangle, pentagon and hexagon. Their shape can also be tube, rod, needle or hollow sphere. Carbon nanotubes are typical examples of the tube-type nanoparticles, while fullerene-based particles can be examples of the hollow sphere.[15] Different shapes of nanoparticles are presented in Figure 5.

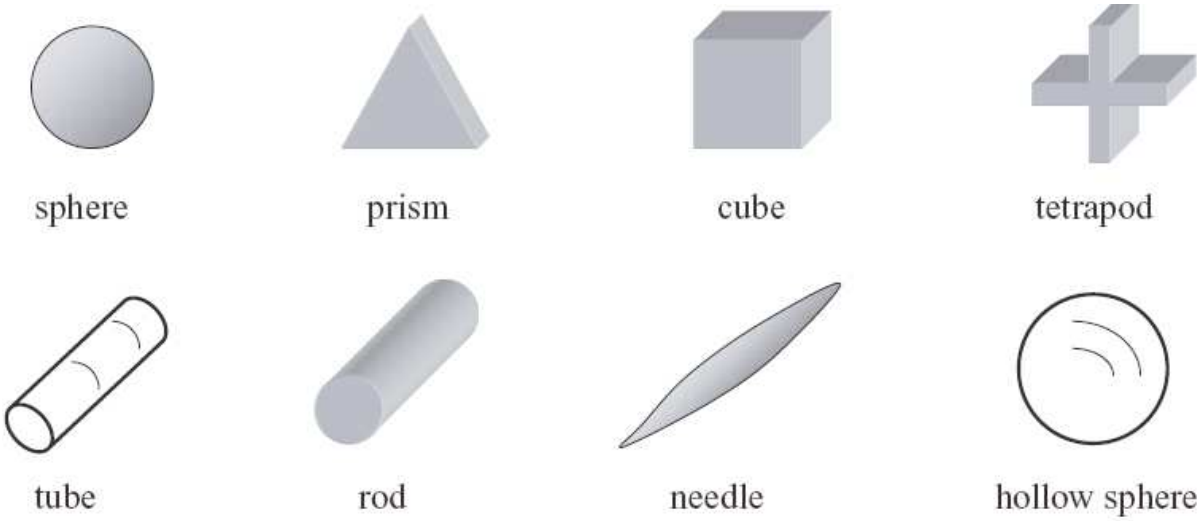

Figure 5. Different shapes of nanoparticles. Figure is taken from reference 15.

Nanoparticles often do not possess suitable surface properties required for specific applications. For this reason, surface-modification techniques are used to transform these materials into valuable finished products.[16] The surface modifications can be done for the purposes of i) passivating a very reactive nanoparticle, ii) stabilizing a very aggregative nanoparticle in a medium, iii) functionalizing the nanoparticles for applications in molecular recognition, or iv) promoting the assembly of nanoparticles. Most commonly used surface modifications methods include: grafting thiolated surfactants or polymers, adsorption of charged surfactants or ligands and attachment of biological molecules such as DNA, peptides or proteins.[13] The enormous diversity of the nanoparticles arising from their wide chemical

nature, shapes and morphologies, the medium at which the nanoparticles are present and possible surface modifications, give nanoparticles great importance in science. Owing to such variety, nanoparticles have potential application in a high performance coatings, electric materials, catalysts, drug delivery carriers, and biomedical materials, etc.

During my Ph. D. research, nanoparticles were used as probes, and such type of nanoparticles will be described in more details in the following paragraph. Nanoparticles, which are used as probes in my experiments, need to fulfil a number of conditions. Such probes should be highly monodispersed, that is, possess ultra – narrow size distribution profile (Figure 6).

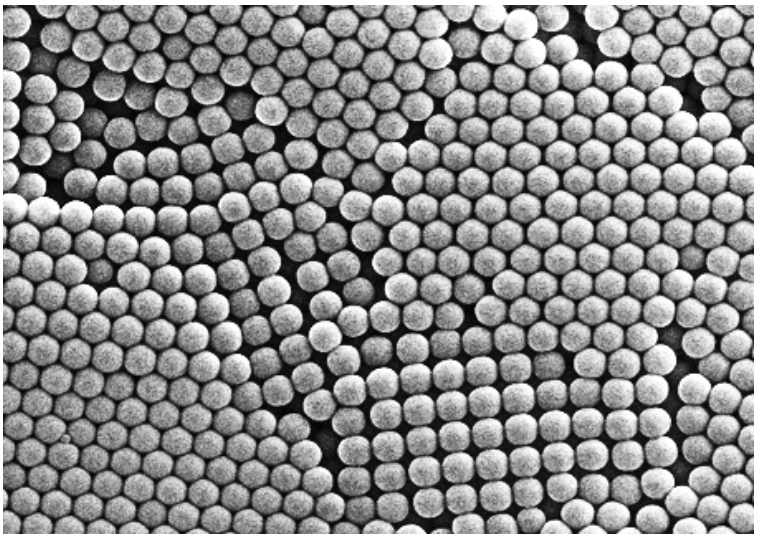

Figure 6. Scanning electron microscope image of monodisperse polystyrene nanoparticles of 100 nanometers in diameter. (Source: http://www.futurity.org/science-technology/tiny-turnstile-counts-nanoparticles/).

Probe nanoparticles should not aggregate in solutions. Stability against aggregation is usually obtained by using proper surface coating. The surface coating of nanoparticles can regulate stability, solubility and targeting. Shape of nanoparticles is also an important factor – the preferred shape of nanoparticles used as a probe is a sphere (Figure 5). At the end, a price also has to be taken into consideration. Those requirements, essential for a perfect probe, are

ideally fulfilled by polymer nanoparticles. Monodisperse polystyrene nanoparticles[17,18] are often used as particle size standards for calibration of size-measuring instruments. They are potentially useful as well as the mass standards for particle mass spectrometry. In my experimental work, I used Nanobead NIST Traceable Particle Size Standard, from Polyscience Inc. Nanobead NIST Traceable Particle Size Standards are monodisperse spherical polystyrene nanoparticles ranging from 40nm to 220nm in diameter. Such nanoparticles are measured on instruments calibrated with NIST (National Institute of Standards and Technology) Standard Reference Materials.

2.2.2. DNA

Deoxyribonucleic acid, DNA, is the supreme "information storage" polymer. The monomer units of DNA are nucleotides, so the polymer is known as a polynucleotide. Each nucleotide consists of 2-deoxyribose, a nitrogen containing base attached to the sugar, and a phosphate group. In DNA, adjacent nucleotides are linked by a phosphodiester bond: a covalent bond is formed between the 5' phosphate group of one nucleotide and the 3'-OH group of another (Figure 7). Each strand of DNA has a "backbone" of phosphate-sugar-phosphate-sugar-phosphate. The backbone has a 5' end (with a free phosphate) and a 3' end (with a free OH group). There are four different types of nucleotides found in DNA, differing only in the nitrogenous base. The four possible nitrogenous bases are adenine (A), cytosine (C), guanine (G), and thymine (T). These bases code the genetic information in DNA and are its primary structure.[19,20]

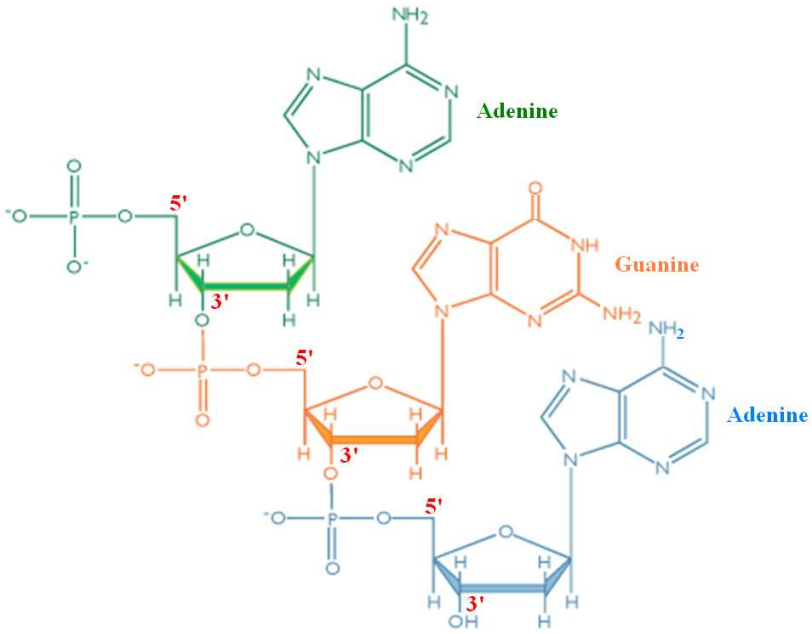

Figure 7. Polynucleotide chain. Each nucleotide is drawn in a different color. Scheme is based on figure from the website: http://cyberbridge.mcb.harvard.edu/dna_1.html

The double helix structure (two DNA strands), discovered in 1953 by James Watson and Francis Crick, is its secondary structure (Figure 8).

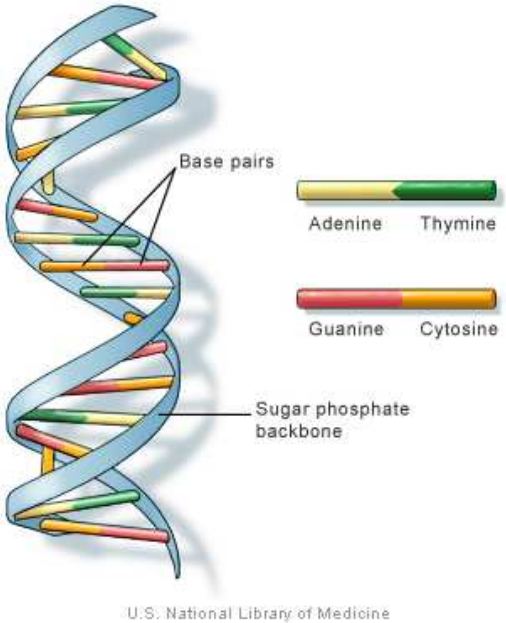

Figure 8. DNA double helix. Two polynucleotide chains are linked together by hydrogen bonds between two base pairs: adenine and thymine and cytosine and guanine (http://www.dna-sequencing-service.com/dna-sequencing/dna-double-helix-3/).

The double helix is formed by two polynucleotide chains wind around each other, each with a pitch of 3.4 nm and a radius of 1 nm. The chains are antiparallel, which means that the one chain runs 5'–3' and the other runs 3'–5' (Figure 7). The chains are held together by hydrogen bonding between A–T and C–G base pairs. The secondary structure of DNA arise primarily from the pattern of this hydrogen bonding between bases of one or more chains.

Long stretches of DNA can fold into a variety of tertiary structures. Such a long section of DNA may form closed circular DNA (ccDNA) by covalent linkage of the two ends of the chain. Next, the twisting of ccDNA can lead to the formation of supercoiled DNA (Figure 9).

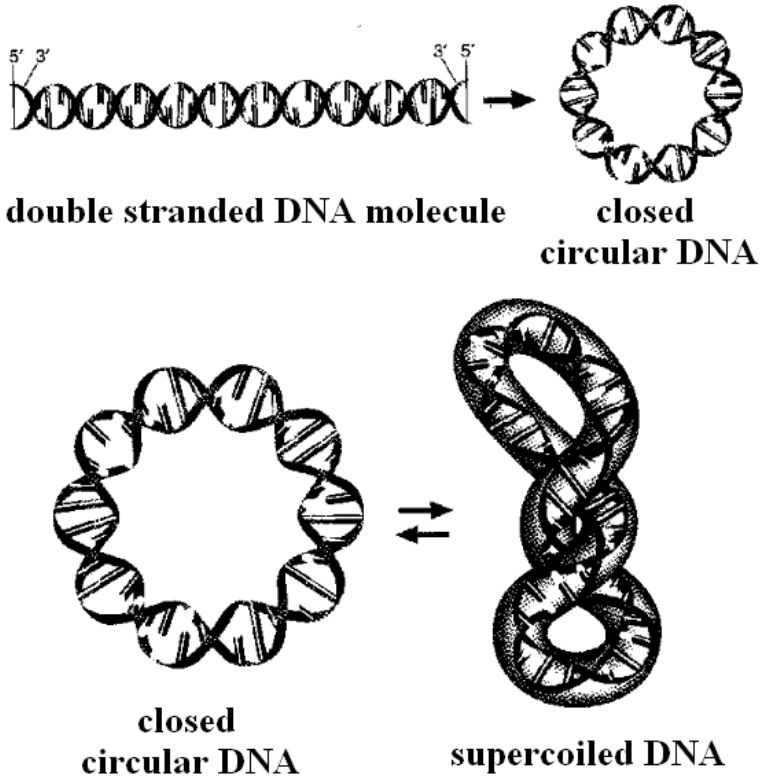

Figure 9. The examples of tertiary structures of DNA. Supercoiled DNA is found in the chromosome and can be visualized as the twisting of closed circular DNA.
(Source:http://members.tripod.com/arnold_dion/RecDNA/notes.html).

Supercoiled DNA is important for DNA packaging within all cells. Because the length of DNA can be thousands of times longer than that of a cell, packaging this genetic material into

the cell or nucleus (in eukaryotes) is difficult. Supercoiling of DNA reduces space and allows for a lot more DNA to be packaged.[21]

In my studies, I used supercoiled plasmid DNA of 4.7k base pairs. I approximated shape of such plasmid by an equivalent rigid cylinder and treat such rod as a probe.

2.2.3. Ions

An ion is an atom or group of atoms, in which total number of electrons is not equal to the total number of protons, giving as a result, a net positive or negative electric charge. There are two basic principles for determining ionic sizes. Anions have a larger ionic radius than their corresponding atomic radii, because although there is the same nuclear charge, the greater number of electrons creates more repulsion and shielding. Thus, the effective nuclear charge drops, and the radius increases. The opposite is true for cations. As they have fewer electrons, there is less repulsion and the cations are therefore smaller than the parent atom.[22] Examples of ionic radii are shown in Figure 10.

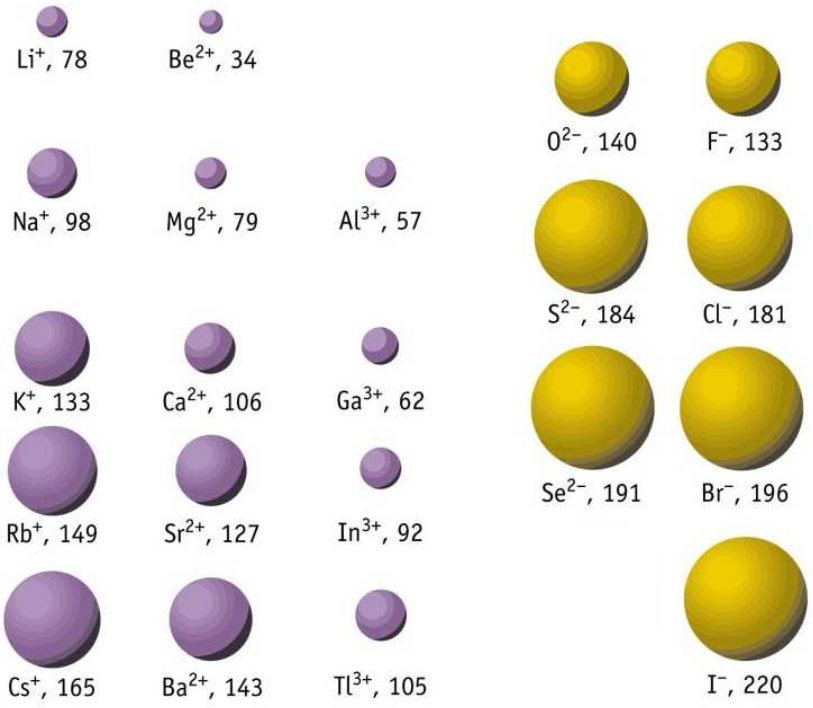

Figure 10. Some of the ionic radii given in picometres. Figure is based on scheme taken from reference 22.

Among ions, there are many anions and cations that have the same number of electrons and they are called isoelectronic ions (e. g. O^{2-}, F^{-}, Na^{+}, Mg^{2+} all possess 10 electrons, see Figure 10). However, the number of protons in the nucleus of the ions is increasing (O^{2-} – 8 protons, F^{-} – 9 protons, Na^{+} – 10 protons, Mg^{2+} – 11 protons). The greater number of protons will tend to pull the electrons more and more towards the centre of the ion - causing the ionic radii to fall. As the number of protons in the nucleus of the ion increases, the electrons get pulled in more closely to the nucleus. To sum up, for isoelectronic ions, the radius decreases as the positive nuclear charge increases.[23]

The role of ions is very important, because they are ubiquitous in solutions. It is known,[24,25] that ions are everywhere in our environment and usually all systems are contaminated by ions. The ionic impurities can be classified as coming from the processes, people and objects. Ionic contamination includes ions in chemicals, ions deposited during handling, ions from the air and ions from cleaning products and equipment. Devices such as semiconductor wafers, microelectromechanical systems, data storage components and flat liquid crystalline panel displays are the most susceptible to ionic impurities. Hence it is essential, to take note of the importance of ions in mentioned materials, especially in experiments with external electric field.

In my studies, I investigated liquid crystal/polymer mixtures, which was contaminated by free ions (ionic impurities). In the external electric field, electrophoretic force pulling free ions plays crucial role in my studies, therefore the electrophoresis was described at some length in the Chapter 2.1.2.

2.3. Complex liquids

According to Gelbart and Ben-Shaul[26] the main feature of a complex fluids is the presence of a mesoscopic length scale which necessarily plays a key role in determining the properties of the system. For example, in polymer solutions, the intermediate length scale can be the size of a polymer chain. Cross-linking between different polymer chains can lead to the formation of a network, with viscoelastic properties intermediate between the elastic behavior of a solid and the viscous flow of a simple liquid. Some other typical examples of complex liquids are liquid crystal solutions. Sufficiently elongated (rod-like) of flat (plate-like) liquid crystalline molecules may lead to additional anisotropic phases, which are "intermediate" between the isotropic liquid and the fully periodic crystal. Mesoscopic length scale is also found in micellar solutions, microemulsions, colloidal suspensions, and after all, in biological fluids, such as blood, cell cytoplasm or biopolymer solutions (DNA).[27] The presence of a mesoscopic scale, gives rise to many of the unusual properties of complex fluids.

In this chapter I will focus on three types of complex liquids system, which were investigated during my Ph. D. research. I will describe in detail: polymers, liquid crystals, and multicomponent system consisted of both polymers and liquid crystal molecules.

2.3.1. Polymers

A polymer (from Greek – *polumeros*) is a large macromolecule consisting of a repetition of smaller chemical units, called monomers. Schematically a polymer can be represented as a chain of recurrent monomers, where *n* stands for a number of monomers in the chain, that is, a degree of polymerization (Figure 11). Degree of polymerization represents a number of recurrent monomers in a polymer chain, therefore is connected with length of this chain.

Many polymers constitute a mixture of chains of variable length and therefore a degree of polymerization is a statistical quantity for a given polymer system.

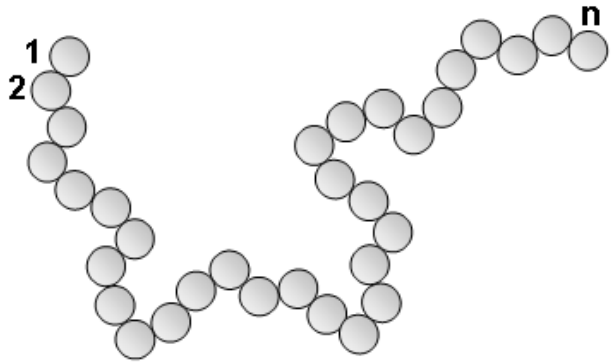

Figure 11. Schematically representation of polymer consisted of *n* monomers.

Degree of polymerization is calculated by dividing an average polymer molecular weight (diminished by final groups' mass) by the molecular weight of single monomer. In case of polymers of very big average molecular weight, final groups' can be ignored, because of very little impact on final macroscopic properties. Degree of polymerization for polymers is greater than $n = 100$ and easily reaches $n > 10^5$. Due to high degree of polymerization, that is big molecular weight, detaching or attaching one of monomers will not significantly change any of chemical or physical properties of the polymer. It differentiates polymers from oligomers, which molecular weight is much lower ($10 \leq n \leq 100$) that detaching or attaching certain monomer, results in noticeable change e.g. in their melting temperature.

With the exception of naturally occurring proteins, it is impossible to find a polymer batch where all macromolecules have exactly the same molecular weight. Typically, polymers have a molecular weight distribution that differs depending on the method of synthesis and on the fractionation procedure.[28] A scheme of a molecular weight distribution profile is shown in Figure 12.

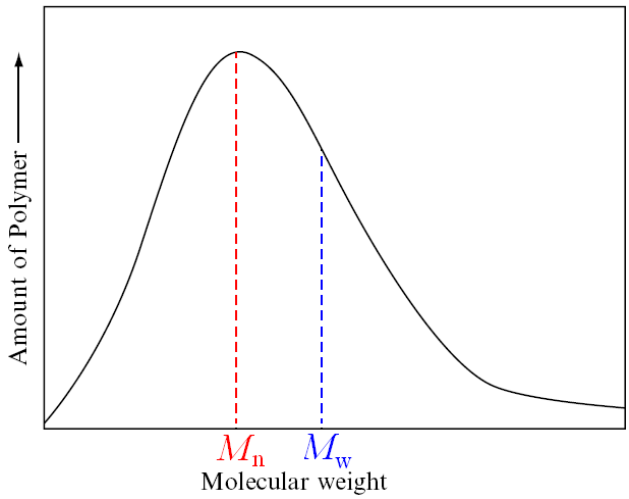

Figure 12. A schematic molecular weight distribution of a polymer.

Polymers are said to be polydisperse, meaning that they have a distribution of molar masses. The distribution of molecular weights is important in many applications, such as adhesion, flocculation or aging behavior.[29] Some physical properties are sensitive to the low molecular weight fraction while other are sensitive to the high molecular weight fraction. Because of difficulties associated with measuring a distribution of molecular weight, some mathematical forms are used to compute the averages measured experimentally. The type of averages depends on the experimental method used to measure it. The simplest average is the number – average molecular weight, M_n, and is defined as follows:

$$M_n = \frac{\sum N_i M_i}{\sum N_i} \tag{9}$$

where N_i is the number of molecules with molecular weight M_i. Because M_n depends on the number of molecules with given molar mass, it can be measured on the basis of colligative properties of the polymer in solution. Colligative properties include: freezing point depression, osmosis, lowering of vapour pressure and elevation of boiling point.[19]

Another definition of molecular weight average is the weight – average molecular weight, M_w, defined as follows:

$$M_w = \frac{\sum wt_i M_i}{\sum wt_i} = \frac{\sum N_i M_i^2}{\sum N_i M_i} \tag{10}$$

where wt_i is the weight of all species with molecular weight M_i. Weight – average molecular weight can be determined from techniques such as size – exclusion chromatography or light scattering (either quasi - elastic or elastic). This molecular weight is sensitive to high molecular weight species and hence is always larger than M_n (Figure 12). Useful measure of the spread of a polymer distribution is a ratio M_w/M_n, called the polydispersity index. For an ideal polymer, this ratio will be equal to one, while in practice, this ratio is always greater than one, typically in range between 1.5 and 2.

Interactions between polymer molecules in solution depend strongly on concentration. Particularly important is a resultant size of the macromolecule. A polymer in solution can be pictured as a coil, however, its shape is continuously changing due to thermal motion. For this reason, when we consider the size of polymer coil it is necessary to take the statistical average over many conformation and chain lengths. There are two useful average measures of the dimensions of polymer coils: the root – mean – square (r. m. s.) end – to – end distance, $< r^2 >^{1/2}$, and r. m. s. radius of gyration, $< R_g^2 >^{1/2}$. The r. m. s. end – to – end distance (Figure 13) is the average separation between chain ends and gives an estimation of a size of polymer in solution. If we consider the simplest model for polymer coil, where chain is supposed to consist of n volume-less links of length l which can rotate freely in space, then r. m. s. end – to – end distance is described as follows:

$$< r^2 >^{1/2} = n^{1/2} l \tag{11}$$

The r. m. s. radius of gyration is a measure of the average distance of a chain from the center of mass of the coil. This quantity has the advantage that can be defined for branched molecules (with more than two ends) and cyclic macromolecules (without ends). The difference between radius of gyration and the distance between chain ends is indicated in Figure 13.

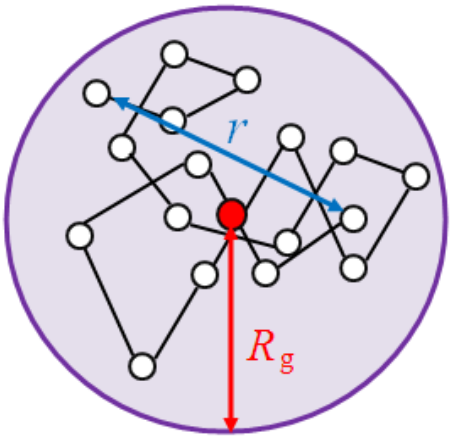

Figure 13. Difference between r. m. s. end – to – end distance, r, and radius of gyration, R_g. Center of mass is pictured as a red circle.

For simple linear chains, radius of gyration and end – to – end distance are related by:

$$< R_g^2 >= \frac{1}{6} < r^2 > \qquad (12)$$

The radius of gyration also depends on a solvent. In a good solvent, polymer chains expand from its unperturbed dimension to maximize the number of segment – solvent contacts. In this case the coil is said to be swollen. In poor solvents, the chains will contract to minimize interaction with the solvent.[19] For example, for poly(ethylene glycol) and water as a solvent, radius of gyration, as a function of molecular mass, M, is given[30] by:

$$R_g = 0.02 M^{0.58} [\text{nm}] \qquad (13)$$

Interactions between polymer molecules depend also on polymer concentration. In a dilute solution, the molecules are well separated and do not interact with each other. Each molecule can be considered as an isolated random coil. With increasing polymer

concentration, less and less space is available between the coils, thus the coils start to overlap. This concentration of polymer in solution is called the overlap concentration, c^*, and is given by:

$$c^* = \frac{M}{\frac{4}{3}\pi R_g^3 N_A} \tag{14}$$

where N_A is the Avogadro's number. If the concentration is increased to a point slightly higher than c^*, the coils become entangled and the solution is called semi – dilute. Polymer chains in dilute, semi – dilute and concentrated regime are presented in Figure 14.

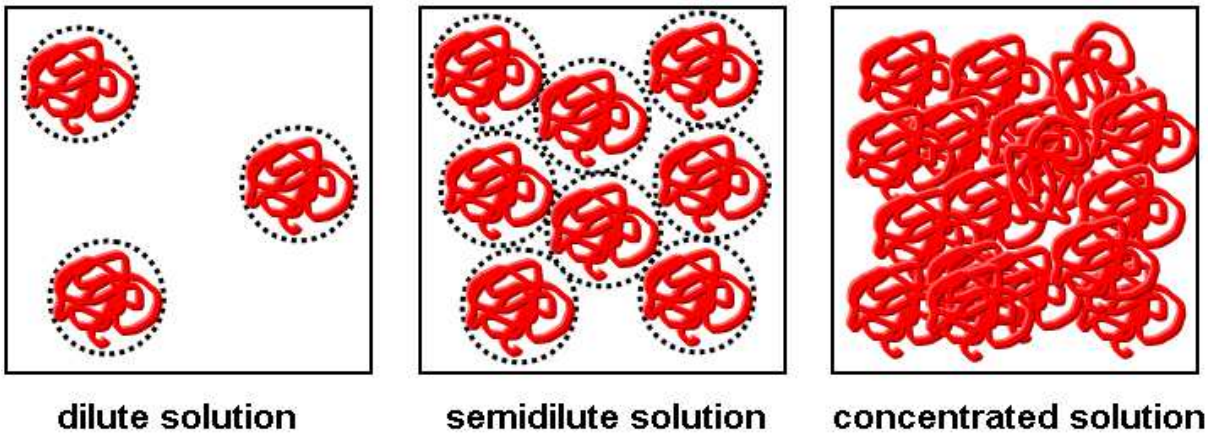

Figure 14. Schematic of the arrangement of polymer chains in different concentration regimes.

In polymer solution we can additionally define a blob size, ξ, also known as a correlation length. The size of blobs is a function of polymer concentration, c, and is described as follows:

$$\xi = R_g \left(\frac{c}{c^*} \right)^{-0.75} \tag{15}$$

The blob size represents the size of the region where all monomers belong to the same polymer. In the semi – dilute solution, the blob size decreases with an increase of concentration and becomes smaller than the coil size. When the concentration is very high, blob size becomes similar to the monomer unit size. In this case the polymer solution is called concentrated solution.

2.3.2. Liquid crystals

Liquid crystals are a state of matter that have properties between those of a conventional liquid and those of a crystal. In the crystal, the molecules are located on a three-dimensional periodic lattice. In the liquid, the centers are not ordered in this sense, and as a result, these two states of matter differ most obviously by their mechanical properties. The statement that liquid crystals have properties between liquid and a crystal, refers to a phase formed between these two states, with a degree of order intermediate between molecular disorder of a liquid and a regular structure of a crystal.[31]

Liquid crystals were first discovered by Reinitzer in 1888 and the first proper classification of liquid crystals was made by Friedel in 1922. Since that time, various new categories have been discovered and named, but certainly, not all of them will be presented here. In this chapter, only types and phases of liquid crystals used while performing the experimental work, will be described in details.

Liquid crystals can be divided into two classes: thermotropic and lyotropic. Thermotropic liquid crystal phases are formed by pure mesogens in a certain temperature range. The prefix thermo-, refers to phase transition induced by temperature changes. Thermotropic mesogens do not need solvent to form liquid crystal phases. In contrast, lyotropic liquid crystal phases are formed by the change of concentration in the solvent (the prefix lyo-, refers to concentration).[19] The most popular lyotropic liquid crystal phases are

those found in surfactant solutions or in solutions of amphiphilic polymers. Surfactant liquid crystals have more variety of structural diversity than thermotropic liquid crystals and usually exist in equilibrium with monomers.[15] Thermotropic liquid crystal phases, which were used while performing experimental work, will be described in more detail in the following paragraph.

Thermotropic liquid crystal phases are formed only by anisotropic molecules. Particles of liquid crystalline substances, as a rule, are like a rod or disc. Figure 15 demonstrates exemplary structural models of rod-like and disc-like particle.

a)

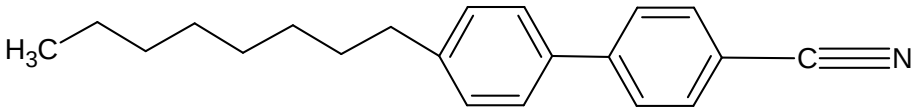

b)

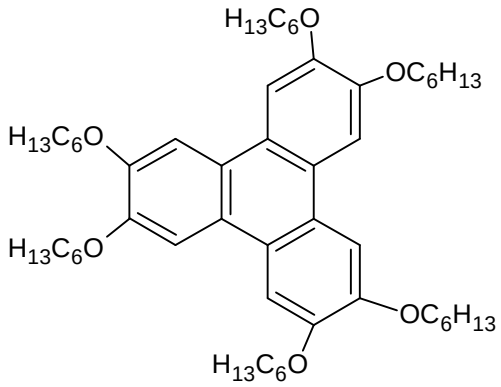

Figure 15. a) rod-like liquid crystal molecule **b)** disc-like liquid crystal molecule

Rod-like particles are presented in the form of an elongated cylinder. It is definitely a simplification, but sufficient enough to understand a character of particles' ordering in mesophases.

In the case of strongly anisotropic particles, two types of orders are taken into account: long-range translational order (that is, ordering of mass centre locations) and long-range

orientational order (that is, ordering of long axes). The direction of average molecular orientation is called the director, usually denoted by a unit vector, $\hat{n}$. To quantify just how much order is present in a material, Freedericksz and Tsvetkov[32] defined an orientational order parameter, *S*, which is described as follows:

$$S = \frac{1}{2}\left\langle 3\cos^2\theta - 1 \right\rangle \tag{16}$$

where θ is the angle between the director and the long axis of each molecule (Figure 16).

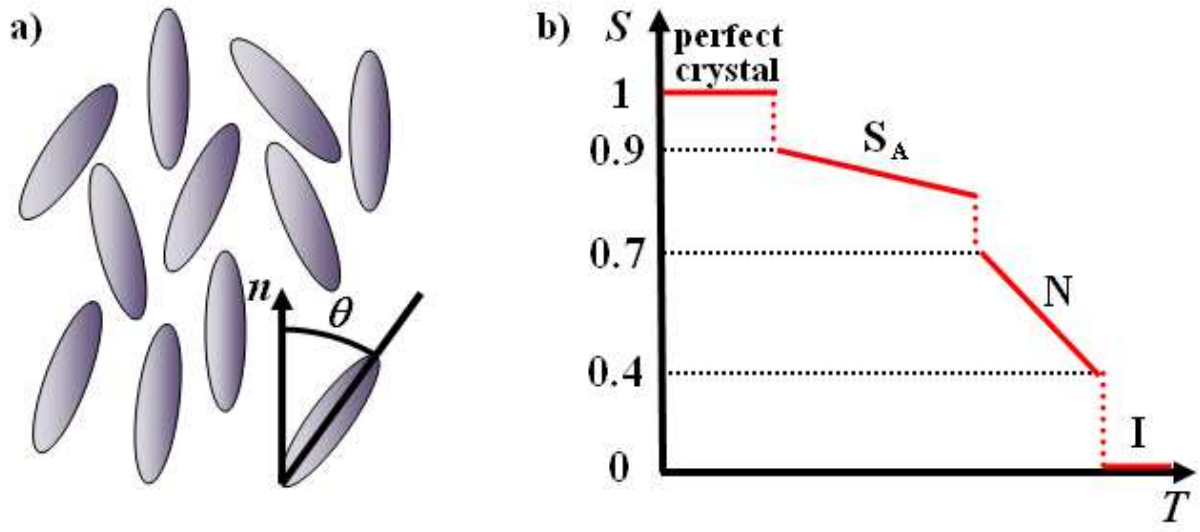

Figure 16. a) Schematic representation of isotropic liquid with order parameter, *S*, equals to zero. **b)** Typical values for order parameter , *S*, for: perfect crystal, smectic A phase – S_A, nematic – N, and isotropic liquid – I.

In the isotropic liquid, the average in equation (16) is zero, therefore the order parameter equals to zero. For a perfect crystal *S* = 1. Typical values for the order parameter of a liquid crystal range between 0.3 and 0.9.

2.3.2.1. Nematic phase

In the nematic phase, there is no long-range translational order, just as in a normal isotropic liquid. However, the phase exhibits long-range orientational order, unlike in a liquid.

Such substance is an anisotropic liquid and remains in the liquid state. This liquid characterizes preferable direction $\hat{n}$, which is determined by the average of molecules orientation. We define the phase of foregoing properties as nematic phase and use N to denote it (Figure 17). Physical characteristics of this phase do not depend on the orientation of $\hat{n}$.

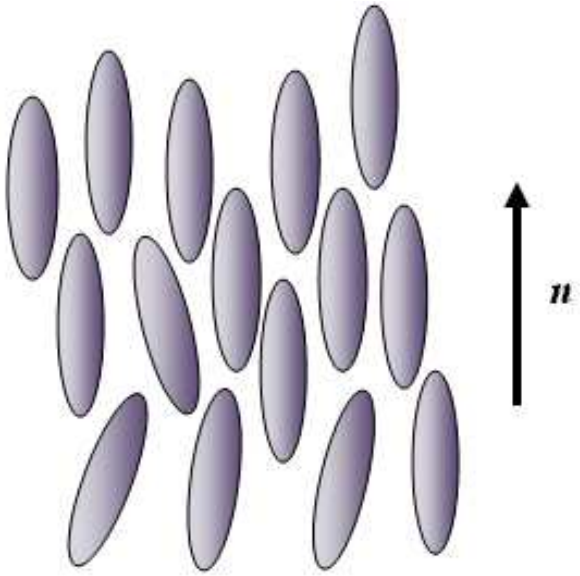

Figure 17. The arrangement of molecules in the nematic mesophase, *n* denotes the director.

The temporary orientations of long axes in nematic phase, differ from that of the director. The probability, that certain particle has orientation close to $\hat{n}$, is much higher than probability, that the orientation differs much from $\hat{n}$. All directions in the plane perpendicular to the director are equivalent, therefore the nematic phase posseses uniaxial symmetry with the axis of symmetry given by $\hat{n}$.

The nematic phase formed by chiral molecules is itself chiral (i.e. different from its mirror image). Such phase is called the cholesteric phase, because the mesogen for which it was first observed contained a cholesterol derivative. This phase has been also observed for

other types of mesogens, therefore now it is called the chiral nematic phase and denoted N*. The arrangement of molecules in chiral nematic phase is illustrated in Figure 18.

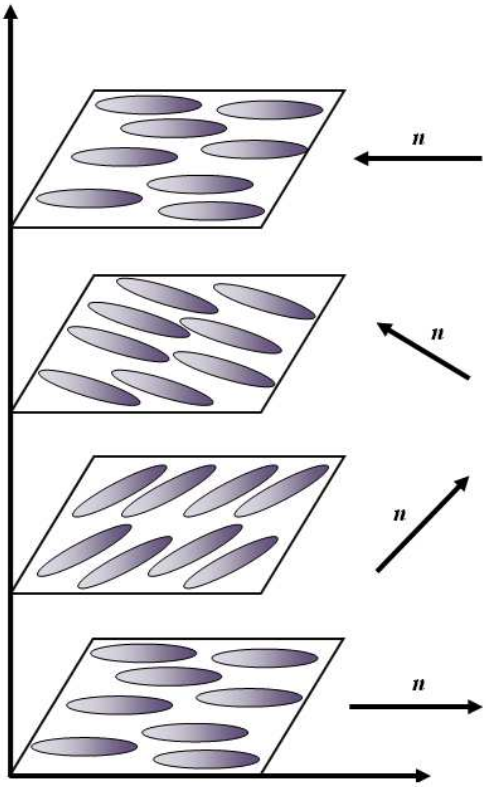

Figure 18. Schematic presentation of chiral nematic or cholesteric phase, where the director *n* undergoes an helical rotation.

Locally, a cholesteric phase is very similar to the nematic phase. The centers of mass have no long-range order and the molecular orientation shows a preferred axis given by the director $\hat{n}$. However $\hat{n}$ in the cholesteric phase is not constant in space, its conformation is helical. The helical structure has a characteristic pitch, or repeat distance along the helix, which can range from a few nanometres to more than 100 nm, i. e. a distance much larger than the molecular dimensions. When the pitch length is comparable to the wavelength of light, the N* phase scatters or reflects visible light, producing colors. The pitch and thus colors are sensitive to the temperature, which is the basis of the thermochromic devices, i.e. those that produce colors change in response to the temperature. The pitch unwinds as temperature is

decreased, leading to observable color changes. These have been exploited in medical thermography, where heat variations across the body surface are mapped.[19]

2.3.2.2. Smectic phase

Between crystalline solid and the nematic phase, there may occur another liquid crystalline phase called smectic phase. All smectics are layered structures, the centers of mass of molecules exhibit ordering in one direction (normal to layers). Particular smectic phases differ from each other through the orientation of director $\hat{n}$ (with respect to the normal to layers) and degree of molecules ordering in the smectic phase. The orientational ordering degree in smectic phases, in general, is higher than in nematic phase and deviations of long axes from the direction $\hat{n}$ are smaller.

The most basic smectic phase is the smectic A, denoted as SmA (Figure 19a). In SmA, normal direction to smectic layers is parallel to $\hat{n}$. Another type of the smectic phase is Smectic C, denoted as SmC (Figure 19b).

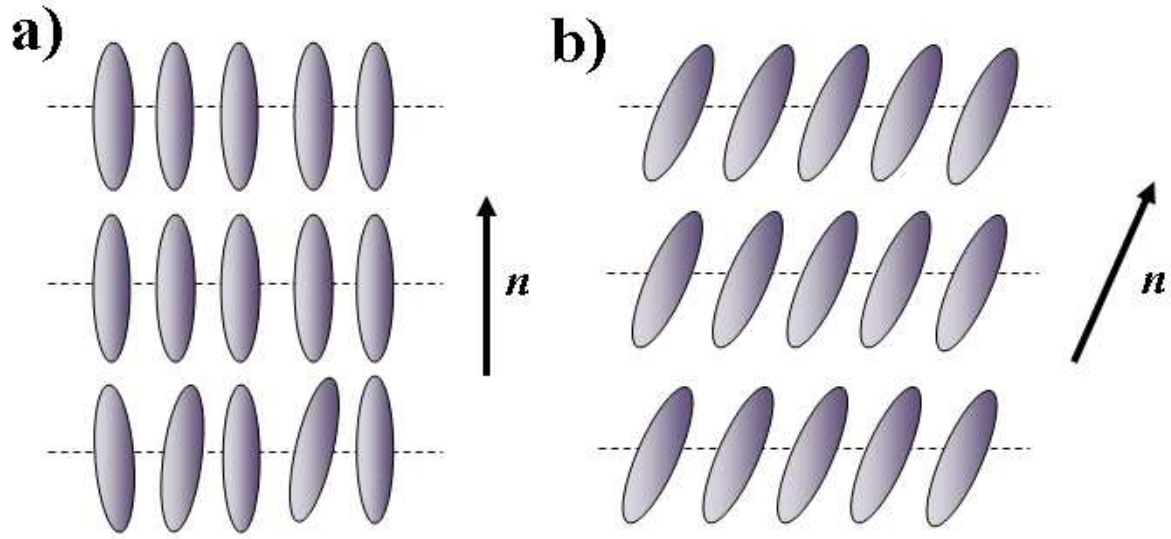

Figure 19. The arrangement of molecules in **a)** smectic A **b)** smectic C.

Smectic C phase has lower symmetry than smectic A, due to two preferable directions: normal direction to layers and a direction of director $\hat{n}$. Phases N and SmA are uniaxially symmetric, but no such symmetry exists in the case of phase SmC. Properties of smectic C are described through two directions: direction of $\hat{n}$ and direction normal to the layers. The angle between these directions is known as tilt angle. Thus smectic C phase has a centre of biaxial symmetry.

Depending on the degree of the tilt of molecules (with respect to the layer plane), smectic F, smectic G, and so forth are also known. Generally, more than 12 different smectic phases have been identified (examples – see Figure 20).

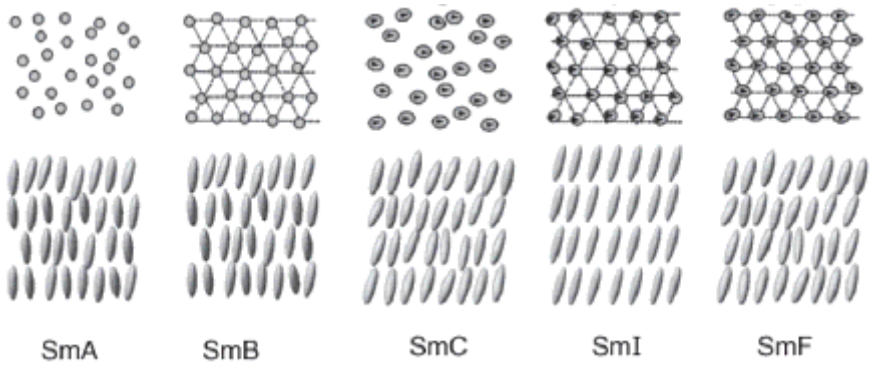

Figure 20. Aggregate structures illustrated with side and top views in various smectic phases. [33]

Smectics with some degree of the tilt of molecules, additionally, can have its "twisted" versions, with helical arrangement of a director. As with the nematic phase, a chiral version of smectic C phase has been observed and is denoted SmC*. In this phase, the director rotates around cone generated by the tilt angle. However, if the helix is unwound by the external force (such as electric fields) so that it becomes infinity, the phase becomes ferroelectric. If there is an alternation in polarization direction between layers, the phase can be ferrielectric or antiferroelectric.

2.3.3. Liquid crystals/polymers mixtures

Mixtures of the polymer and liquid crystals may be classified into two groups, depending on concentration ratio. If the concentration is greater than 20% by weight, we obtain a system, in which liquid crystalline domains are dispersed in a polymer matrix (Figure 21a). System of such properties is called Polymer Dispersed Liquid Crystal – PDLC. However, if the concentration is lower than 10% by weight, we have a system, in which the stabilizes the liquid crystal phase (Figure 21b). Such system is known as Polymer Stabilized Liquid Crystals - PSLC.

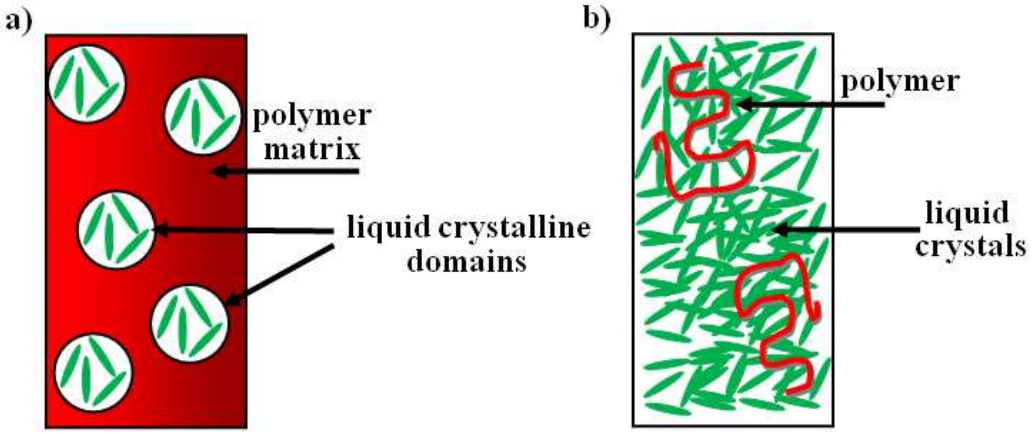

Figure 21. a) Polymer Dispersed Liquid Crystal – PDLC **b)** Polymer Stabilized Liquid Crystal – PSLC.

Exemplary phase diagram for a polymer/liquid crystal mixture is shown in the Figure 22. Region 1 on the diagram is a stable area of one homogeneous phase occurrence. In region 2, mixture is unstable and phase separation into two phases occurs. In region 2', between the spinodal and binodal curves, we also observe the homogeneous phase, but in the metastable state.

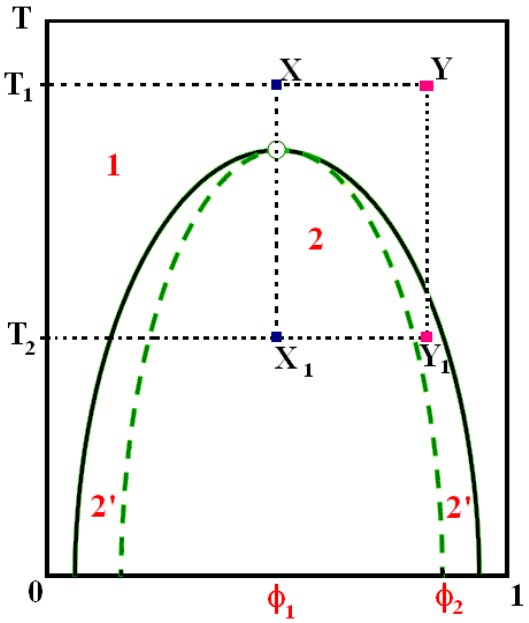

Figure 22. Exemplary phase diagram for polymer/liquid crystal mixtures with upper critical solution temperature. The solid line represents binodal curve and the dashed line spinodal curve.

Certain regions are separated from each other by curves. Solid line is called coexistence curve or binodal curve. Above this curve, the mixture is homogenous, in the stable state. Dashed green line is known as a spinodal curve. Between binodal and spinodal curves, the mixture is in the metastable state and may (but does not have to) separate into two phases. Below spinodal curve, the mixture is unstable and separation always occurs.

Dynamics of phase separation can be divided into two category: the nucleation and growth; and spinodal decomposition (Figure 23).

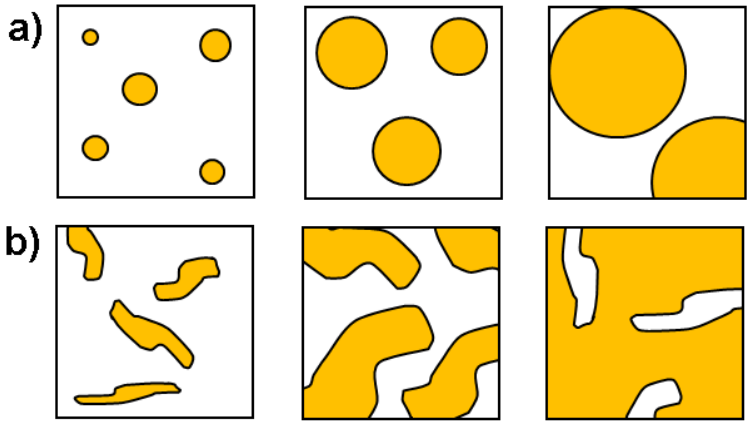

Figure 23. Schematic of structures observed in the early stage of phase separation in a polymer/liquid crystal mixtures by **a)** nucleation and growth **b)** spinodal decomposition.

If reduction of a temperature (X - X_1) forces a separation of a mixture of a composition φ_1 (Figure 22), the separation will occur through the spinodal decomposition mechanism. However if we reduce temperature (Y - Y_1) of mixture of a composition φ_2, the separation mechanism will be the nucleation and growth.

2.4. Fundamental concepts of experimental methods

2.4.1. Light scattering phenomena

Light is commonly known as visible part of electromagnetic radiation to which the human eye is sensitive. The wavelength of visible light ranges from 400nm (violet) to 750nm (red) and each wavelength between this range is perceived to correspond to a different color. In science, the term light comprises adjacent radiation regions of ultraviolet (10nm – 400nm) and infrared (750nm - 300μm) not visible to human eye.[34,35]

To describe the interaction of light with matter, it is essential to consider that light has both particle-like and wave-like character. As a wave, light has wave-like properties such as frequency, wavelength, interference, and as a particle, light has particle-like properties i.e. consists of quanta of light with well defined momentum and energy (photons). Treating light within the classical wave picture (Figure 24), is a simple way to understand the origin of phenomenon of light scattering.

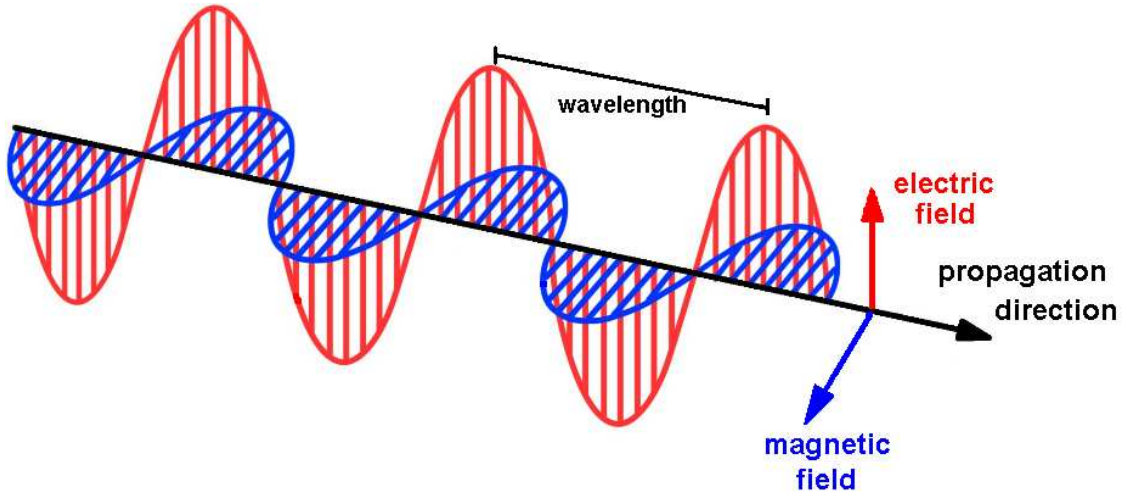

Figure 24. Electromagnetic waves are formed when an electric field (red color) couples with a magnetic field (blue color). The magnetic and electric fields of an electromagnetic wave are perpendicular to each other and to the direction of propagation of the wave.

All matter consists of atoms, which themselves are built from negative and positive charges. When the oscillating electric field of electromagnetic radiation interacts with the electrons in a particle, the particle constitutes an oscillating dipole or electric oscillator. The oscillating dipole moment develops with a magnitude proportional to the polarizability of the particle, that is, ability to shift charges within particle. This oscillating dipole acts as an emitter of an electromagnetic wave of the same wavelength as the incident one. The wave is emitted isotropically in all directions (Figure 25). This is the simplest description of the process called the elastic light scattering – ELS. The term elastic refers to the fact that the incident and scattered photons have the same frequency and hence the same energy. In ELS, the scattering signal which is detected is the time-averaged light intensity, thus its frequency deviation from the incident light is usually not measured.

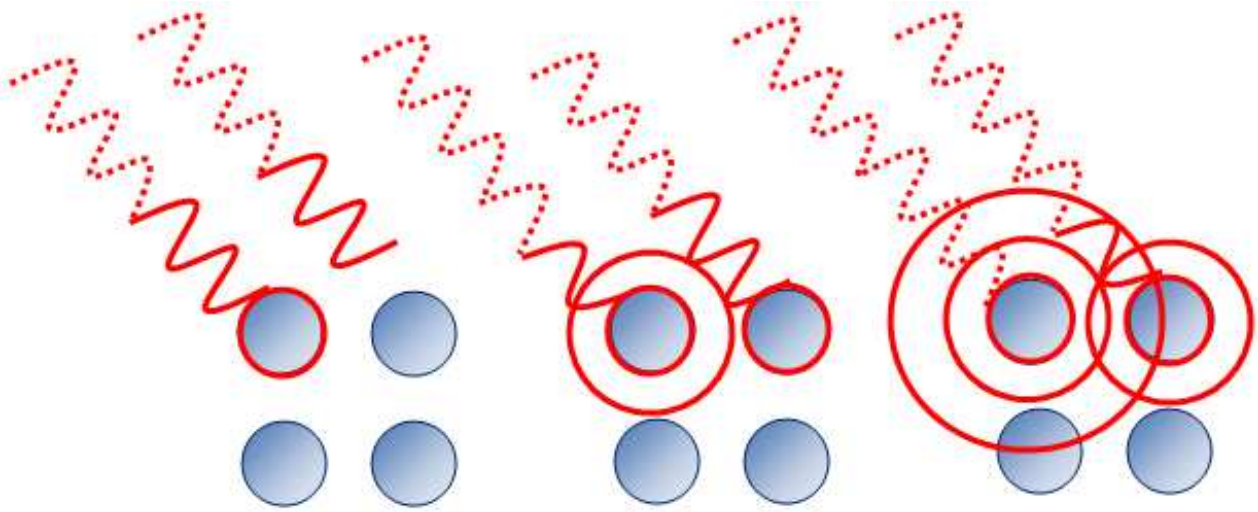

Figure 25. Interference pattern of light scattered from particles.

However not always frequency of emitted waves remains the same, hence quasi–elastic (QELS) or inelastic light scattering (IELS) can be distinguished. In QELS, the frequency of scattered light is slightly different from that of the incident light (from a few Hz to a few hundred Hz). These frequency differences come from the translational and rotational motions

of the particles and its value, is directly related to the particles' motions. In IELS, the scattered frequency differs by the amount much larger than few hundred Hz from that of the incident light. Such big difference is caused by involvement of other forms of energy, such as the vibrational and rotational energy of particles, for example in Raman scattering.[35]

It is worth mentioning, that scattering is only observed if the medium is inhomogeneous, as in an imperfect crystal or a solution of macromolecules. When a material is in itself heterogeneous, either due to local density fluctuations in the pure material or due to the presence of dispersed particle in the medium, radiation is scattered into all direction as well. If the medium is perfectly homogeneous, as in perfect crystal, the radiation scattered by individual molecules interferes destructively in all directions, except the direction of propagation of the incident radiation.[35,36]

Classical light scattering theory was derived in 1871 by Lord Rayleigh[37] and now is called the Rayleigh theory. By the Rayleigh scattering we mean scattering of light by particles with diameters much smaller than the wavelength of the incident radiation ($d << \lambda$, usually taken to be $d < \lambda/20$). In the regime of the Rayleigh scattering, the scattering intensity is inversely proportional to the fourth power of the wavelength, so shorter wavelength radiation is scattered more intensely than longer wavelengths. Moreover, the light scattering intensity depends on the scattering angle, θ.[34,35,38] Shape of scattering intensity as a function of scattering angle is shown in Figure 26. The maximum scattering intensity is at $\theta = 0°$ and the minimum scattering intensity is at $\theta = 90°$. The origin of this effect is that the intensity of the electromagnetic wave emitted by an oscillating dipole is strongest perpendicular to the axis of its oscillation which corresponds to a scattering angle $\theta = 0°$. At $\theta = 90°$, the scattering intensity is almost zero since there is no scattering in the direction of dipole moment oscillations. For the Rayleigh scattering the scattering intensity for forward scattering is equal

to the intensity for back scattering at the corresponding angle. In other words, the scattering intensity at angle θ is equal to the scattering intensity at the angle 180 - θ.

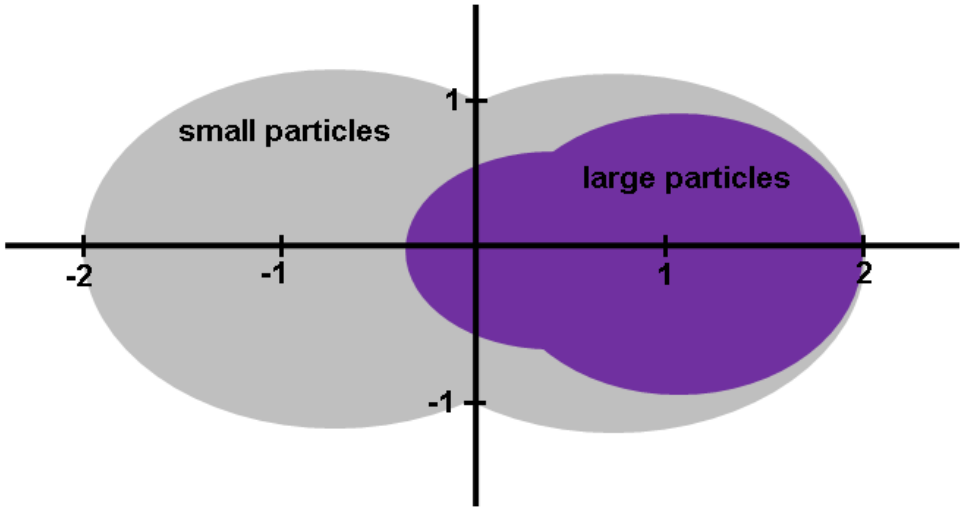

Figure 26. Shape of scattering intensity for both small particles (grey region) and large particles (violet region). The source of light is on the left side of the picture. The large particle scattering diagram shows asymmetry in scattering – the back scattering intensity is much reduced from the forward scattering intensity.

For molecules or particles smaller than the wavelength, but not too much, (i. e. $d < \lambda$, for size of the molecule at about one-tenth of the wavelength of incident radiation) we are in the Rayleigh – Debye – Gans regime and the analysis of the scattering is more complicated. The dimension of particle is larger than that, which can be treated as a single dipole, so the approach is to treat the particle as several of these oscillating dipole within one given particle. Each of these scattering elements gives rise to Rayleigh scattering independent of other scattering elements in the particle. Scattering in a given direction from all these elements results in interference, because of different locations of these elements in the particle. Light scattering from different parts of the particle will reach the detector by traveling different path lengths and these difference in path lengths can lead to destructive interference that reduces the intensity of the scattered light. Accordingly, interference of the scattered light emitted from such particle leads to nonisotropic angular dependence of the scattered light intensity.

The net effect is that the scattering diagram for large particles is reduced in intensity from the scattering diagram for small particles (Figure 26). At $\theta = 0°$, the path lengths will always be identical and there will be no destructive interference. At θ not equal to zero there will be destructive interference. As θ increases, the destructive interference will increase reaching a maximum at $\theta = 180°$. The back scattering intensity is much reduced from the forward scattering intensity as is presented in Figure 26. Universally, the scattering intensity in light scattering experiments is described as follows:

$$I(q) = P(q)S(q) \tag{17}$$

where *I(q)* is total scattering intensity, *P(q)* is particle form factor describing scattering from a single particle and *S(q)* is the structure factor. *S(q)* describes interferences between light scattered from different particles and can be neglected for very diluted solutions. To describe a large particle size effect, a function called particle form factor, $P(q)$, is defined. The form factor takes into account the interference pattern of intraparticular scattered light and is characteristic for size and shape of the scattering particles. When the molecule is much smaller than the wavelength of incident radiation (Rayleigh regime) then $P(q) \approx 1$ and particle form factor can be neglected. Particle form factor is determined for dilute solutions, when $S(q) = 1$. We know that there is no effect at zero angle scattering that $P(q) = 1$ and $P(q) < 1$ for all other θ, because destructive interference can only cause a reduction in intensity. The large effect on back scattering than on forward scatter means that $P(\theta < 90) > P(180 - \theta)$.

P(q) is characteristic for size and shape of the scattering particle. As a consequence, it provides the quantitative means for the characterization of particle in very diluted solution ($S(q) \approx 1$). In this case, the detected scattered intensity will depend on total number of scattering centers in a particle proportional to the mass of the particle.

2.4.1.1. Static Light Scattering

In Static Light Scattering (SLS), the scattering signal, which is detected, is the time-averaged light intensity. The SLS experiment may be described as elastic light scattering, thus frequency deviation from the incident light is often not measured. The intensity of scattered light is a function of the optical properties of the particles and the medium, the dimension and mass of the particles, sample concentration and observation angle and distance.[35]

Figure 27 shows a scheme of instrumentation used for static light scattering. The light from a laser impinges on the sample and, as a result, the incident beam is scattered. The scattered beam follows toward detector where intensity of scattered light is measured. Figure 27 also defines the scattering wavevector, $\vec{q}$. The wavevector, $\vec{q}$, provides a quantitative measure for the length scale of the static light scattering experiment. The wavevector is experimentally determined by the scattering angle θ and the wavelength of the laser light λ. Figure 27 shows how the value of $\vec{q}$ is derived from a given scattering geometry. $\vec{q}_{\text{in}}$ and $\vec{q}_{\text{out}}$ are the wavevectors of the incident and of the scattered light beam, respectively. The scattering wavevector $\vec{q}$ is a difference between the two wavevectors, i.e. $\vec{q} = \vec{q}_{out} - \vec{q}_{in}$. For an elastic scattering process, $|\vec{q}_{in}| = |\vec{q}_{out}| = \frac{2\pi}{\lambda}$, and therefore:

$$|\vec{q}| = q = \frac{4\pi \cdot n}{\lambda} \sin\left(\frac{\theta}{2}\right) \tag{18}$$

where *n* is the refractive index of the sample itself, which has to be taken into account since it changes the wavelength of the incident light compared to its value in air.[34]

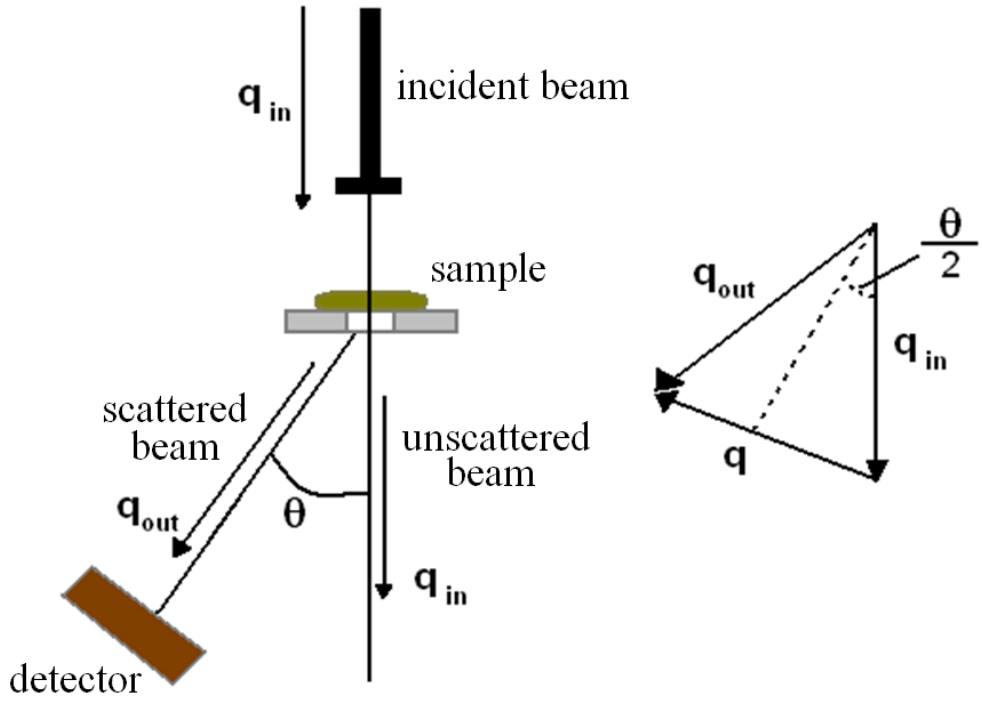

Figure 27. Scheme of instrumentation used for static light scattering.

Scattering is due to the inhomogeneity of the index of refraction. When the phase separation process occurs, different phases are characterized by different indices of refraction. For this reason, I used SLS to investigate kinetics and dynamics of phase separation processes.

2.4.1.2. Dynamic Light Scattering

Particles in solution exhibit a random motion (Brownian motion) caused by thermal density fluctuations of the solvent. As a consequence of the temporal changes in interparticle positions, the interference pattern and the resulting scattered intensity detected at given angle also change with time (Figure 28).

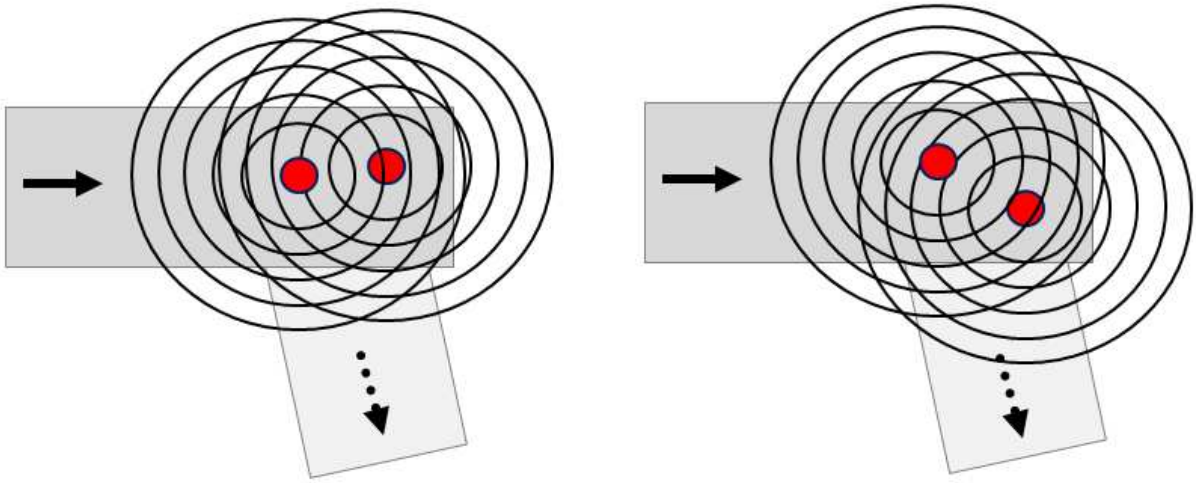

Figure 28. Sketch of the change in the interference pattern of scattered intensity with time. Resulting scattered intensity detected at given angle also change with time, reflecting the Brownian motion.[34]

This phenomenon provides the basis for the Dynamic Light Scattering (DLS), an experimental procedure which yields a quantitative measure for the mobility of scattering particles in solution as characterized by their selfdiffusion coefficient.[34] Dynamic Light Scattering technique is also known as quasi-elastic light scattering (QELS) or Photon Correlation Spectroscopy (PCS), because the frequency of scattered light is slightly different from that of the incident light. These frequency differences come from the translational and rotational motions of the particles and their value is directly related to the particles motions.

Fluctuations in light scattering intensity depend on the diffusion coefficient, D, which is a measure of the rate of molecular motion and is given by the Stokes – Sutherland - Einstein relation:

$$D = \frac{k_B T}{f} \tag{19}$$

where k_B is a Boltzmann constant, T is temperature and f is a frictional coefficient. For a spherical particle of radius R in a solvent of viscosity η, the frictional coefficient is given by Stokes's relation:

$$f = 6\pi\eta R \tag{20}$$

To quantitatively analyze the particle diffusion by light scattering, it is helpful to express the scattering intensity fluctuations in terms of correlation functions. The method is shown in Figure 29.

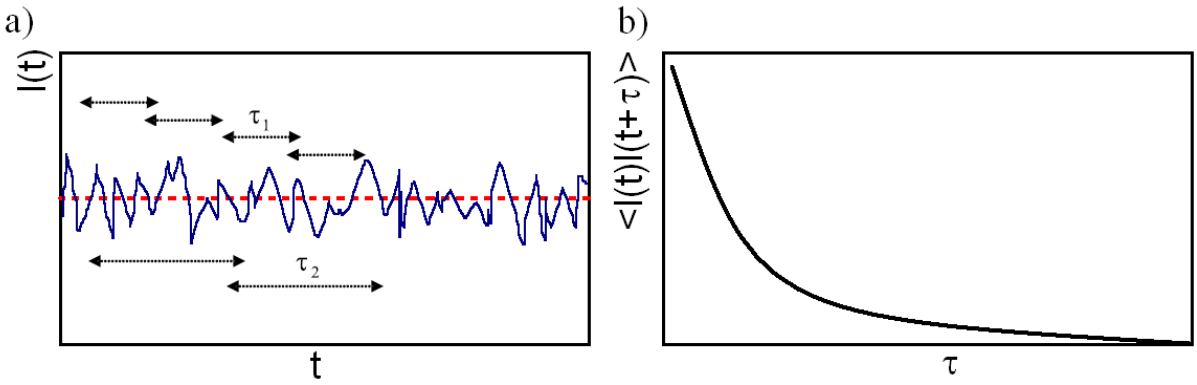

Figure 29. Principle of DLS technique. **a)** The average scattered intensity is indicated by the dotted red line (measured in static light scattering) and the detailed analysis of the fluctuating intensity is indicated by solid blue line (measured in dynamic light scattering). **b)** The fluctuation pattern is translated into the intensity autocorrelation function.

In DLS we measure time – dependent fluctuation in the scattering intensity $I(t)$ (Figure 29a – dark blue solid line). The signal looks very noisy and a way to extract some information is to calculate the autocorrelation function, $g_1(q,\tau)$ (Figure 29b). The autocorrelation function of a random process describes the correlation between the process at different points in time. In

DLS, the time-dependent scattered intensity is multiplied by itself after it has been shifted by an internal distance τ in time.

$$g_1(q,\tau) = < I(q,t) I(q,t+\tau) > \quad (21)$$

For monodisperse samples, $g_1(q,\tau)$ is a single exponential ($g(q,\tau)=A\exp(-2\tau/\tau_0)$) with decay rate $\Gamma = Dq^2$ (or relaxation time $(Dq^2)^{-1}$). In other words, by measuring how long it takes for the autocorrelation function to go to zero, we can tell how fast the particles are moving. The decay rate provides translational diffusion coefficients. From them the hydrodynamic radius of the constituent particles can be obtained by using the Stokes – Sutherland – Einstein equation. Moreover, by determining the diffusion coefficient, we can obtain information about dynamic properties of particles such as conformation of macromolecular chains, crystallization processes, micellization or aggregation. DLS has truly become a mature and popular technique for probing the dynamic properties of particulate materials either in solution or in suspensions.

2.4.2. Imaging techniques

Microscopes are devices designed to magnify visual or photographic images. The aim is to observe details that human eye is not able to see. The microscope must fulfill three tasks: produce a magnified image of the sample, separate the details in the image, and make them visible to the human eye or camera. This group of instruments not only consists of multiple-lens designs, but also very simple single lens instruments that are often hand-held, such as a loupe or magnifying glass.[39]

Microscopes can be divided into several different types. One classification relies upon what interacts with the specimen to produce the image. It can be: light (optical microscopes), electrons (electron microscopes) or a probe (scanning probe

microscopes). Another grouping is based on whether microscopes analyse the specimen via a scanning point (confocal optical microscopes, scanning electron microscopes and scanning probe microscopes) or analyse whole sample straight away (wide field optical microscope and transmission electron microscopes). The development of microscopy revolutionized biology and still remains a key technique in the life and physical sciences. During my Ph. D. research I used optical microscope, which I describe more precisely in next chapter.

2.4.2.1. Optical Microscopy

First optical microscopes (OM) were designed around 1600. The optical microscope is a kind of microscope that uses visible light, therefore it is usually called as the light microscope. The light microscope is a simple instrument, being essentially an extension of our own eyes. It magnifies small objects, enabling us to directly view structures that are below the resolving power of the human eye (100 μm).[40]

The light microscope is in principle a simple lens system for magnifying small objects. The first lens is called the objective and creates an image of the object in the intermediate image plan (Figure 30). This intermediate image can be looked at with another lens, called the eyepiece, which can provide further magnification.[41,42]

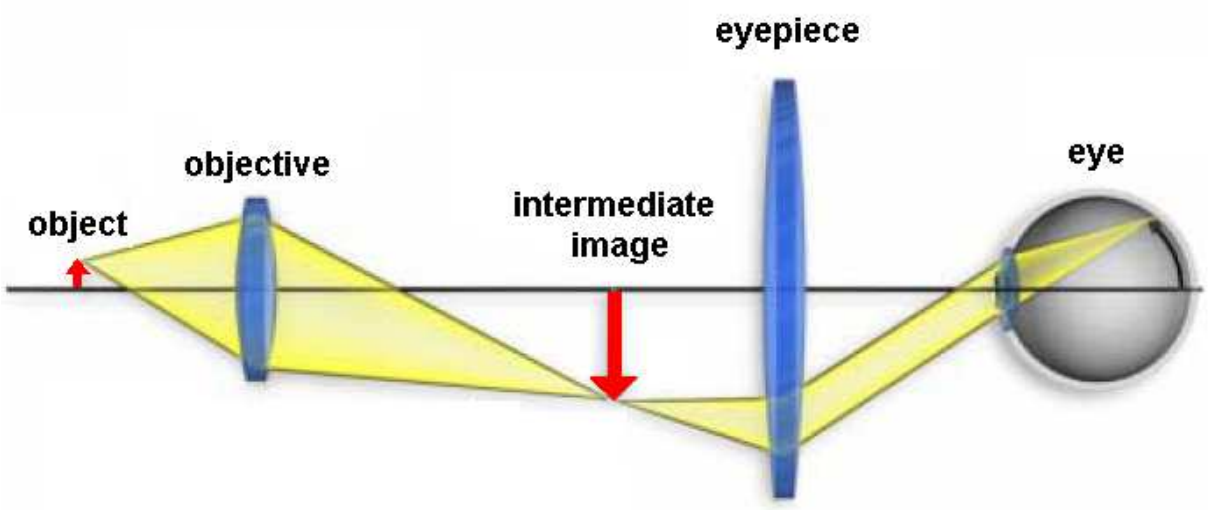

Figure 30. Principle scheme of an optical microscope, based on Davidson and Abramowitz.[42]

By using more lenses microscopes, we can provide further magnification, but it does not always mean that more details can be seen. The amount of detail depends on the resolving power of a microscope, which is the smallest separation at which two separate objects can be distinguished (or resolved). The resolution of an optical microscope is defined as the shortest distance between two points on a specimen that can still be distinguished by the observer or camera system as separate entities. The classic Rayleigh equation[42] describing resolution is given by:

$$d_{\min} = 1.22\frac{\lambda}{2NA} \tag{22}$$

where $d_{\min}$ is a space between two adjacent particles (still allowing the particles to be perceived as separate), λ is the wavelength of illumination, and NA is the numerical aperture of the objective. NA depends on refractive index of the medium between the cover glass and the objective front lens and advantageous high value of NA can be obtained only by using oil-immersion objectives.

In order to improve specimen contrast or highlight certain structures in a sample, some special techniques can be used. One of these techniques is polarized light microscopy, contrast – enhancing technique that improves the quality of the image obtained with birefringent materials.[43] The polarized light microscope is designed to observe specimens that are visible primarily due to their optically anisotropic character. Such microscope must be equipped with both a polarizer (positioned in the light path before the specimen) and an analyzer (a second polarizer) – Figure 31. Image contrast arises from the interaction of plane – polarized light with birefringent specimen to produce two individual wave components that are perpendicular to each other.

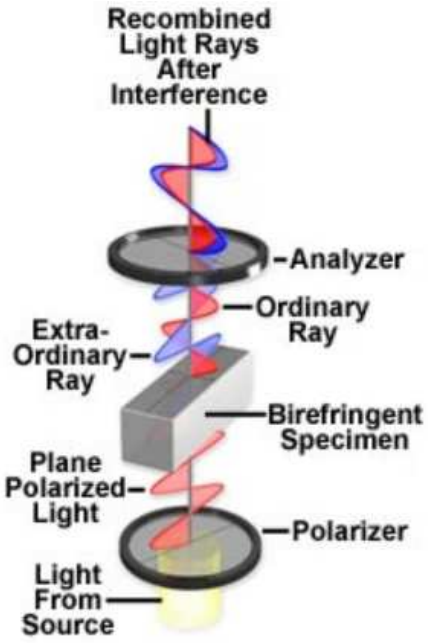

Figure 31. Scheme of polarized light microscope – figure from Nikon MicroscopyU web page.[43]

Polarized light microscopes have a high degree of sensitivity and can be used for quantitative and qualitative studies targeted at wide range of anisotropic specimens. This technique can be also utilized to distinguish between isotropic and anisotropic substances and reveals detailed information concerning the structure or composition of materials. Generally, the polarized light microscopy is an outstanding tool for chemistry, materials sciences, geology, biology, metallurgy and even medicine.

3. Results and discussion

The experimental part is divided into three main subsections: **3.1** *Diffusion of nano-particles in polymer solutions*, **3.2** *Diffusion of plasmid DNA in polymer solutions* and **3.3** *Ions motion in liquid crystal/polymer mixtures.* Every parts present dynamics of nano and micro objects in complex liquids but each from different point of view. In the first section I will analyze the diffusion of spherical nanoparticles in aqueous solutions of poly(ethylene glycol), PEG, covering a wide range of molecular masses of PEGs (M=3400 to 520 000), concentrations (0.1 to 50%) and viscosities (10^0 cP to 10^4 cP). In the second section I will focus on the diffusion and viscosity which is experienced by the biomolecules (plasmid DNA and restriction enzyme) in polymer solution. I will also analyze the influence of crowded environment on DNA cleavage by restriction enzyme in polymer solutions. The last subsection demonstrates what prospective application can have the motion of nano and micro objects in complex liquids. I show that free ions can be used to accelerate the phase separation process in the liquid crystal/polymer mixtures.

3.1. Diffusion of nano-particles in polymer solutions

This chapter is based on article entitled "Crossover regime for diffusion of nanoparticles in polyethylene glycol solutions: influence of depletion layer" (Natalia Ziębacz et al. Soft Matter 2011, DOI: 10.1039/C0SM01357A).

The viscosity in soft matter system is scale dependent quantity.[44,45] In polymer solutions the viscosity of nanoprobes of size R approaches the macroviscosity when R exceeds the radius of gyration of polymer, R_g. Hence, the nano to macroviscosity crossover occurs for $R \sim R_g$. In the following Chapter, I will analyze diffusion of nanoparticles in polymer solution in the crossover regime. I determine experimentally a relation of the diffusion coefficient of nano-particles to the nano-viscosity in polymer solutions, covering a range of two orders of magnitude of size ratios R/R_g and four orders of magnitude in the solution viscosity. In the crossover regime at $R \sim R_g$ I observe a scale dependent diffusion and explain the phenomenon by the simplified model of diffusion with and within the depletion layer - the layer around diffusing particle depleted from polymer chains.

3.1.1. Introduction

Small proteins and nano-particles diffuse surprisingly fast in living cells and in other high viscosity complex liquids.[46,47] Their diffusion coefficients are often orders of magnitude larger than expected from the Stokes-Sutherland-Einstein (SSE) relation and solution macroscopic viscosity, η_{macro}. These observations could not be explained on the basis of any single effective viscosity of complex liquids.[48]

The system of polyethylene glycol (PEG) solutions became a paradigm of soft matter system for the study of diffusion and mobility of nanoparticles. Following the work of Langevin and Rondelez,[49] Cheng et al.[50] showed that for nanoobjects of radius R smaller than the radius of gyration of the PEG polymer, $R<R_g$, the diffusion coefficient in PEG solution is given by:

$$\frac{D}{D_S} = \exp\left(-b\left(\frac{R}{\xi}\right)^a\right) \tag{23}$$

where a and b are two parameters of the order of 1, ξ is the blob size in the polymer solution and D_s is the diffusion coefficient in the solvent, given by the Stokes-Sutherland-Einstein equation:

$$D_S = \frac{k_B T}{6\pi\eta_S R} \tag{24}$$

where η_s is the viscosity of the solvent. The scaling relation given by equation (23) was originally proposed by de Gennes.[51] In the opposite limit $R>R_g$ it has been verified for different polymer systems[52-54] that the diffusion coefficient of nanoparticles is given by equation similar to the equation (23), but with the solution macroviscosity i.e.:

$$D = \frac{k_B T}{6\pi\eta_{\text{macro}} R} \tag{25}$$

In the recent paper[44] we established experimentally that diffusion coefficient of protein (lyzozyme) and fluorescent dye (5(6) – carboxy – tetramethylorodhamine) and their mobility in PEG solution satisfy the following relation:

$$\frac{D}{D_s} = \frac{\mu}{\mu_s} = \frac{\eta_s}{\eta} \tag{26}$$

D was determined from the fluorescence correlation spectroscopy measurements and μ, the electrophoretic mobility of the same probe, was determined independently from the capillary electrophoresis measurements (the subscript s describes to the diffusion or mobility

coefficients of same nanoparticles in the solvent). Equation (26) was also used as the definition of the viscosity η at the nanoscale. Additionally it was found[44] that for PEG solutions the macroscopic viscosity is described by the following relation:

$$\frac{\eta_{macro}}{\eta_s} = \exp\left(b\left(\frac{R_g}{2\xi} \right)^a \right) \tag{27}$$

with the same exponent *a* and parameter *b* as in equation (23). From equations (23), (25) and (27) it follows that the coefficient of viscosity depends on the length-scale at which it is probed. The viscosity η reaches η_{macro} for $2R$ approaching R_g and the diffusion coefficient of nanoparticles obeys the SSE equation,[53,54] but with scale dependent viscosity. Such crossover from nano to macroviscosity was earlier demonstrated experimentally for the solution of rigid elongated micelles made of hexaethylene-glycol-monododecyl-ether surfactants.[45] Summarizing, previous studies[44,45,49-54] concentrated mostly on two regimes $R>R_g$ or $R<<R_g$. In both regimes normal (scale-independent) diffusion was observed.[44,52-54] Here I focus my study on the crossover regime i.e. at $R\sim R_g$ and at $R>R_g$.

Weitz et al.[55,56] and Kang et al.[57] investigated systems which shared a common feature: $R\sim R_g$ e.g. R = 210 nm in a PEG solution of a molecular mass of 4M (R_g = 135 nm) or spheres of sizes 250 to 500 nm in the solution of the *fd* virus (size 880 nm). They observed a scale dependent diffusion coefficient and concluded that such systems depart from the SSE equation. Mason and Weitz assumed that diffusion occurs in a homogeneous medium and described the particle motion in terms of anomalous diffusion[56] and the special modification of the SSE equation involving its Laplace'a transform.[55] A competing description was developed by other groups[58-64] on the basis of the concept of depletion layer.[62,63] The depletion layer (Figure 32) is a layer surrounding particle which is depleted from polymer. The formation of the depletion layer around a particle in polymer solution has deep consequences for diffusion. The viscosity around the particle is non-uniform and changes

from solvent viscosity close to the particle to the macro-viscosity over a distance of the depletion layer i.e. tens of nanometers.

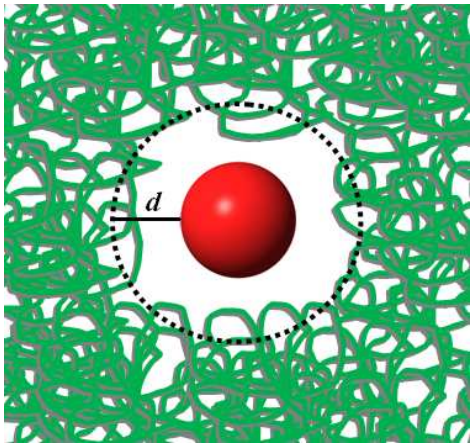

Figure 32. Schematic picture of a sphere in a polymer solution with a depletion layer of size *d*.

In the following Chapter, I show that the motion of particles in polymer solution can be approximated by two-scale diffusion in the crossover regime ($R \sim R_g$): fast diffusion of particle at small length scale inside the depletion layer and slow diffusion of the particle together with its depletion layer at large length-scale. I determine approximately, from the fit of very simple model to experimental data, i) the thickness of the depletion layer; ii) the diffusion coefficient of the fast diffusion; iii) the diffusion coefficient of the slow diffusion; and iv) the relation of the diffusion coefficient of the slow mode to the nano and macro-viscosity over a wide range of sizes and viscosities.

3.1.2. Materials and methods

3.1.2.1. Characterization of polymer solution

I used aqueous solutions of poly(ethylene glycol), PEG, covering a wide range of molecular masses (M=3400 to 520 000), concentrations (0.1 to 50%), viscosities (10^0 cP to 10^4 cP) and R/R_g (0.35 to 19.9). PEG polymers were purchased from Sigma Aldrich (PEG 6K, 20K, 35K, 600K, 2M, 8M) but their molecular masses, M, were determined using the Gel

Permeation Chromatography. As it can be seen in Figure 33b and Table 2, molecular masses determined from the GPC differ considerably from molecular masses given by Sigma Aldrich, hence in all calculations including *M*, I use number average molecular mass determined by GPC.

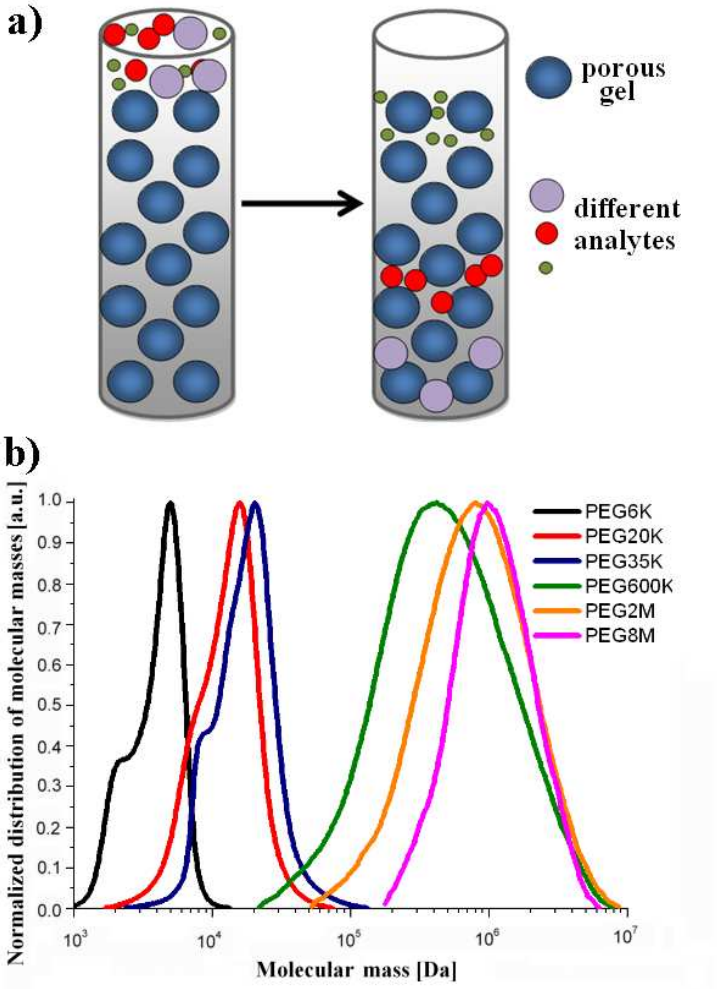

Figure 33. a) Gel permeation chromatography (GPC) technique separates analytes on the basis of size. The smaller analytes enter the pores more easily and therefore spend more time in these pores. Conversely, larger analytes spend little time in these pores, therefore are eluted more quickly. **b)** Molecular masses distribution profile (for PEG6K, 20K, 35K, 600K, 2M and 8M) determined from the gel permeation chromatography (GPC).

PEGs radius of gyration in water (Figure 34), as a function of M is given[65] by $R_g = 0.02M^{0.58}$ [nm] (this relation is specific for PEG polymers). The size of blobs (Figure 35), ξ, is a function of polymer concentration, c, and is given[51] by $\xi = R_g(c/c^*)^{-\beta}$, where c^* is the polymer concentration at which polymer chains start to overlap. The overlap concentration (Figure 36)

is given[51] by $c^* = M/(4/3\pi R_g^3 N_A)$, where N_A is the Avogadro's number. The exponent $\beta = 0.75$ guarantees that ξ does not depend on the molecular mass of the polymer.[51]

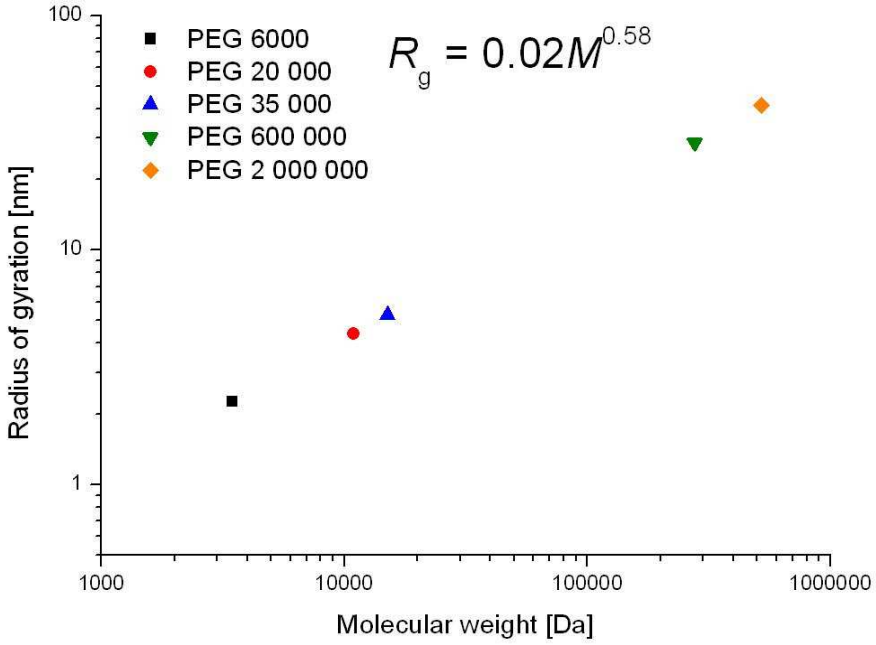

Figure 34. Radius of gyration for PEG in water as a function of molecular mass.

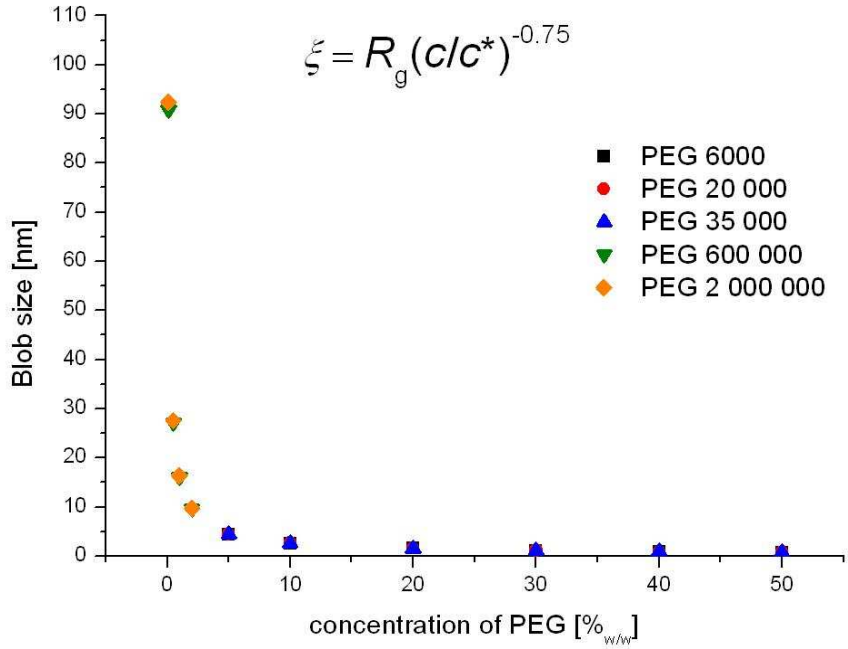

Figure 35. The size of a „blob" inside which all monomers belong to the same chains as a function of polymer concentration.

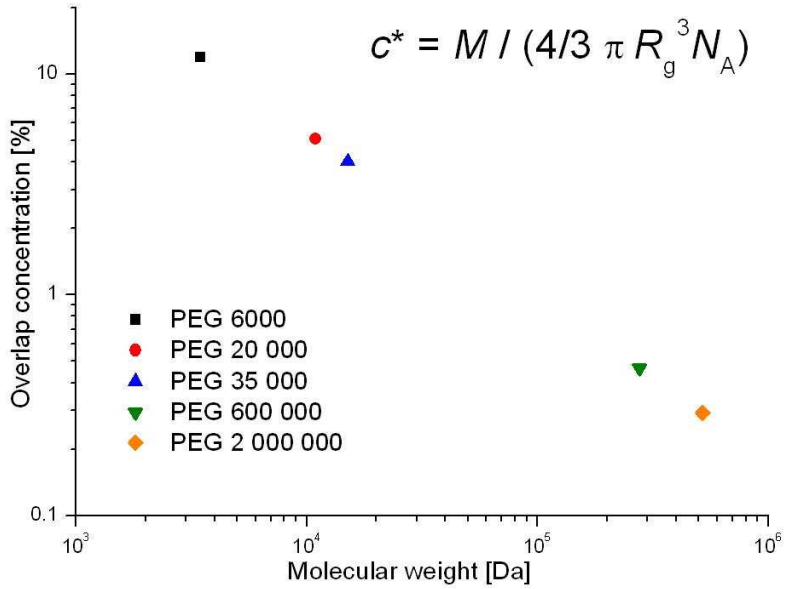

Figure 36. Concentration at which polymer chains start to overlap, *c**, as a function of molecular mass.

I also measured the macroscopic viscosity of the PEG solutions in the rheological experiments, using the Falling Ball Viscometer KF10 from RheoTec Messtechnik GmbH. The macroscopic viscosity is used further in the study of large particles in PEG solution ($R>R_g$). Data for η_{macro} as a function of polymer concentration is shown in Figure 37.

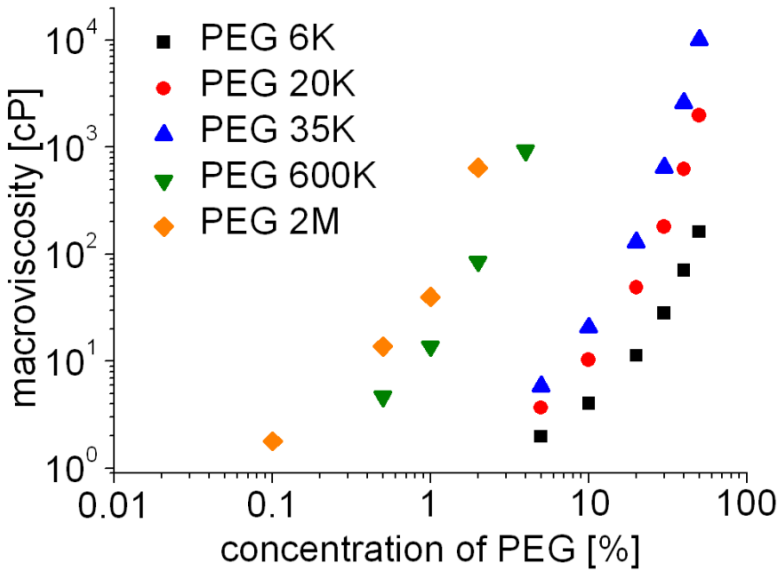

Figure 37. The macroviscosity of PEG solution for the following polymers (PEG6K, PEG20K, PEG 35K, PEG600K, PEG 2M) versus polymer weight fraction. Data measured using Falling Ball Viscometer.

As described in Introduction (page 47), in our previous work it was found[44] for PEG solutions the macroscopic viscosity is described by equation (27), so all macroscopic data should collapse on a single master curve given by this equation. Indeed, Figure 38 (relating η_{macro} to $R_g/2\xi$) confirms our previous results,[44] however I observed that the scaling is influenced by the polydispersity of polymer solutions.

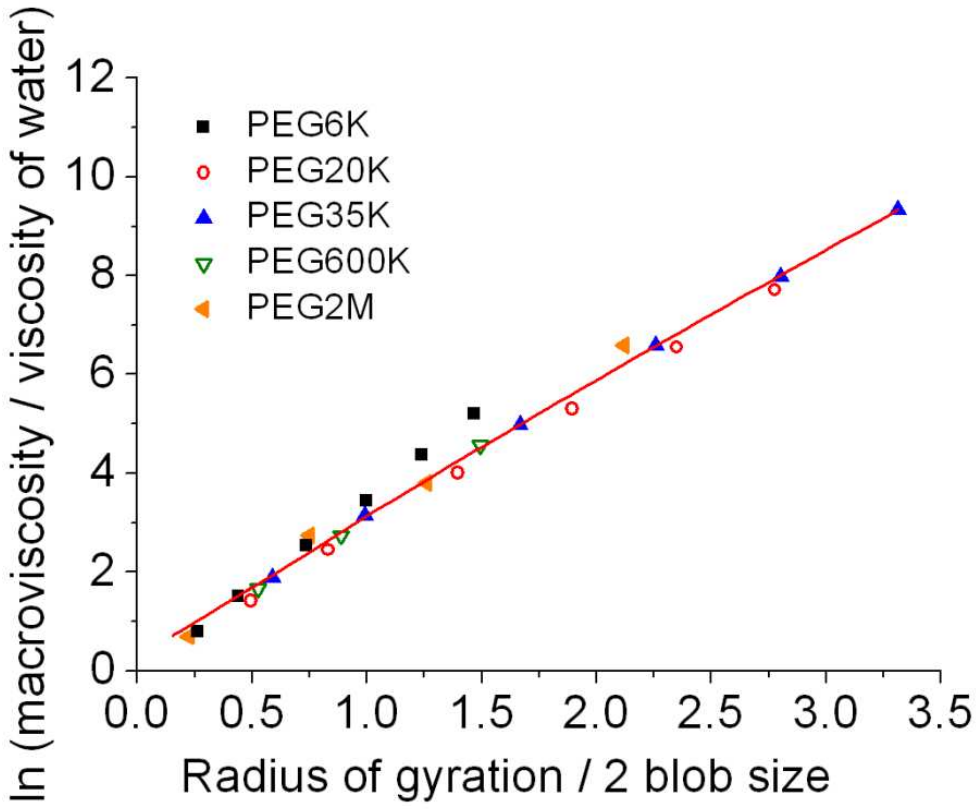

Figure 38. The normalized plot for the natural logarithm of macroviscosity of PEG solutions (see also Figure 37), $\ln(\eta_{macro}/\eta_s)$, as a function of $R_g/2\xi$ (equation (27)). R_g is the radius of gyration of polymer and ξ is the blob size. All data points collapse on a single master curve with a=0.9±0.2 and b= 3.0 ±0.50. The value of b depends on the definition of the blob size. Errors in a and b are most probably a consequence of the polydispersity in molecular masses of the polymer (Figure 33b). Macroviscosity is more sensitive to the fraction of high molecular mass polymers in a polymer batch.

I summarized all data necessary for polymer characterization in Table 2.

Table 2. Molecular masses, radius of gyration, overlap concentration, range of concentration and macroviscosity for different molecular mass PEGs.

	PEG6K	**PEG20K**	**PEG35K**	**PEG600K**	**PEG2M**	**PEG8M**
Number average molecular masses, M_N [Da]	3461	10944	15040	276872	521565	854096
Weight average molecular masses M_W[Da]	4151	14177	19369	778886	1110260	1286520
Polydispersity index PDI	1.20	1.30	1.29	2.81	2.13	1.51
Radius of gyration, R_g [nm]	2.26	4.40	5.29	28.68	41.41	55.12
Overlap concentration, c^* [%]	11.92	5.09	4.02	0.47	0.29	0.2
Concentration range [%]	5 - 50	5 - 50	5 - 50	0.5 - 2	0.1 - 2	0.1 – 1
Macroviscosity range at 25^0C, η_{macro} [cP]	1.9- 162.4	3.7-1993.5	5.9- 10103.2	4.7 - 85	1.8- 643.2	3 – 245.8

As nano-probes I used two types of Polystyrene (PS) spheres (Polysciences, Inc; Nanobead NIST Traceable Particle Size Standard) of average radius R = 10 and R = 45 nm with standard deviation less than 3%. They are packaged in convenient, easy to use dropper bottles at 1% solids (w/v) in an aqueous suspension. Diffusion coefficient of PS beads was determined using Dynamic Light Scattering and, as it is shown in Figure 39, the volume fraction of PS spheres till $2 \cdot 10^{-4}$ does not influence on diffusion coefficient. Hence, in all measurements done with PS beads, volume fraction of PS spheres was below $2 \cdot 10^{-4}$.

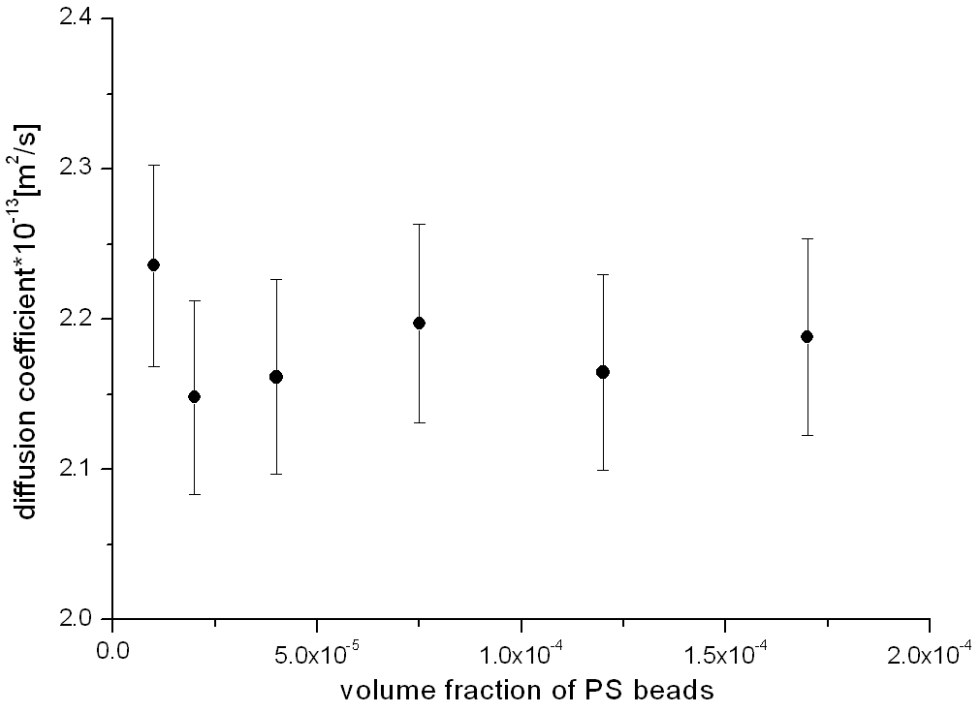

Figure 39. Diffusion coefficient of PS beads in 10% PEG 35 K solution versus concentration of the spheres. As it is shown the volume fraction of PS spheres till $2 \cdot 10^{-4}$ does not influence the diffusion coefficient.

3.1.2.2. Dynamic Light Scattering apparatus

I determined diffusion coefficients of the PS spheres in polymer solutions in Dynamic Light Scattering (DLS) experiments (Figure 40). These measurements were carried out using a BI-200SM Goniometer (Brookhaven Instruments Corp.) equipped with the Stabilite 2017 Argon ion laser (wavelength, λ=514.5 nm) at various angles, θ, from 30° to 150°. I measured the Fourier transform of the intensity-intensity correlation function $g(q,\tau)$ as a function of the scattering wave vector, q:

$$q = \frac{4\pi n}{\lambda} \sin\frac{\theta}{2} \tag{28}$$

and time τ. All measurements were carried out at 25°C.

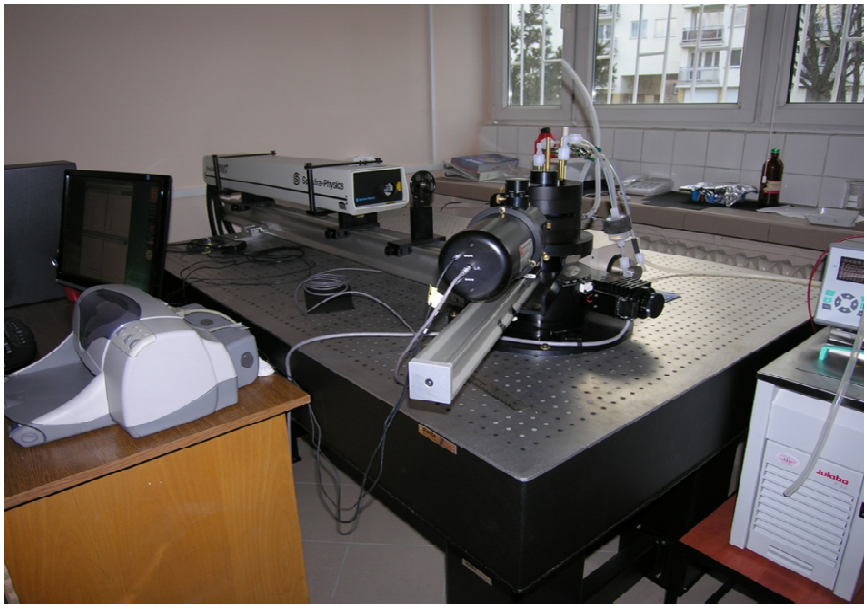

Figure 40. The dynamic light scattering apparatus, standing in our laboratory.

I also used standard Abbe refractometer (manufactured by Carl-Zeiss, Germany) to measure index of refraction *n* of polymer solutions (Figure 41). As it is seen the refractive index does not depend on molecular mass of polymer, as it was expected.

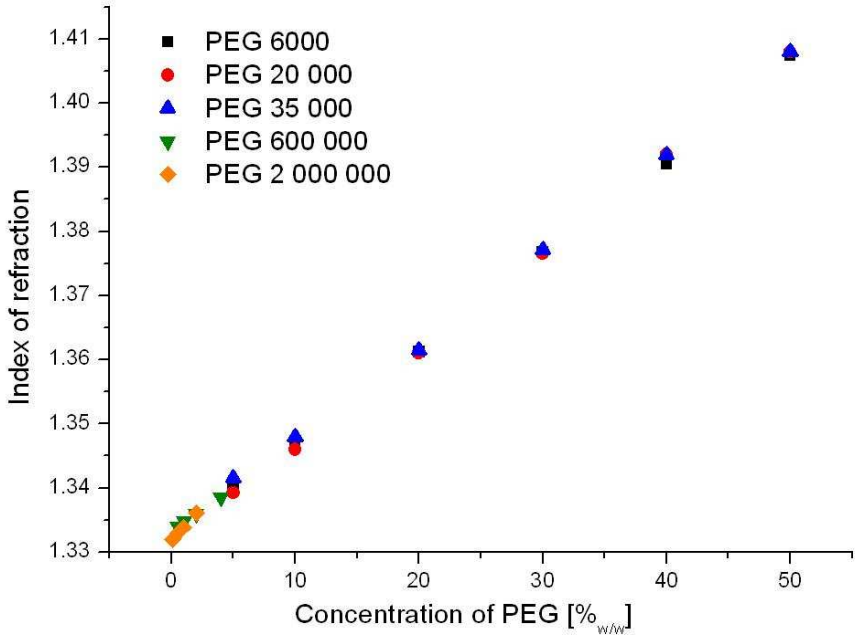

Figure 41. Index of refraction as a function of polymer concentration. Index of refraction was measured using the Abbe refractometer.

3.1.3. Experimental results

3.1.3.1. Results for $R > R_g$

When radius of the probe, R is much bigger than the radius of gyration of the polymer R_g, (Figure 42a) the depletion layer is much smaller than R and therefore can be neglected. For volume fraction of PS spheres below $5 \cdot 10^{-7}$ the measured $g(q,\tau)$ has two well-separated decay modes. The fast decay time, τ_1, is 3 orders of magnitude smaller than the slow decay time, τ_0, and does not depend on PS spheres volume fraction. The fast decay mode in $g(\tau)$ reflect the dynamics of entangled polymer network. The slow decay mode comes from the dynamics of the PS spheres diffusing through this polymer network. For volume fraction of the PS spheres larger than 10^{-5} the signal from the PEG dynamics is no longer visible. The intensity – intensity autocorrelation function, in this case, is monoexponential i.e. $g(q,\tau)=A\exp(-2\tau/\tau_0)$ (Figure 42b) with the characteristic relaxation time $\tau_0 = 1/Dq^2$. D is the scale-independent diffusion coefficient of the PS spheres.

Using Dynamic Light Scattering technique, I measured the diffusion coefficient of the PS spheres in PEG 6K and PEG 35K solutions as a function of polymer concentration. These data were compared to equation (25), where the macroviscosity was determined using Falling Ball Viscometer (Figure 37). The experimental results shown in Figure 42c agree, as expected,[52-54] with the calculated diffusion coefficient from the Stokes – Sutherland – Einstein (SSE) equation (equation (25)) relating the diffusion coefficient of spheres to the macro-viscosity, η_{macro} of the polymer solution.

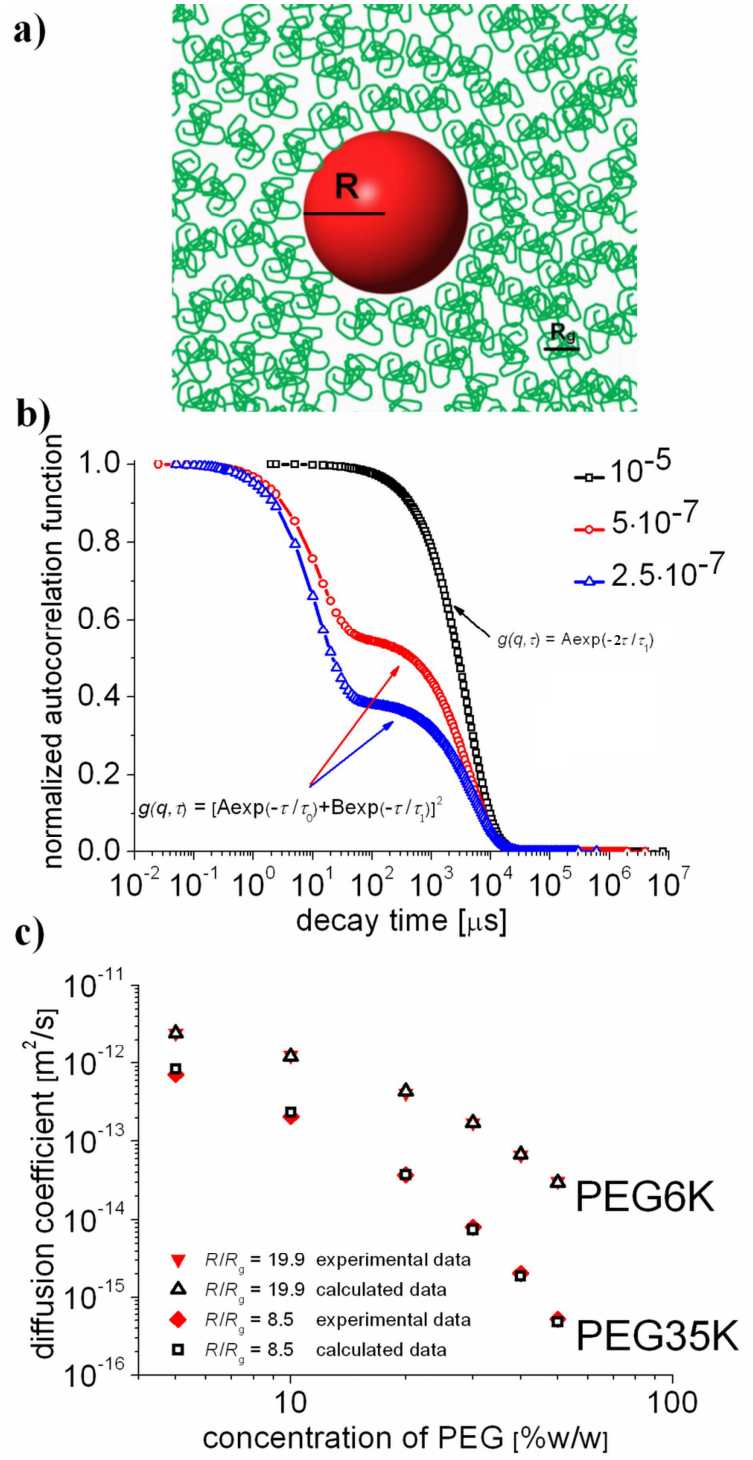

Figure 42. a) A schematic picture of a sphere in a polymer solution for $R>R_g$ i.e. with negligible depletion layer **b)** Typical intensity – intensity autocorrelation function, $g(q,\tau)$, as a function of time τ for PS spheres (R=45 nm) in 10%PEG35K/H_2O (R/R_g = 8.5) solutions at a scattering angle of 90° i.e. $q=(2\pi n/\lambda)\sqrt{2}$. For larger volume fraction of PS spheres (above 10^{-5}) the signal from the PS spheres is mono exponential with one decay time, τ_0, originating solely from the diffusion of PS spheres. Volume fractions of PS spheres are indicated on the plot. **c)** The diffusion coefficient of the PS spheres in PEG 6K and 35K solutions (measured using DLS) as a function of polymer concentration. These data were compared to equation (25). The macroviscosity in equation (25) was determined in separate rheological experiments (Figure 37). R/R_g = 19.9 corresponds to PEG6K and R=45nm, R/R_g = 8.5 corresponds to PEG35K and probe of R=45nm.

3.1.3.2. Results for $R \leq R_g$

When the radius of the probe, R, is comparable to the radius of gyration of polymer R_g, the signal originating from probe cannot cover the signal from polymer (in contrary to the previous case (for $R>R_g$) shown in Figure 42b). In this regime, the measured intensity-intensity autocorrelation function, $g(q,\tau)$, has two decay modes, and is described by a double exponential law within the whole range of wavenumbers (Figure 43). The fast decay time, τ_1, reflect the dynamics of entangled polymer network, while the slow decay mode, τ_0, comes from the dynamics of the PS spheres diffusing through this polymer network (Figure 43). I determined the signal from the polymer network in order to distinguish which characteristic relaxation time (in $g(q,\tau)$ with two decay modes) originate from the dynamics of the PEG polymers and which from the PS spheres. In my studies, I was interested only in the analysis of the slow relaxation time (originating from the PS spheres), given by $\tau_0 = 1/Dq^2$ (see also data on Figure 43). This slow relaxation time described the dynamics of the PS spheres in the PEG solution.

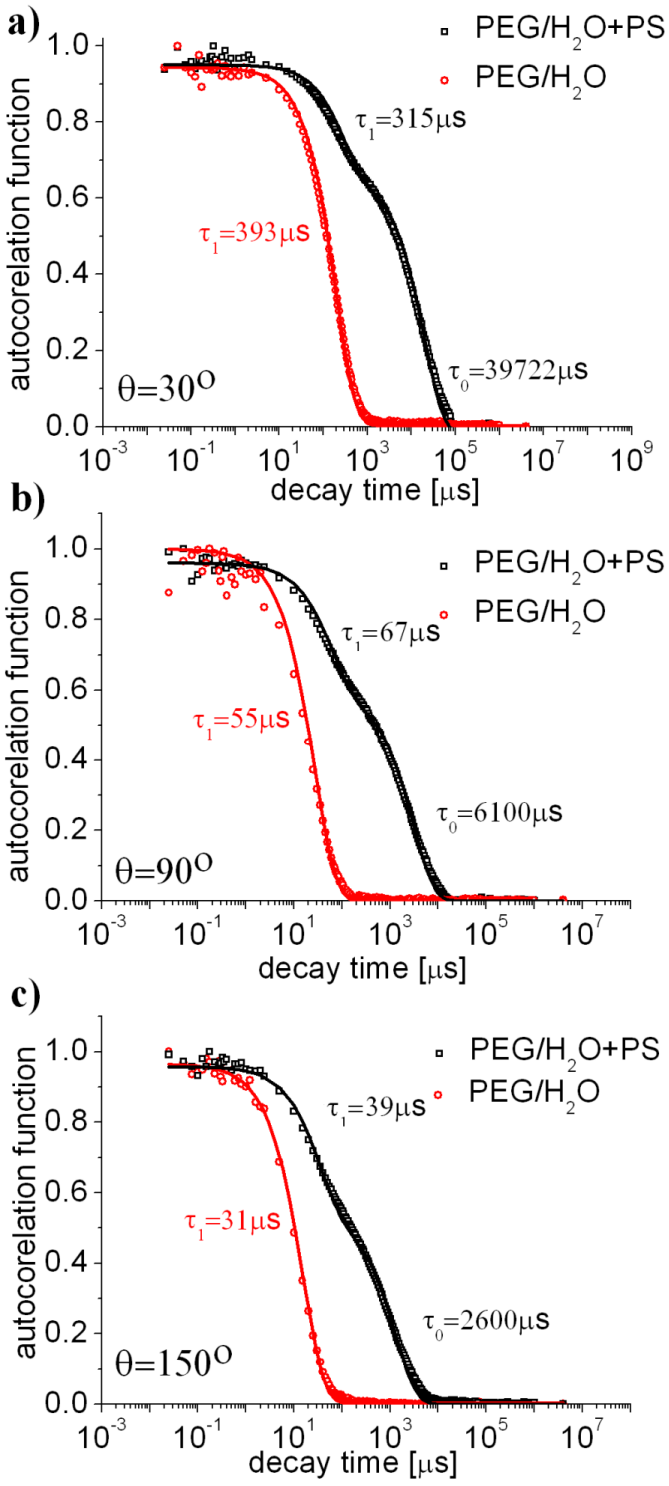

Figure 43. Experimental intensity-intensity autocorrelation function for 2%PEG600K/H_20 (red circles) and for 2%PEG600K/H_20+PS spheres (R=10 nm) (black circles) together with the exponential fit (solid lines red or black) (one component fit for the PEG solution given by the red line and two component fit for the PEG solution with PS spheres given by the black line)**.** The characteristic relaxation time, τ_1, for PEG polymers (red curve) is very close to the shorter characteristic time for the solution of PEG polymers with PS spheres (black curve). Further analysis of the dynamic light experiments in this case is unambiguous and the second relaxation time, τ_0, (black curve) is ascribed to the dynamics of the PS spheres in the PEG solution. Data obtained for the following scattering angles: **a)** θ=30° **b)** θ=90° **c)** θ=150°

For $R \leq R_g$ (R/R_g=1.1 and 0.35) the inverse of the decay time $1/\tau_0=Dq^2$ versus q^2 is not a straight line indicating that D depends on q (Figure 44b), contrary to the case of $R>R_g$ (exemplified on Figure 44b by R/R_g=2.3). I interpret this scale dependent diffusion as consequence of the formation of equilibrium depletion layer (Figure 44a) around PS spheres. Formation of this layer[62,63] is due to the entropy of polymer chains, which strongly (exponentially) decreases when a distance between the center of mass of a polymer and the surface of the sphere decreases below R_g. Macroscopic viscosity of the PEG solution is an exponential function of polymer concentration.[44] Therefore the viscosity around a sphere in polymer solution is non-uniform and decreases rapidly from the macroscopic value far from the sphere to the solvent value close to the surface of the sphere. I compare the model (presented in the following subsection) to the experimental results and determine: i) the size of the depletion layer (Figure 44c), ii) the diffusion coefficient inside the layer and iii) the long time diffusion coefficient of the particle together with its depletion layer (Figure 44d).

3.1.3.3. Simplified two scale diffusion model

The motion of a particle in polymer solution is characterized by an effective scale-dependent diffusion coefficient D_{eff}. The form of D_{eff} follows from the two-scale diffusion model: I consider a spherical particle of radius R trapped in a spherical cave of the radius $R_c > R$ (Figure 44a). Both the particle and the cave perform Brownian motion with the diffusion coefficient D_0 and D, respectively, with $D_0 > D$. The particle is reflected at the boundaries of the cave and the diffusion inside the cave does not affect the motion of the cave. Because the particle moves much faster inside the cave than the cave itself, I simplify the problem and divide the displacement r of the center of the particle into two parts: First the particle has to travel the distance $r-d$ confined in the cave with the diffusion coefficient D, and then diffuse

over the distance d within the cave with the diffusion coefficient D_0. The quantity $d = R_c - R$ is the size of the depletion layer (Figure 44a).

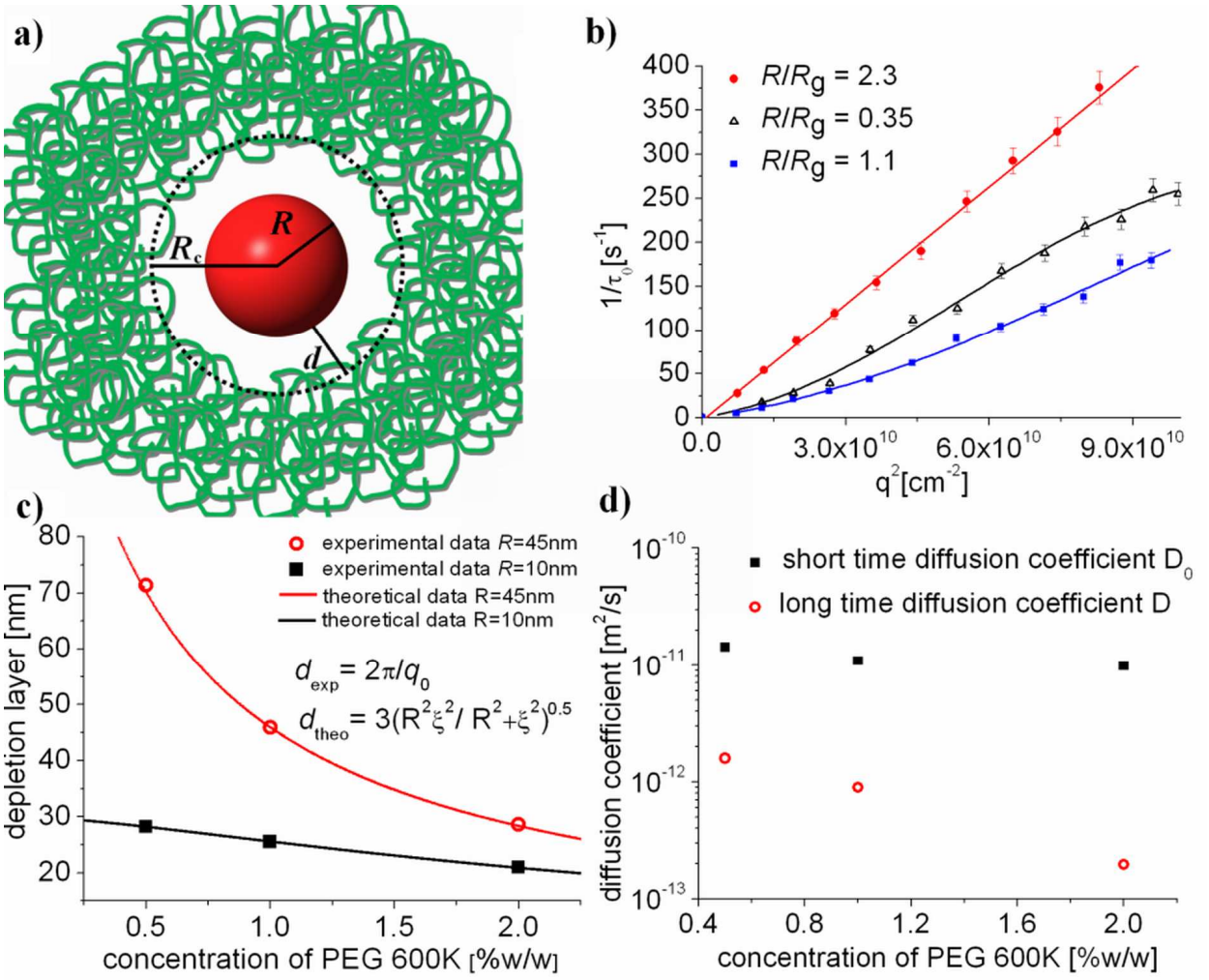

Figure 44. a) A schematic picture of a sphere in a polymer solution with a depletion layer. In the limit $R>R_g$ the size of the depletion layer can be neglected in comparison to R (Figure 42a). As shown in Figure 44b the depletion layer is negligible for R/R_g as small as 2.3 (PEG20K, R=10nm) **b)** The inverse of the relaxation time $1/\tau_0$, versus q^2 for three ratios of R/R_g: R/R_g=2.3 (PEG20K, R=10nm); R/R_g=1.1 (PEG2M, R=45nm); R/R_g=0.35 (PEG600K, R=10nm) plotted with the theoretical fit to equation (29). **c)** The depletion layer thickness d versus concentration of the PEG solution from the fit of equation (29) to the data (the fit is shown in Figure 44b). The solid line is the prediction of the theoretical model proposed by Fleer et al.[61] In this model d is related to the size of the probe R and the correlation length in the polymer solution ξ (see inset). **d)** Diffusion coefficients – D and D_0 – calculated from equation (29) for R/R_g = 0.35 (fit shown in Figure 44b).

The mean-squared displacements $\langle r^2 \rangle$, $\langle (r-d)^2 \rangle$, and $\langle d^2 \rangle$ are additive and obey the relation $\langle r^2 \rangle = \langle (r-d)^2 \rangle + \langle d^2 \rangle$. The characteristic diffusion time τ_r in which the particle travels over the distance r is a sum of two contributions $\tau_r = \tau_{r-d} + \tau_d$. The first contribution, $\tau_{r\text{-}d}$, is the characteristic time required for the cave to diffuse over the distance $r - d$ with diffusion coefficient D; the second contribution, τ_d, is the characteristic time in which the particle diffuse over the distance d with diffusion coefficient D_0. In terms of the wave vector, $q = 2\pi/r$, one has $\tau_r^{-1} = D_{eff}/r^2 = D_{eff}q^2/4\pi^2$. Therefore, the characteristic diffusion time and the characteristic relaxation time, τ_0, are linked by the following relation: $\tau_0^{-1} = 4\pi^2 \tau_r^{-1}$.

The two-scale diffusion model described above is valid provided that the particle travels over the distance that is bigger than the width of the depletion layer, that is, when $r > d$. Otherwise, the motion is characterized simply by the diffusion constant D_0 of the particle within the cave. In this case we have $\tau_0^{-1} = D_{eff}q^2$ with $D_{eff} = D_0$. Therefore, the characteristic relaxation time is given by the following conditional equation, which defines D_{eff} in terms of D and D_0:

$$\frac{1}{\tau_0} \approx \begin{cases} \dfrac{D_0 q^2}{\left(\dfrac{q}{q_0}\right)^2 + \beta\left(1 - \dfrac{q}{q_0}\right)^2} & \text{for } q < q_0 \\ D_0 q^2 & \text{for } q > q_0 \end{cases} \tag{29}$$

where $q_0 = 2\pi/d$ and $\beta = D_0/D$. In the limit $q/q_0 \to 0$ equation (29) reproduces the relation $\tau_0^{-1} = Dq^2$. This limit is achieved when the particle diffuses over a distance r much larger than the size R_c of the cave. Note that the limit $\beta \to \infty$ corresponds to the particle moving inside an immobilized cave. In this case the effective (apparent) diffusion coefficient of the particle tends to zero. As expected, in this limit, equation (29) yields infinitely large decay time corresponding to $D_{eff} \to 0$. The limit $\beta \to 0$ corresponds to the situation when the diffusion coefficient of the particle inside the cave is much smaller than that of the cave. This case

contradicts the assumption of presented model. This limit is also not correct from the physical point of view since we expect that the depletion layer is depleted from polymer, i.e., viscosity inside the depletion layer should be smaller than that of the bulk polymer solution.

It should also be noted, that in DLS experiment the largest $q^2 \sim 10^{11} cm^{-2}$, while the smallest $q_0^2 \sim 10^{12}$ cm^{-2} (see e.g. Figure 44bc). In order to probe in detail the regime $q > q_0$ I should use soft-x-rays dynamic light scattering technique which in principle works as DLS, but with soft-x-rays instead of light.[66] Unfortunately, I did not have the opportunity to perform such measurements.

From the fits shown in Figure 44b to equation (29) I obtain two diffusion coefficient D, D_0 and the size of the depletion layer $d = 2\pi/q_0$. The thickness of the depletion layer decreases with increase of concentration[61] and depends strongly on the size of the probe and the blob size ξ (Figure 44c). Fast diffusion occurring at small length scale inside the depletion layer, D_0, is much larger than the long scale diffusion coefficient, D (Figure 44d). Large ratios of D/D_0 are expected on the basis of the structure of the depletion layer (Figure 44a). On the basis of fit of equation (33) to the data shown in Figure 44b I calculate the characteristic decay time originating from the motion of the particles inside the cage using following formula: $\tau_d^{-1} = D_0 q^2$. For example, for 2%PEG600K/$H_2$0 and PS spheres of R = 10 nm, short time diffusion coefficient $D_0 = 9.8 \cdot 10^{-12}$ m^2/s (Figure 44d). Hence, for scattering angles $\theta = 30^o, 90^o, 150^o$ I obtain τ_d = 1428 µs, 192 µs, 102 µs, respectively. Calculated characteristic decay times are contained in range of decay times for intensity-intensity autocorrelation functions (Figure 43), as it was expected. This result suggest that ”inside” intensity-intensity autocorrelation functions I can find signal originating from long and short time scales. Additionally the relaxation times of the bulk PEG solution, also shown in Figure 43 is roughly 3 times shorter than the short relaxation time of PS spheres diffusing inside the depletion layer. The autocorrelation curves shown in Figure 43 are double-exponential with one

relaxation time characterizing pure polymer and the second relaxation time depending on the *q*-vector (equation (29)). Therefore a simple autocorrelation function based on the mean-square displacement in the real space cannot be directly used to fit the data (such function would show two characteristic times for spheres depending on the angle of scattering). More theoretical work is needed to develop full model of the two-scale diffusion and replace oversimplified equation (29).

In the final step, I analyzed the long scale diffusion coefficient, *D*, for all experimental cases i.e. for R/R_g from 0.35 to 19.9. The following analog of the Stokes-Sutherland-Einstein relation well represents all the data (see also equation (25)).

$$D = \frac{k_B T}{6\pi\eta(R+d)} \tag{30}$$

where the scale dependent viscosity is given by:

$$\eta = \eta_s \exp\left(b\left(\frac{R_{\text{eff}}}{2\xi}\right)^a\right), \qquad R_{eff} = \sqrt{\frac{R_g^2(2R+2d(\xi))^2}{R_g^2+(2R+2d(\xi))^2}} \tag{31}$$

where η_s is water viscosity. The form of R_{eff} as a function of the depletion layer size *d*, radius of the PS spheres *R* and the radius of gyration R_g was inspired by the theoretical model proposed by Fleer et al.[61] and additionally by the crossover which was established in our previous paper.[44] R_{eff} has a correct limiting behaviour for $R>R_g$ (equation (25) and also for $R<<R_g$ as given in Reference 44). However, it is not fully understood why in these equations we need to use the diameter of the sphere instead of its radius. The thickness of the depletion layer, $d(\xi)$, depends on polymer concentration via ξ. Theoretical thickness of depletion layer proposed by Fleer et al.[61] ($d_{\text{theo}} = 3(R^2\xi^2/R^2+\xi^2)^{0.5}$ – see also inset in Figure 44c) is in agreement with my experimental measurements (Figure 44c). Equations (30) and (31) describe the diffusion coefficient *D* for all *R* including quantitatively the regime $R\sim R_g$, where

the depletion layer with concentration dependent size $d(\xi)$ leads to the scale dependent diffusion (see Figure 44b). There are only two fitting parameters (a and b) in equations (27) and (31) and both should be of the order of unity. In Figure 45 I compared experimentally determined D with equation (30) and (31) and presented the data in the scaling form. Figure 45b shows D as a function of polymer concentration and Figure 45c is the scaling plot of D versus $R_{eff}/2\xi$, where all data fall onto a single curve for a=0.9±0.2 and b=3.0±0.50 same as in the limiting case of the macroscopic viscosity (see Figure 38).

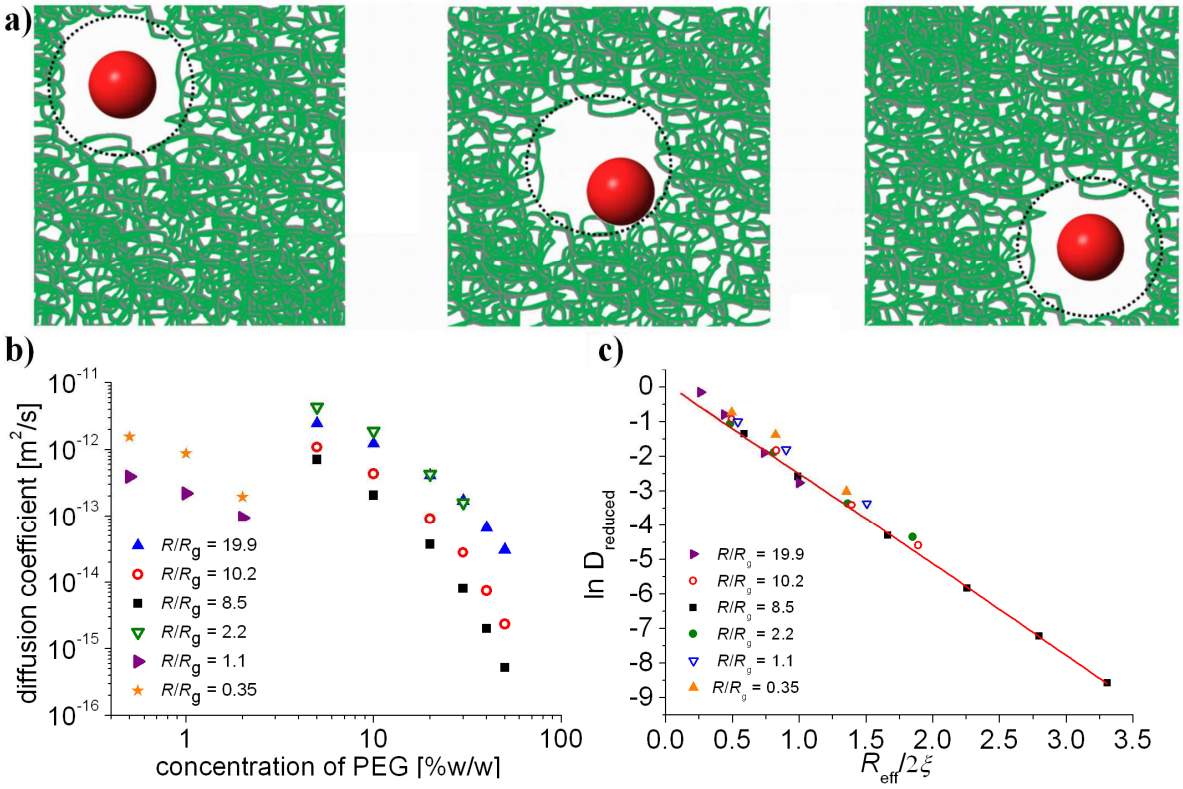

Figure 45. a) A schematic picture of a sphere diffusing in a polymer solution. Spherical particle is trapped in a spherical cave. The particle and the cave both perform Brownian motion. The particle is reflected at the boundaries of the cave and diffusion inside the cave does not affect the motion of the cave. This model represents a case when the particle together with the cave travel the distance much larger than the radius of the cave. The motion of the particle in the cave is characterized by the diffusion coefficient D_0 (fast diffusion) and the motion of the cave with a particle inside by the diffusion coefficient D (slow diffusion). The long time diffusion coefficient D obeys the equations (30) and (31) **b)** The diffusion coefficient, D, versus concentration of PEG polymer for different sizes of the particles and polymers (R/R_g is 0.35, 1.1, 2.3, 8.5, 10.2 and 19.9 **c)** Scaling of D versus $R_{eff}/2\xi$. All data collapse onto a single curve with a=0.9±0.2 and b=3.0±0.50. The long time dimensionless diffusion coefficient $D_{reduced}$ follows the scaling relation (equations (30) and (31)) i.e. $D_{reduced} = xD = f(y)$ where $x=[6\pi\eta_s(R+d)]/(k_BT)$, $y=R_{eff}/2\xi$ and f does depend neither on R nor on the molecular mass of the polymer. I covered in this study 4 orders of magnitude of the diffusion coefficients and two orders of magnitude of polymer concentration.

3.1.4. Conclusions

Equations (30), (31) and Figure 45 summarize results contained in this Chapter. The long time diffusion coefficient, *D*, is related quantitatively to the nano-viscosity and to the size of the depletion layer. The limiting case of this relation, i.e. for $R>R_g$, leads to the scaling plot of the macro-viscosity (Figure 38) in agreement with previous measurements of the motion of small dyes and proteins in polymer solutions.[44] I model the particles motion in polymer solution by two-scale diffusion (Figure 45a). This scale dependent diffusion is caused by the non-uniform viscosity, arising from the structure of the depletion layer, and should not be interpreted as anomalous diffusion.[67] The model used in this Chapter is certainly oversimplified and more work is needed in order to elucidate all aspects of this scale dependent diffusion and the role of the depletion layer in the motion of nanoparticles in the crossover regime. Also the effective radius R_{eff} in equation (31) is most certainly also a crude approximation, but its form is a good starting point for further theoretical studies. The detailed experimental study of the motion of PS spheres inside the depletion layer requires application of the soft-x rays dynamic light scattering technique.[66, 68]

Presented analysis can be applied in several distinct areas: in complex liquids the scaling plot of the macroviscosity can be used to characterize the material yielding pertinent length scales. Also the same macroscopic rheological measurements would provide information concerning transport at the nanoscale i.e. providing data (*a* and *b* parameters) for equations (27) and (31). The concept of nano-viscosity which depends on the scale of flow calls for the reinvestigation of the Navier-Stokes equations at the nanoscale i.e. below the characteristic crossover length scale. Furthermore biochemical reactions in a high viscosity complex liquids should be diffusion-limited and therefore according to the equations (27) and (31) should exponentially depend on reagents sizes. Additionally, rotations of reagents inside

depletion layer should be fast due to the local low viscosity[69] and as a result enhance reaction rate. Summarizing, presented results are pertinent to hydrodynamics at the nanoscale and biochemistry in a crowded environment.[70]

3.2. Diffusion of plasmid DNA in polymer solutions

This chapter is based on article entitled "Influence of nano-viscosity and depletion interactions on cleavage of DNA by enzymes in glycerol and poly(ethylene glycol) solutions: qualitative analysis" (Sen Hou, Natalia Ziębacz et al. Soft Matter 2011, 7, 3092 – 3099). Sen Hou performed biochemical reaction and used biochemist assays while my work was the analysis based on DLS experiments.

Biochemical reactions in living systems take place in an environment crowded by various macromolecules and ligands. Such environment strongly affects the dynamics of biomolecules in living cells, but not in an evident way. For example, the crowded environment, which is featured by large viscosity, does not always decrease diffusion coefficients of biomolecules appreciably, as we could expected from the Stokes – Sutherland – Einstein (SSE) equation. In the following Chapter, I present a qualitative study of diffusion of biomolecules in polymer and in low molecular mass agent solutions.

3.2.1. Introduction

Typical biochemical experiments done in buffers do not reflect *in vivo* conditions. In living cells, various macromolecules and lipids constitute up to 40% of the volume.[71,72] Consequently, biological reactions *in vivo* inevitably occur in a crowded environment.[73] Such environment strongly affects the stability of proteins,[74] the diffusion coefficient of biomolecules, the activity of enzymes,[75] and the association rate of proteins.[76] Biochemistry in a crowded environment *in vitro* is a new emerging field of research which might give an insight into biochemical reactions *in vivo*.[77] Many soft matter systems (e.g. polymer[70]) can

serve as paradigms of crowded environment mimicking the conditions inside of cells. In this Chapter, I present exactly such study, in which polymer solutions were used as crowding agents to mimic conditions in living cells.

I have used glycerol, poly(ethylene glycol) (PEG) 6000 and PEG 8 M solutions (polymer characterization - see Table 2 and Figure 33b) to investigate the influence of the crowded environment on cleavage of plasmid DNA by restriction enzyme HindIII. Restriction enzymes (restriction endonucleases) are enzymes that cleave DNA at specific nucleotide sequences. Such restriction enzyme bind to DNA at any position and then travel along the strand of DNA until they reach a recognition sequence. As a result, DNA molecule can be cut to produce two DNA fragments from one (see Figure 46).

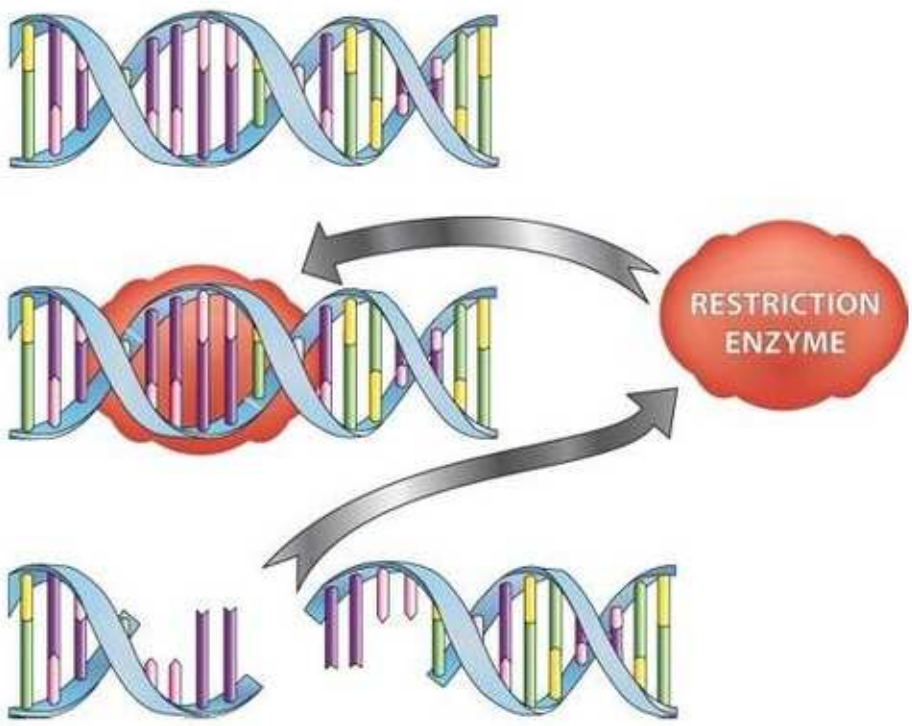

Figure 46. A restriction enzyme breaking both strands of DNA. Figure is taken from http://www.biotechlearn.org.nz/themes/dna_lab/images/restriction_enzyme

The sequence recognized is often four to six nucleotides long. It is the recognition sites that provide the key to how one DNA fragment can be cut into two in a specific manner. There are

three different types of restriction enzymes. Type I cuts DNA at random locations as far as 1000 or more base-pairs from the recognition site. Type III cuts at approximately 25 base-pairs from the site. Types I and III require ATP and may be large enzymes with multiple subunits. Type II enzymes, which are predominantly used in biotechnology, cut DNA within the recognized sequence without the need for ATP, and are smaller and simpler.[78] HindIII is a kind of type II restriction enzyme that digests the double-stranded DNA at the palindromic sequence AAGCTT (The palindromic sequence is a nucleic acid sequence that is the same whether read 5' to 3' on the complementary strand with which it forms a double helix – Figure 47).

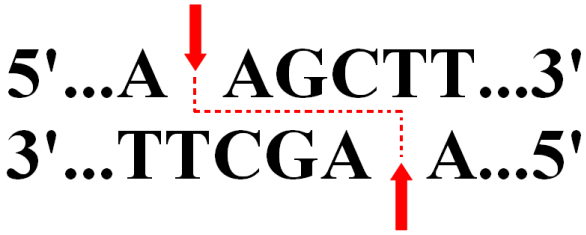

Figure 47. Restriction enzyme HindIII cut double-stranded DNA at the palindromic sequence AAGCTT.

DNA cleavage by restriction enzyme HindIII is important in nucleic acid metabolism,[79] protection against virus attack,[80] and biotechnology.[81]Although many studies have been done to investigate the structure, stability and function of type II restriction enzymes,[82-84] only a few of them have been done in crowded environment.[83,84] These studies however, are not coherent – showed that crowded environment had different influences on different enzymes.[83,85] Such differences indicated a lack of universal rule describing enzymes activity in crowded environment.

The viscosity is one of the characteristics of crowded environment that affects cleavage of DNA. From the Stokes – Sutherland – Einstein equation, an increase of viscosity decreases the diffusion coefficient of enzyme and DNA in the solution, and as a result, bioreaction is slowed down. However, the crowded environment, which is featured by large

viscosity, does not always decrease diffusion coefficients of biomolecules appreciably. Some small proteins move fast in various cell compartments such as nucleus[86] or mitochondria,[87] despite high viscosity in these systems. According to the Stokes – Sutherland – Einstein equation, this fast diffusion indicates that the proteins experience a viscosity much smaller than the macro-viscosity measured by a standard viscosimeter. Our researches provided an explanation for this phenomenon in study of tracers (proteins, dyes) mobility in polymer solutions.[44] The nano-viscosity experienced by the tracers in polymer solutions has been connected with the size of the polymer molecules. When the diameter of the tracer, *d*, is bigger than the polymer radius of gyration R_g, the tracers experience the macro-viscosity of the polymer solution. On the other hand, when *d* is much smaller than R_g the tracers experience a nano-viscosity much smaller than the macro-viscosity.[44] Therefore I made a clear distinction between macro- and nano viscosity in this study of cleavage of DNA in polymer solution.

Another characteristics of crowded environment which affect the cleavage of DNA are depletion interactions.[88,89] PEG can induce DNA collapse into a compacted structure through attractive depletion interaction between DNA fragments.[90,91] Depletion interactions are caused by the osmotic pressure which arises when two DNA molecules are in close proximity, closer than the radius of gyration of the polymer. In such a case, the space between DNA molecules is depleted from polymer coils and consequently an imbalance in osmotic pressure occurs. It leads to an effective attraction between DNA fragments of the same DNA molecule. The same interactions are responsible for the formation of large aggregates, when acting between different DNA molecules. For long DNA molecules monomolecular collapse dominates[90] and for short DNA molecules aggregation of DNA molecules dominates.[92] As a result DNA forms a compact state.[90] The structural changes inside DNA can in principle strongly affect its interactions with enzymes and consequently affect the cleavage process of the DNA.

In the following chapter, I investigate the influence of complex liquids (glycerol, PEG 6000 and PEG 8 M solutions) on the dynamics of biomolecules (DNA and restriction enzyme HindIII). I show that PEG 6000 solution decreases the diffusion coefficient of DNA and HindIII more efficiently than glycerol solution of the same concentration or PEG 8 M solution of the same macro-viscosity. I explain the DNA cleavage in PEG and glycerol solution by the concept of size dependent nano-viscosity. I also compare the size of DNA obtained by Dynamic Light Scattering (DLS) measurement with that obtained by theoretical analysis and demonstrate formation of aggregates of plasmid DNA in PEG 6000 solution due to depletion interactions.

3.2.2. Experimental results

3.2.2.1. DNA cleavage in the crowded environment

The DNA plasmid is composed of two components, presented in Figure 48a and b. Component I DNA is the supercoiled double - stranded DNA and component II DNA is the loose circular DNA, which results from single-stranded cleavage of component I. Restriction enzyme HindIII can cut double-stranded DNA at the palindromic sequence AAGCTT (Figure 47) and transform it into a linear form of DNA (component III – Figure 48c). These three components of DNA have different mobilities caused by the difference in their structure, therefore should be presented as three distinguishable bands in electrophoresis assay.[93] From this reason, the electrophoresis assay was used[94] to monitor the cleavage of DNA by HindIII in glycerol, PEG 6000 and PEG 8 M solutions respectively (Figure 49).

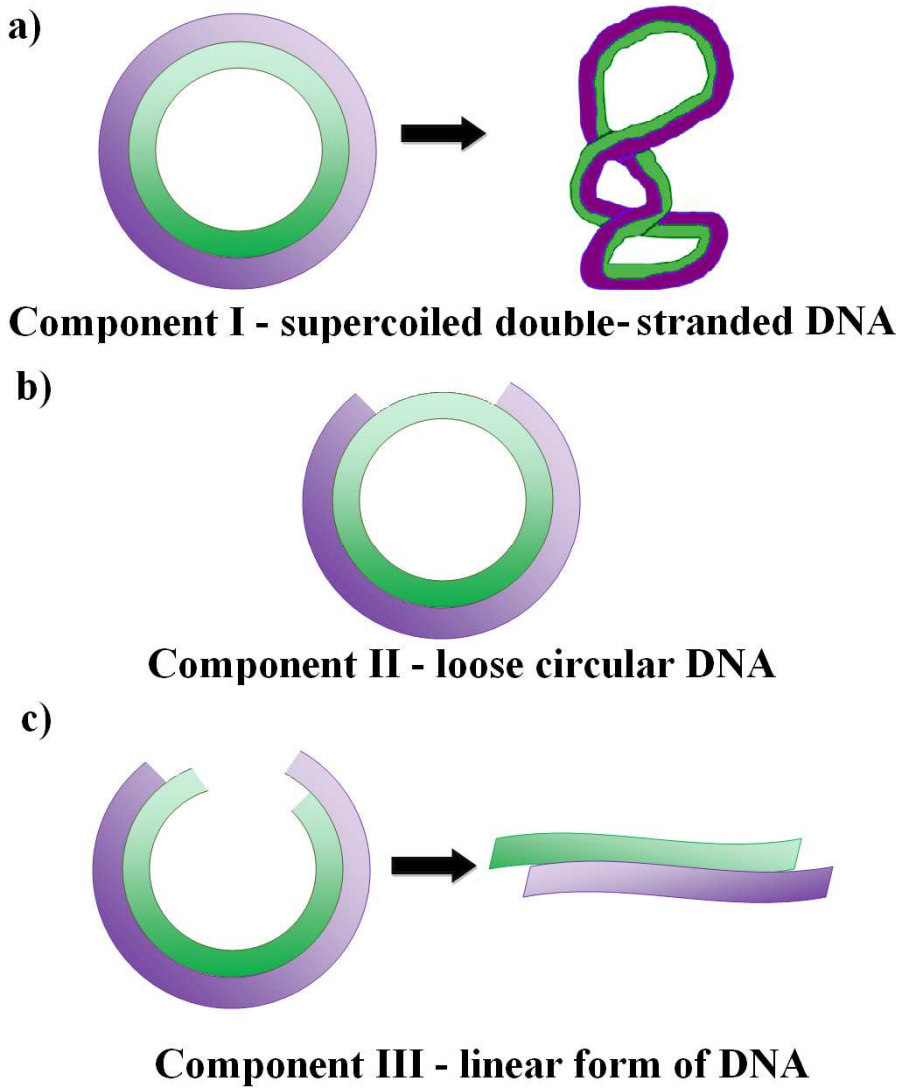

Figure 48. PUC19 plasmid DNA is composed of two components: **a)** Component I and **b)** Component II. Restriction enzyme cut double – stranded DNA and transform DNA into **c)** linear form of DNA – Component III.

Component III DNA moves faster than component I and component II DNA in electrophoresis assay, as was expected from the difference in their structure. Figure 49 shows that PEG 6000 solution can efficiently inhibit the cleavage of DNA. A large amount of DNA is not changed to component III DNA in the presence of high concentration of PEG 6000 solution (line 4 – 7, Figure 49a). On the contrary, PEG 8M solution does not show any

influence on DNA cleavage process (line 2 – 6, Figure 49c). It is also visible, that glycerol solution of the same concentration as the PEG 6000 solution also slows down the cleavage of DNA but with low efficiency. PEG 6000 solution is characterized as crowded and viscous, glycerol solution is characterized as crowded but not viscous and PEG 8 M solution is characterized as viscous but not crowded.

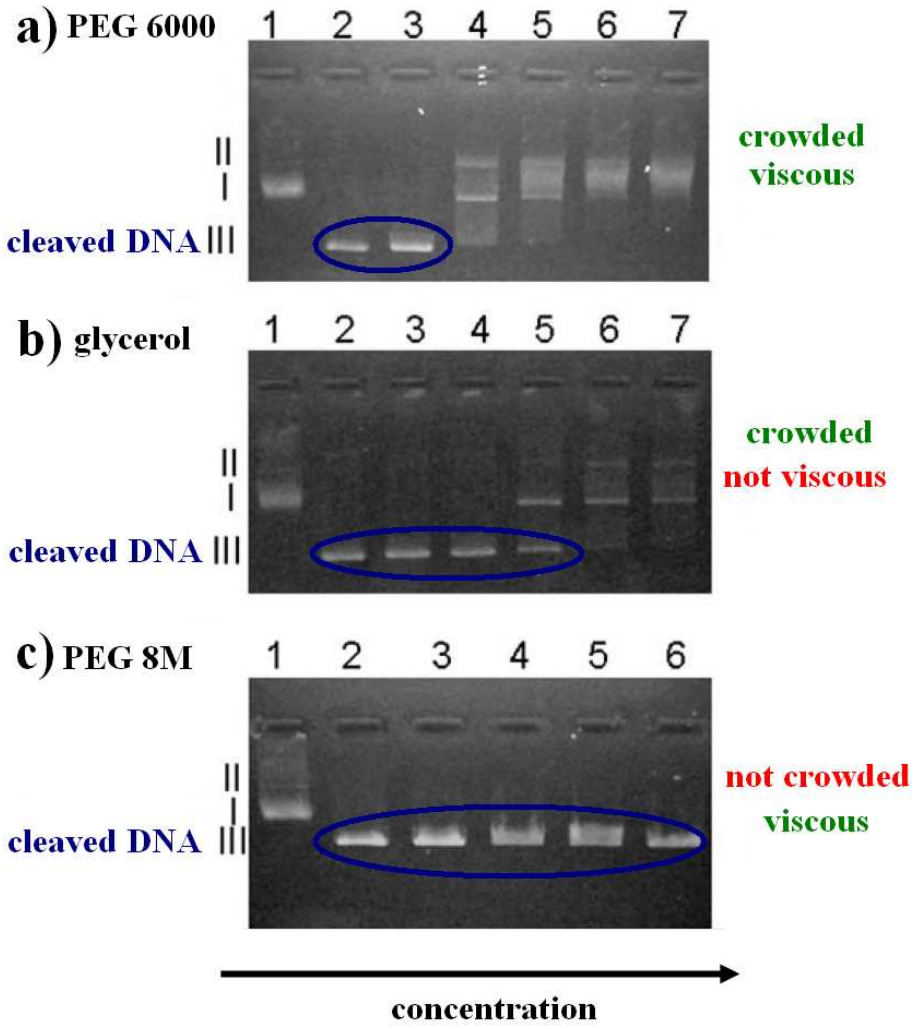

Figure 49. The photograph of the gel electrophoresis assay (experiment made by Sen Hou[94]) performed after the cleavage of the DNA by HindIII in PEG 6000, glycerol and PEG 8M solutions. The reaction time (1 h) was the same for all solutions. The photograph shows three separate bands for I, II, and III components of the plasmid DNA. Component III is the linear DNA which results from the cleavage process of circular DNA plasmid. This component has the highest mobility. Lane 1 is the control lane showing DNA without any cleavage (same in all cases). Lanes 2 to 7 denote solutions with different PEG 6000 **a)** or glycerol **b)** concentrations i.e. 0, 7, 14, 21, 29 and 36 w/w% respectively. In the case of PEG 8 M **c)** lanes 2 to 6 correspond to 0, 0.14, 0.49, 0.63 and 0.7 w/w% respectively.

Following two chapters explain what nanoscopic mechanism is hidden behind the unusual cleavage of DNA in the crowded environment. It will be also shown how viscosity (Chapter 3.2.2.2) and depletion interactions (Chapter 3.2.2.3) influence on DNA cleavage process.

3.2.2.2. Influence of viscosity on DNA cleavage process

In this part, I precisely investigate the influence of viscosity on the cleavage of DNA. Glycerol, PEG 6000 and PEG 8 M solutions are three examples of crowded environments of different viscosity characteristics (Figure 50).

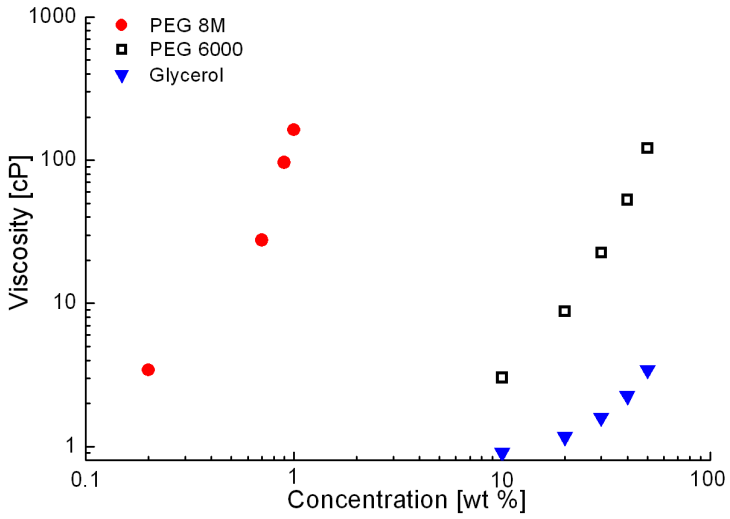

Figure 50. Viscosity as a function of concentration of glycerol, PEG 6000 and PEG 8M in TE buffer at 37°C.

As it is seen in Figure 50, the viscosity of glycerol, PEG 6000 and PEG 8M solutions increases with their concentration. However, the glycerol solution has much smaller viscosity than the PEG 6000 solution of the same concentration, while PEG 8 M solution has much smaller concentration than the PEG 6000 solution of the same viscosity. The viscosity of PEG solution grows[44] with polymer concentration c as $\exp(3/2(c/c^*)^{0.53})$. Here $c^*=M/(4/3\pi R_g^3 N_A)$ is the overlap concentration i.e. the concentration at which polymer's chains start to overlap. M is the molar mass of polymer, N_A is Avogadro's number and $R_g=0.02M^{0.58}$ [nm] is the

radius of gyration of PEG chain.[65] The overlap concentration is 0.12 g/cm^3 for PEG 6000 (average molecular mass M = 3461 Da) and 0.002 g/cm^3 for PEG 8M (average molecular mass M = 854096 Da, see Figure 33b and Table 2). Consequently, the concentration of PEG 6000 solution is larger than that of PEG 8 M solution of the same viscosity (see Figure 50).

In glycerol and PEG 6000 solutions, the diffusion coefficient D of HindIII or DNA is inversely proportional to the viscosity η of the solution according to the Stokes–Sutherland–Einstein equation, $D=k_BT/(6\pi\eta R)$. Here k_B is the Boltzmann's constant and T is the temperature. The viscosity of polymer solutions is much larger than that of TE buffer (η_{TE}=0.727cP at 37^{o}C), thus the diffusion coefficients of HindIII and DNA in crowded environment are much smaller than those in TE buffer. Small diffusion coefficient of HindIII and DNA increases the time for these reagents to encounter in the crowded environment. Consequently, the cleavage of DNA in crowded environment is slower than that in TE buffer (Figure 49a and b).

The viscosity-determined, diffusion-limited theory well explains the slow cleavage of DNA in glycerol and PEG 6000 solution. But it cannot explain why PEG 8 M solution, which is also characterized by large viscosity, does not affect the cleavage of DNA (Figure 49c). In order to explain this unusual phenomenon it is necessary to employ the concept of nano-viscosity. In previous section (Chapter 3.1 *Diffusion of nano-particles in polymer solutions*) and in recent studies,[44] it was shown that when the radius of gyration of the polymers, R_g, is larger than the diameter d of the probe, $R_g > d$, the probes experience a nano-viscosity. In contrary, when $R_g < d$, the probes experience a macro-viscosity. The size of HindIII (estimated on the basis of its molecular mass 69.9 kDa) is d = 5.6 nm, while the radius of gyration of PEG 8M is R_g = 55.12 nm. Hence, in PEG 8M solution ($R_g > d$), HindIII experiences a nano-viscosity, which means that it can move relatively freely in PEG 8M solution (see Figure 51a and Table 3). That is why PEG 8M does not affect the cleavage of

DNA. The effective length of the DNA based on the equivalent rod model is 266 nm, which is much larger than R_g = 55.12 nm of PEG 8 M and thus DNA can be treated as immobile in comparison to the motion of the enzyme of size d = 5.6 nm.

The radius of gyration, R_g, for PEG 6000 is 2.26 nm and for glycerol is even smaller. That is why HindIII of size d = 5.6 nm > R_g experiences the macro-viscosity in these solutions (see Figure 51b and Table 4). The time needed to cut DNA in these solutions should be proportional to the macro-viscosity and that is why the cleavage time grows with the concentration of glycerol or PEG 6000 (see Figure 49 and Figure 50).

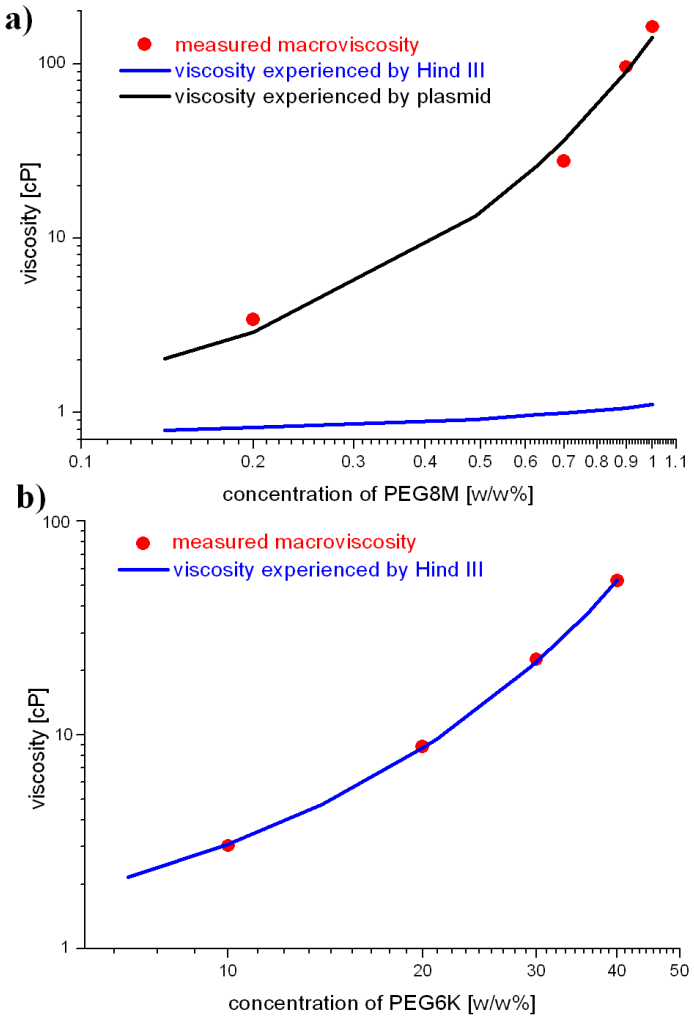

Figure 51. a) Viscosity as a function of concentration of PEG8M at 37°C. Viscosity experienced by Hind III, η_{nano}, is calculated from $\eta_{nano} = \eta_0 \exp(b(d/\xi)^a)$, where η_0 is the viscosity of water, a and b are constant of the order of 1, d is the size of HindIII and ξ is the mesh size of polymer network.[94] Accurate data are included in Table 3. **b)** Viscosity as a function of concentration of PEG6K at 37°C. Viscosity experienced by Hind III, η_{macro}, is calculated from $\eta_{macro} = \eta_0 \exp(b(R_g/\xi)^a)$, where η_0 is the viscosity of water, a and b are constant of the order of 1, R_g is the radius of gyration and ξ is the mesh size of polymer network.[94] Accurate data are included in Table 4.

Table 3. Accurate data for macroviscosity, viscosity experienced by HindIII and viscosity experienced by plasmid as a function of concentration of PEG8M at 37°C.

PEG 8M at 37°C			
Concentration [w/w%]	**Macroviscosity [cP]**	**Viscosity experienced by HindIII [cP]**	**Viscosity experienced by plasmid [cP]**
0	0.73	0.73	0.73
0.14	1.55	0.79	2.03
0.2	3.42	0.82	2.89
0.49	9.54	0.91	13.34
0.63	20.66	0.97	26.26
0.7	27.63	0.99	36.49
0.9	96.02	1.06	90.76
1	162.85	1.11	141.27

Table 4. Accurate data for macroviscosity and viscosity experienced by HindIII as a function of concentration of PEG6K at 37°C.

PEG 6K at 37°C		
Concentration [w/w%]	**Macroviscosity [cP]**	**Viscosity experienced by HindIII [cP]**
0	0.73	0.73
7	1.91	2.16
10	3.03	3.07
14	4.79	4.75
20	8.8	8.69
21	9.88	9.57
29	20.59	20.11
30	22.6	21.99
36	37.72	37.13

Previous study[83] concerning EcoRV kinetics in Ficoll solutions also mentioned that the slow diffusion of proteins caused by viscosity influences the cleavage of DNA. However, the authors did not relate the cleavage of DNA to the nano-viscosity. I showed in this study that it is the nano-viscosity rather than the macro-viscosity that affects the cleavage of DNA in the crowded environment.

3.2.2.3. Influence of depletion interactions on DNA cleavage

I observe that the cleavage process at high concentration of PEG 6000 is too slow to be explained by the changes of the nano or macro-viscosity. The viscosity of 14 w/w% PEG 6000 is about 7 times larger than that of TE buffer. Hence, according to the Stokes

Sutherland–Einstein equation, the diffusion coefficient of HindIII in 14 w/w% PEG 6000 is about 7 times smaller than that in TE buffer. Because the cleavage of DNA in TE buffer solution is completed in 10 min (line 2 in Figure 52a), HindIII should complete the cleavage in the 14 w/w% PEG 6000 solution in 70 min. However, the cleavage process is not completed even in 1080 min (line 4 in Figure 52b), showing that there had to be other factors influencing the cleavage of DNA in PEG 6000 solution.

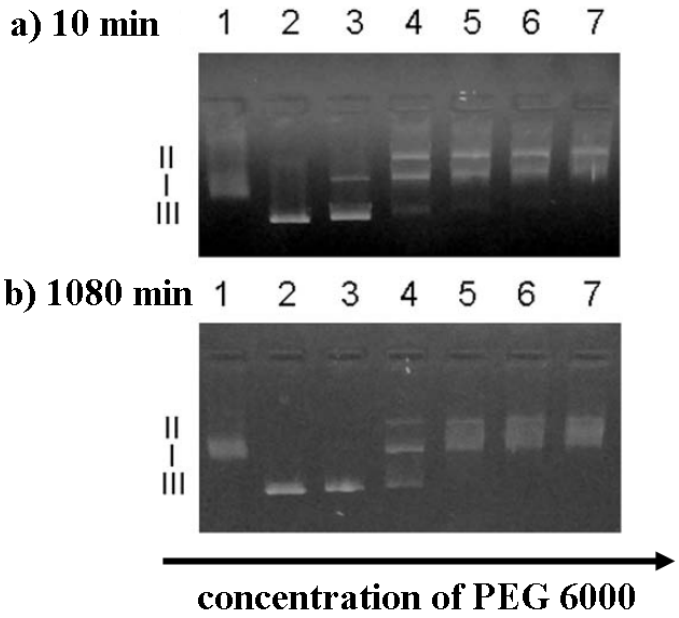

Figure 52. The photograph of the gel electrophoresis assay (experiment made by Sen Hou[94]) presenting an influence of the incubation (reaction) time on DNA cleavage process in PEG 6000 solutions. Lane 1 is native DNA. The concentration of PEG 6000 solution from lane 2 to lane 7 is 0, 7, 14, 21, 29 and 36 wt% respectively. The incubation time at 37^{o}C is 10 min **a)** and 1080 min **b)** respectively. The presence of I, II and III bands in lane 4 in **a)** and **b)** indicate that the process is not completed in 1080 min. Intensity for the third component III is similar in **a)** and **b)** showing that the process is extremely slow.

The cleavage of DNA in crowded environment involves various nonspecific interactions of biomolecules with solution constituents apart from the viscosity. One of such interactions are depletion interactions between DNA molecules in polymer solutions.[90,91] The influence of this interaction on reaction rates was strong in our solutions, although indirect. The origin of depletion interactions can be traced back to the conformational entropy of polymer chains.[88] The center of mass of a polymer molecule cannot get closer to the DNA fragment than the

certain characteristic distance, because it would result in a decrease of its conformational entropy. This distance is proportional to the sum of the radius of gyration of a polymer, R_g, and a radius of a DNA fragment, r. If two DNA fragments are close to each other, separated by a distance smaller than $2r + 2R_g$, a polymer cannot enter between them. This depletion zone (zone depleted from polymers) causes an imbalance of osmotic pressures (induced by polymers outside the zone between the DNA fragments). The osmotic pressure pushes the DNA fragments together and collapses DNA into a compacted structure. If the DNA fragments belong to the same DNA molecule we call it condensation.[90,91] If the DNA fragments belong to different DNA molecules we call it aggregation.[92] DNA condensation decreases the volume of DNA molecules and increases their diffusion coefficient; while DNA aggregation increases the volume of DNA molecules and decreases their diffusion coefficient. Both processes compact the structure of DNA and spatially inhibit the approach of HindIII to its target DNA. As a result the cleavage of DNA is slowed down. In order to prove aggregation of DNA molecules in PEG 6000 solution at high concentration, I have performed DLS experiments and theoretical analysis for the diffusion coefficients of the plasmid DNA. It is thoroughly described in the following paragraphs.

I used plasmid DNA PEGFP-C1 (4.7k base pairs) and both 7 and 36 w/w% PEG 6000 solutions (in TE buffer) in DLS measurement at 25^{o}C and 37^{o}C (details of the apparatus - see subsection 3.1.2.2 *Dynamic Light Scattering apparatus* and Figure 40). The concentration of plasmid DNA was 72 ng/μL. I also added the same concentration of enzyme buffer into the solution to mimic the cleavage system. I used TE buffer containing the same amount of plasmid DNA as a control. The experimental results were fitted according to the typical DLS procedure. The characteristic diffusion time for DNA, τ_0, and PEG 6000, τ_{0p}, was obtained by evaluating the time-dependent homodyne autocorrelation function.

$$g(q,t) = \langle I(q,t)I(q,t+\tau)\rangle \tag{32}$$

where *I(q,t)* is the intensity of light scattered from the samples at time *t* and at the wavevector *q*. Here, the modulus of the scattering vector of the optical arrangement, *q*, is given by $q=(4\pi n/\lambda)\sin(\theta/2)$, where *n* is the refractive index of the liquid solution (measured by a standard Abbe refractometer), λ is the wavelength of the laser in vacuum and θ is the scattering angle. The autocorrelation function *g(q,t)* for one diffusion mode is represented by a single exponential type of decay function for DNA in TE buffer solution,

$$g(q,t) = A + B\left[\exp(-\tau/\tau_0)\right]^2 \tag{33}$$

or a double exponential type of decay function for DNA in PEG 6000 solution,

$$g(q,t) = A + [B\exp(-\tau/\tau_0) + C\exp(-\tau/\tau_{0p})]^2 \tag{34}$$

where *A*, *B* and *C* are experimental constants. The inverse of the characteristic diffusion time depends on *q* as follows:

$$Dq^2 = 1/\tau_0 \tag{35}$$

Here *D* is the diffusion coefficient, which does not depend on *q*. For each sample I measured the autocorrelation function using five different scattering angles (*q* wavevectors) and used above equation to determine *D*.

According to the method developed by Seils and Pecora,[95] I approximated shape of the supercoiled plasmid DNA by an equivalent rigid cylinder (Figure 53, see also Figure 9 on page 14).

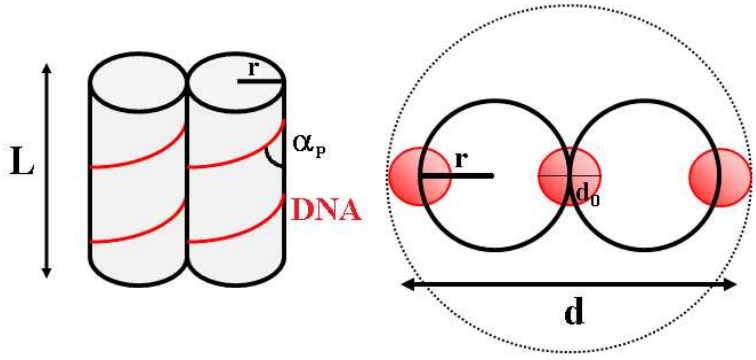

Figure 53. Schematic approximation of supercoiled plasmid DNA shape through equivalent rigid cylinder of length *L*, diameter *d* and helical pitch α_P. d_0 represents the diameter of the relaxed DNA and *r* is the radius of helix. See also Figure 9 on page 14.

The dimensions of the cylinder are calculated on the basis of the DNA superhelix in the following way. The length of this cylinder, L, is half of the contour length of DNA, l, corrected for the helical pitch, α_P:

$$L = \frac{l}{2}\cos(\alpha_P) \tag{36}$$

The diameter of the cylinder d is defined as

$$d = 4r + d_0 \tag{37}$$

where d_0 represents the diameter of the relaxed DNA and r is the radius of helix,

$$r = \frac{l\sin(\alpha_P)}{4\pi n_\theta} \tag{38}$$

and n_θ is the number of helical turns.

$$n_\theta = \delta_b\, n_b/n_h \tag{39}$$

where n_b is the number of base pairs in DNA, n_h is the number of base pairs for one turn, and δ_b is the number of superhelical turns per base pair. For PEGFP-C1, I substituted definite data following Seils and Pecora[95] $\alpha_P = 55^o$, $n_b = 4700$, $n_h = 10$, $\delta_b = 0.079$ and $l = 1626.2$ nm. From these data I got the equivalent cylinder dimension: $L = 466$ nm and $d = 13.4$nm. For PUC19, $\alpha_P = 55^o$, $n_b = 2686$, $n_h = 10$, $\delta_b = 0.079$ and $l = 924.4$ nm and I obtained the equivalent cylinder dimension: $L = 266$ nm and $d = 13.4$ nm.

For the equivalent cylinder, the translational self-diffusion coefficient D_0 can be described as

$$D_0 = \frac{1}{3}(D_{II} + 2D_\perp) \tag{40}$$

where $D\perp$ describes the diffusion perpendicular to the long axis of the cylinder and $D\parallel$ describes the diffusion parallel to the long axis of the cylinder.

$$D_\perp = \frac{k_B T}{4\pi\eta L}(\ln(\rho) + \upsilon_\perp) \qquad D_{II} = \frac{k_B T}{2\pi\eta L}(\ln(\rho) + \upsilon_{II}) \tag{41}$$

k_B is the Boltzmann constant, T is the absolute temperature, and $\upsilon_{\perp}$ and υ_{II} are ‘‘end-effect corrections’’

$$\upsilon_{\perp} = 0.839 + 0.185/\rho + 0.233/\rho^2 \quad (42)$$

$$\upsilon_{II} = -0.207 + 0.980/\rho - 0.133/\rho^2 \quad (43)$$

with axial ratio $\rho = L/d$.

As described above, Seils and Pecora[95] use an equivalent rod as a model for the plasmid DNA to compute its diffusion coefficient. This model is fitted to the experimental data in TE buffer (Figure 54) showing perfect agreement between theory and experiment. However, in polymer solution theoretical model and experimental results disagree by a factor of 2 to 4. It can be observed, that DNA molecules diffuse slower than expected at both 25^{o}C and 37^{o}C (Figure 54a and b). For example the DNA molecules in 36 w/w% PEG 6000 solution at 37^{o}C diffuse 2.3 times slower than expected on the basis of the model and the value of the macroviscosity. The only way to reconcile these data with the theoretical model is the large increase (2.3 times) of the size of DNA. Such increase in the linear size indicates aggregation of many DNA coils. Because the volume of the aggregate scales as the cube of the size I can give a lower limit of the number of DNA coils in the aggregate *i.e.* $N=2.3^3=12$. Such aggregation is possible because DNA coils are not separated by large distances in the solution. The concentration of DNA is about 23.2 nmol/L. So the average distance between DNA molecules is about 400 nm. The size of supercoiled pEGFP-C1 DNA is also about 460 nm so the average distance between DNA molecules and the size of DNA molecules are comparable and thus aggregation is probable. Both intermolecular DNA aggregation and intra-molecular DNA condensation can be induced by the depletion interactions. It is also possible, that DNA aggregation is additionally accompanied by DNA condensation.

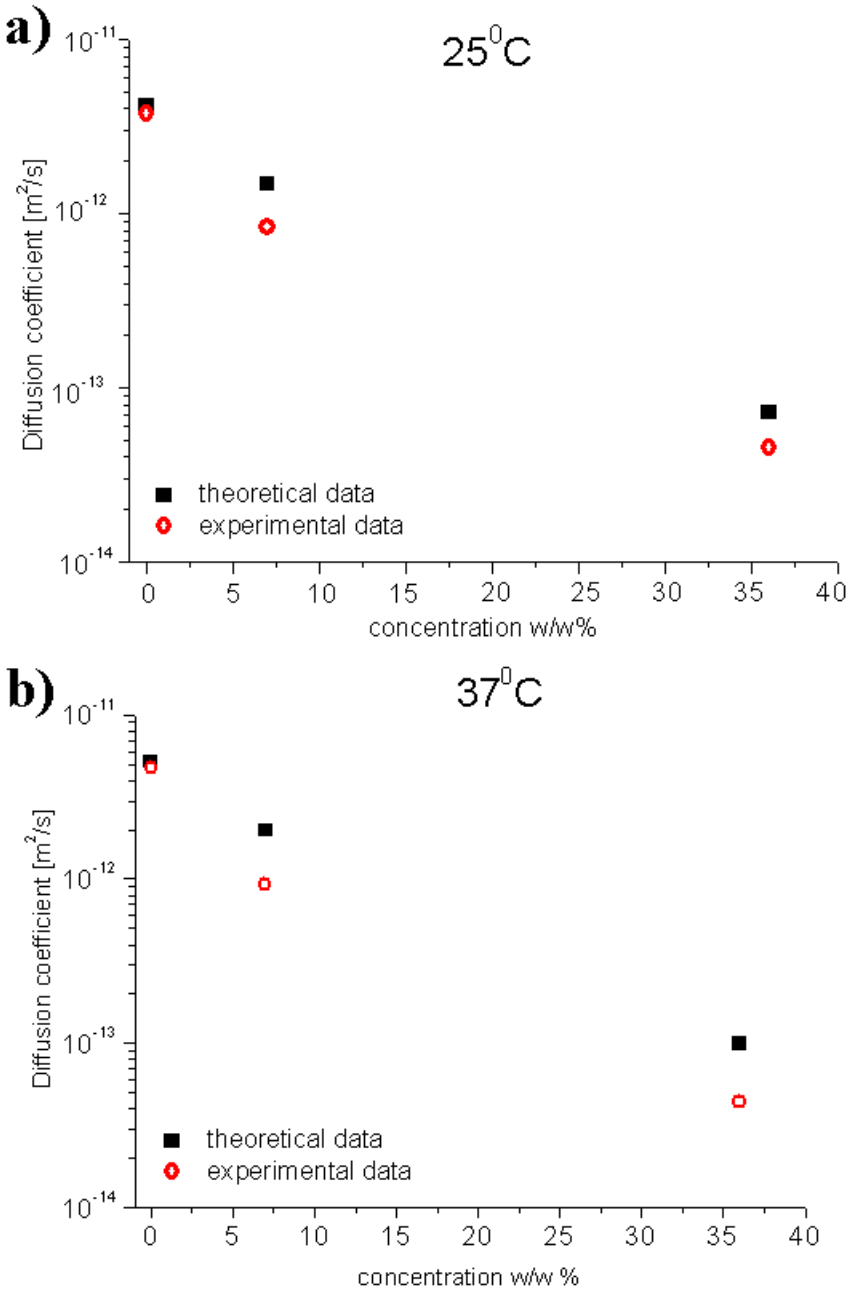

Figure 54. Diffusion coefficient of plasmid DNA measured by DLS versus the theoretical data at **a)** 25°C and **b)** 37°C. Disagreement between theory (calculated for a single molecule of native DNA) and experiment indicates aggregation of plasmid DNA in polymer (PEG 6000) solution.

Finally, I had to verify whether the slow cleavage of DNA is caused by the other factor such as deactivation of HindIII by polymer molecules. This factor, however, was rejected because some researches[70,96] indicate that crowding agents as glycerol and PEG solution do not deactivate HindIII.

3.2.3. Conclusions

I investigate influence of viscosity on the DNA cleavage process by HindIII in crowded environments composed of glycerol, PEG 6000 and PEG 8 M. I find that PEG 6000 solution could effectively slow down the cleavage process. However, neither PEG 8 M solution of the same viscosity as PEG 6000 solution nor glycerol solution of the same concentration as PEG 6000 solution slows down the cleavage of DNA appreciably. I show that the viscosity experienced by the biomolecules (nano-viscosity) is responsible for this effect. Large nano-viscosity of crowded environment (as in PEG 6000) decreases the diffusion coefficient of DNA and HindIII and thus reduces the frequency of encounters between DNA and HindIII. As a consequence the cleavage of DNA slows down. On the contrary PEG 8 M of high macro-viscosity does not influence the cleavage process because the nano-viscosity for HindIII is close to that of water. Additionally the depletion interactions between DNA also slow cleavage of DNA by inducing aggregation of DNA coils. When the concentration of PEG 6000 is high, DNA molecules form big aggregates due to depletion interactions, inhibiting the approach of HindIII to its target DNA. Such research indicates a convenient way to control the DNA cleavage rate by performing this reaction in a suitably chosen crowded environment.

3.3. Ions motion in liquid crystal/polymer mixtures

This chapter is based on article entitled "Thousand-fold acceleration of phase decomposition in polymer / liquid crystal blends" (Natalia Ziębacz et al. ChemPhysChem 2009, 10, 2620 - 2622) and patent application entitled "Sposób przyspieszania separacji faz w układach niejednorodnych, zwłaszcza w układach polimer/ciekły kryształ i polimer/polimer" (Biuletyn Urzędu Patentowego 2010, 3, 13).

A free ions (ionic impurities) inevitably contaminate liquid crystal and polymer systems. All experiments, which I present in this section, prove that such ions can be used to accelerate the phase separation process in the liquid crystal/polymer mixtures. In other words, dynamics of even such small objects as ions can have an influence on phenomenon in macro scale such as phase separation.

3.3.1. Introduction

Micro phase separated blends of liquid crystals (LC) and polymers are widely used for display applications, gas flow sensors, optical gratings and memories.[97-100] The phase separation process in such blends is an important object of research, especially that in such mixtures, the final industrial products have mechanical, transport and electrical properties which depend on the kinetics and dynamics of the separation process used in their formation.[101,102] Generally, the phase separation process is slow, both in the sense of actual time (of minutes to hours or even days) and—as it is controlled by diffusion—also in the sense of the power law evolution of the mean size of the domains. In this context, it would be favourably to control and even accelerate the phase separation processes. In addition to the traditional adjustment of the natural parameters of the process (temperature, composition)

conceptually new advances attempt to affect the phase separation with an external electric field (EF). Use of electric field, however, brings into focus the role of ionic constituents. It is known[24], that all liquid crystals contain some concentration of ionic impurities. Even if the original material is very pure, charges may appear in the liquid crystal due to the alignment layers, high intensity laser field, high electric field or UV illumination. Therefore it is essential, to take note of an importance of ions in liquid crystals, especially in experiments with external electric field.

Tsori et al.[103] showed theoretically an induction of the hexagonal to bcc phase transition in diblock copolymers upon application of direct current electric field (DC EF) above a critical magnitude, and that free ions can reduce the value of the critical field by an order of magnitude: from 70 V/μm to 6 V/μm. Tsori and Leibler followed[104] with a result that ions can influence the phase separation process also in binary mixtures through a mechanism based on a contrast of conductivity—due to different chemical potential of ions—in each of the two phases and on motion of the interface as a result of the electrophoretic force acting on the ions. It was also shown[105] that low frequency oscillating EF (OEF) can induce a dynamic charge separation (dyCHASE) even over macroscopic distances (mm) in a LC meniscus.

In this part, I demonstrate experimentally, that 1) OEFs can be used to accelerate the rate of phase separation even by three orders of magnitude, and 2) free ions are responsible for the acceleration of the phase separation process in the liquid crystal/polymer mixtures.

3.3.2. Materials and methods

3.3.2.1. Materials description

A binary mixture consisted of polystyrene (PS) from Fluca Chemical Co. characterized by the index of refraction n_{PS} = 1.589, molecular weight M_w = 74500 g/mol and the polydispersity index M_w/M_n = 1.03 (M_w is the weight average molecular weight and M_n is the

number average molecular weight). The liquid crystals: 4-cyano-4'-n-pentylbiphenyl (5CB) and 4-cyano-4'-n-octylbiphenyl (8CB) were purchased from the Military University of Technology, Warsaw, Poland. The chemical structure of all used compounds is shown in Figure 55.

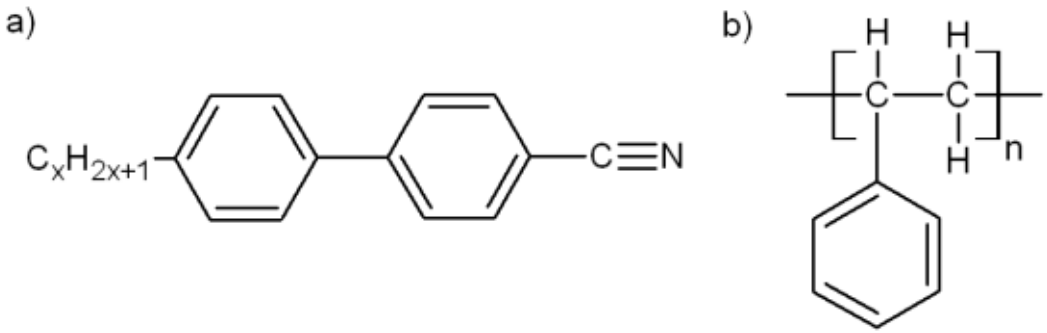

Figure 55. a) The rod like liquid crystals 5CB and 8CB which differ from each other only in the length of alkyl chain, x = 5 or 8, respectively. **b)** Monomer of polystyrene with degree of polymerization n = 715.

Pure 5CB is an isotropic liquid for temperatures above T_1 = 35°C, crystalline below T_2 = 24°C, and nematic for $T_1>T>T_2$. In the isotropic phase, the 5CB index of refraction n_{5CB} = 1.5878, so $\Delta n_1 = n_{PS} - n_{5CB} = 0.0012$. Pure 8CB is an isotropic liquid for temperatures above T_1=40.8 °C, smectic-A below T_2=33.8 °C, and nematic for $T_1>T>T_2$. In the isotropic phase the refractive index of 8CB is n_{8CB} = 1.566, so for 8CB we $\Delta n_2 = n_{PS} - n_{8CB} = 0.023$. Due to the small difference in the refractive indices of 5CB, 8CB and PS ($\Delta n_1 << 1$, $\Delta n_2 << 1$) the multiple scattering of light in these mixtures can be neglected for small sizes of the studied system. It was estimated[106] that for such differences in the refractive indices the mean free path of light in the sample consisting of the polymer-rich domains and the LC-rich domains (in the isotropic phase) 1000 micrometers, thus in order to avoid multiple scattering of light I have used samples of thickness less than 100 micrometers.

3.3.2.2. Sample preparation

I prepared thin films for optical microscopic and static light scattering experiments using the following procedure. 5CB or 8CB and PS were dissolved in toluene and then stirred mechanically for 48h at 65°C, just above the cloud point temperature. The resulting mixtures (40% toluene solution) were placed on a glass of size 1 cm in diameter, cut from microscope cover glass. Microscope glass was covered by indium thin oxide (ITO) layer, which was etched on the edges to prevent short circuit (Figure 56).

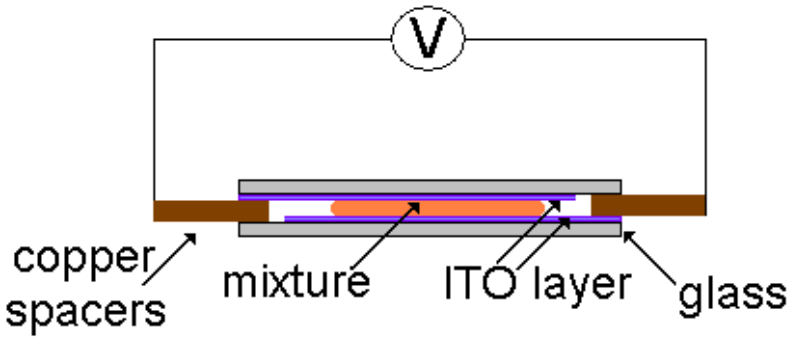

Figure 56. Schematic illustration of my sample.

Next, the films were dried and annealed for 36 to 48h at a temperature of 65 °C. After evaporation of the toluene, the films were covered by the second glass plate. The distance between the plates was set by copper spacers.

3.3.2.3. Static light scattering apparatus and optical microscope

I used Static Light Scattering (SLS) to monitor the evolution of the size of the domains during phase separation. SLS was equipped with a standard He-Ne (5mW) laser which radiates wavelength λ = 632.8 nm. The scattering of light was monitored on a linear array of 512 photodiodes, and the scattering intensity $S(q,t)$ was determined as a function of the scattering wavevector q and time t. The scattering angles, θ, in this experiment were between

θ = 0.5° – 25° and the corresponding wavevectors were between q = 0.2 – 6.9 μm^{-1}. In real space we could in principle observe the domains of size $L = 2\pi/q$ i.e. as small as 1 μm and as large as 31 μm. In practice, the first few photodiodes are too close to the main beam to give reliable results, therefore in practice the range of L that could be observed in our apparatus was between 1 – 5 μm. The values of scattered light intensity $S(q,t)$ as a function of time t were registered every 5s at the beginning of the experiment, and with a lapse of time, this interval time was adjusted between 5 and 180s depending on how fast the process was going. I monitored the position of the peak in $S(q,t)$ as a function of the scattering wavevector. Figure 57 shows SLS apparatus standing in our laboratory.

Figure 57. The static light scattering apparatus.

Optical Microscopy (OM) was used to determine the phase diagrams of 5CB/PS and 8CB/PS systems. For microscopic observations, I used the optical polarizing microscope Nikon ECLIPSE E 400 equipped with Nikon Digital Camera DXM 1200 and a heating/cooling stage LINKAM THMS 600 with 0.01° control of the temperature. Figure 58 shows picture of OM standing in our laboratory.

Figure 58. The optical polarizing microscope Nikon ECLIPSE E 400 equipped with Nikon Digital Camera DXM 1200 and a heating/cooling stage LINKAM THMS 600 with 0.01° control of the temperature.

3.3.2.4. Phase diagram determination

I performed the thermo-microscopy studies to obtain the phase diagram of 5CB/PS. The phase diagram of 8CB/PS was determined by Małgorzata Graca during her Ph. D. studies.[107] The obtained diagrams are shown in Figure 59. The measurements were done for five compositions of 5CB/PS: 58/42, 63/37, 72/28, 84/16, 95/5% by weight and for pure 5CB. For 8CB the measurements were performed for seven composition of 8CB/PS: 46/54, 50/50, 60/40, 70/30, 90/10 wt% and for pure 8CB.

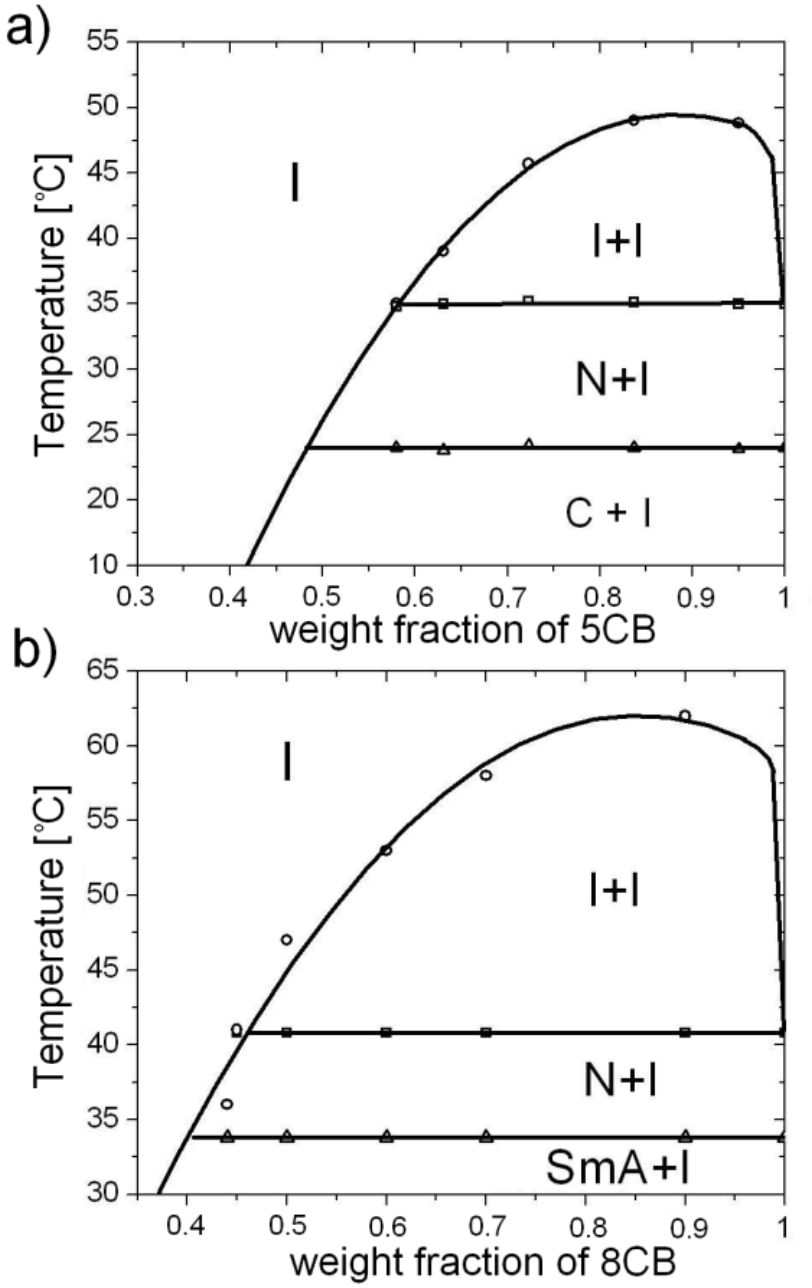

Figure 59. a) Equilibrium phase diagram of PS (M_w=74500 g/mol) / 5CB: temperature vs the concentration of 5CB. The symbols in this diagram represent experimental data obtained by optical microscopy (OM). Triangles represent the transition temperature from crystalline state 5CB + isotropic PS (C+I) to nematic 5CB + isotropic PS (N+I), squares represent the transition temperature from nematic 5CB + isotropic PS (N+I) to isotropic 5CB + isotropic PS (I+I), circles represent the transition temperature from isotropic 5CB + isotropic PS (I+I) to homogenous, isotropic mixture (I). **b)** Equilibrium phase diagram of PS (M_w=74500 g/mol) / 8CB: temperature vs the concentration of 8CB (obtained by Małgorzata Graca[107]). The symbols in this diagram represent experimental data obtained by OM. Triangles represent the transition temperature from smectic-A phase + isotropic PS (SmA+I) to nematic 8CB + isotropic PS (N+I), squares represent the transition temperature from nematic 8CB + isotropic PS (N+I) to isotropic 8CB + isotropic PS (I+I), circles represent the transition temperature from isotropic 8CB + isotropic PS (I+I) to homogenous, isotropic mixture (I).

Samples were first annealed at a temperature above phase separation (60°C for 5CB/PS and 65°C for 8CB/PS) in the homogeneous isotropic phase of the binary mixture. Next, by cooling the samples I studied the textures of the system (exemplary textures of liquid crystal catch during phase separation process are shown in Figure 60).

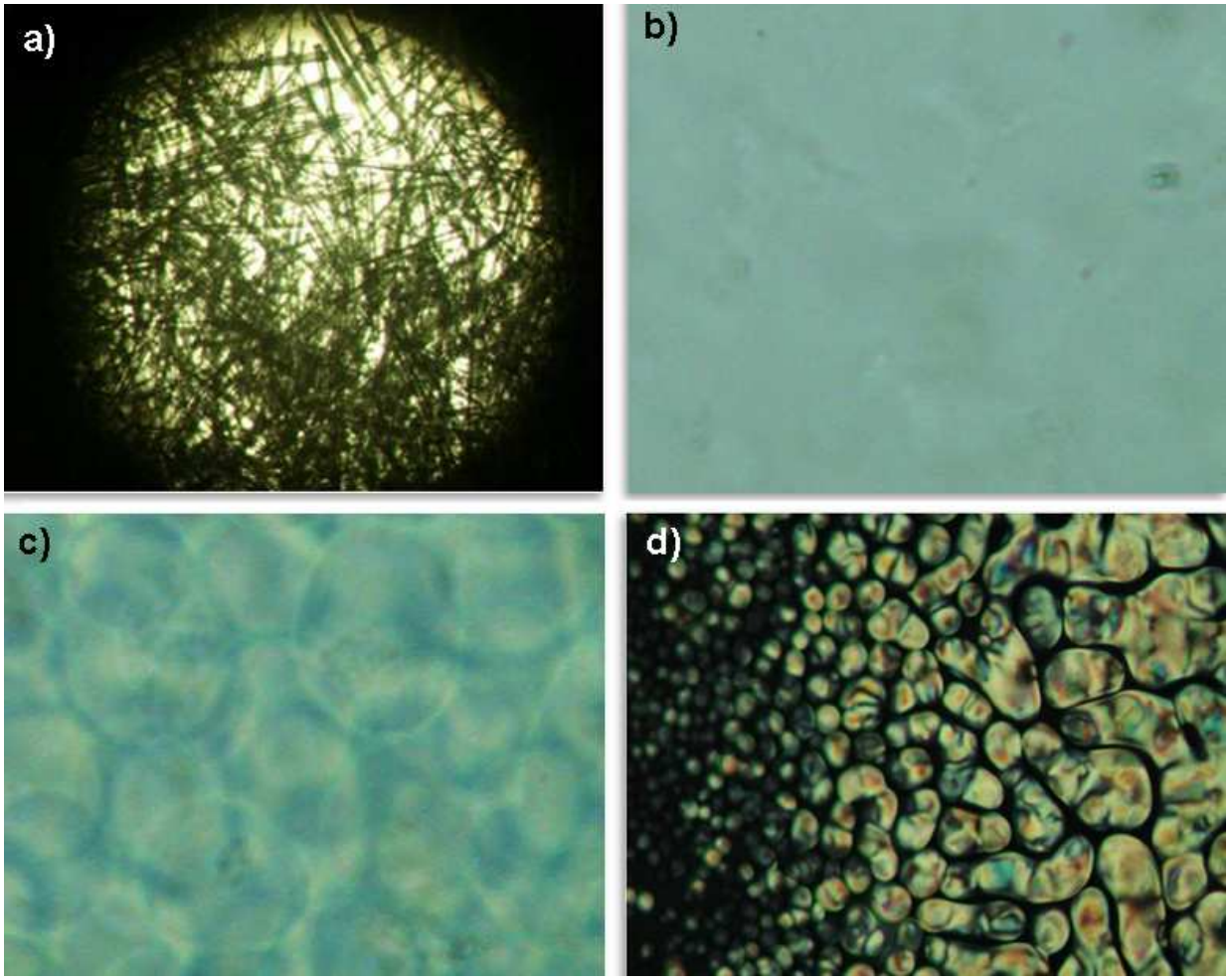

Figure 60. Photographs obtained from the direct observations under the optical microscope for 5CB/PS mixtures**. a)** pure 5CB in crystalline state (C) **b)** homogenous, isotropic mixture (I) **c)** isotropic 5CB + isotropic PS (I+I) **d)** nematic 5CB + isotropic PS (N+I).

Figure 59a presents three phase transition lines separating four different regions, depending on the ordering of liquid crystal/polymer. In a separating mixture 5CB/PS the 5CB-rich phase can be in the isotropic I, nematic N or crystalline C phase. In the 8CB/PS mixture the 8CB-

rich phase can be in the isotropic I, nematic N, or smectic-A phase (SmA). For low temperatures 8CB is in the crystalline C phase (not shown in Figure 59b). The polymer-rich phase can only form an isotropic I phase. The transition temperatures to the nematic (N+I) and smectic-A (SmA + I) region as well as crystalline state (C+I) region phases of the liquid crystal do not depend on the composition of the mixture within the experimental error of 0.2°C. The phase diagrams exhibit a large miscibility gap (I+I), which size increases with the molecular weight of PS. For a small molecular weight of PS (of the order of 10 000), the (I+I) region disappears.

3.3.3. Experimental results

3.3.3.1. Phase separation in liquid crystal/polymer mixtures

The samples were first annealed for 24 hours at temperature above 60 °C or 65 °C in the homogeneous state. Next, I cooled the samples to I+I or N+I region of the phase diagram (Figure 59), where the samples were allowed to demix until the peak (in the scattering intensity) did not leave the region of wavevectors accessible in my experiment. The dominating wavevector component ($q_{\max}$) gives the position of the peak in the scattering intensity *S(q,t)*, and this position is inversely proportional to the size of the domains $L(t) \sim 1/q_{\max}(t)$.

First I have studied the phase separation process in the absence of electric field. Figure 61 shows typical plots of time evolution of the light scattering intensity *S(q,t)* obtained for 5CB/PS mixture (84/16 wt%) in the I+I region. The peak is clearly visible and its location is determined by the wavevector $q_{\max}$. The average size of the polymer domains in the I+I and N+I region given by the peak position $L(t) \sim 1/q_{max}(t) \sim 1/t^{\alpha} \sim t^{-\alpha}$ changes algebraically in time with the exponent $\alpha = -0.3 \pm 0.04$, the same for all investigated concentrations of 5CB/PS and

8CB/PS. Similar results for 8CB with PS, irrespective of polymer mass, were obtained in my department in previous years.[106,108,109]

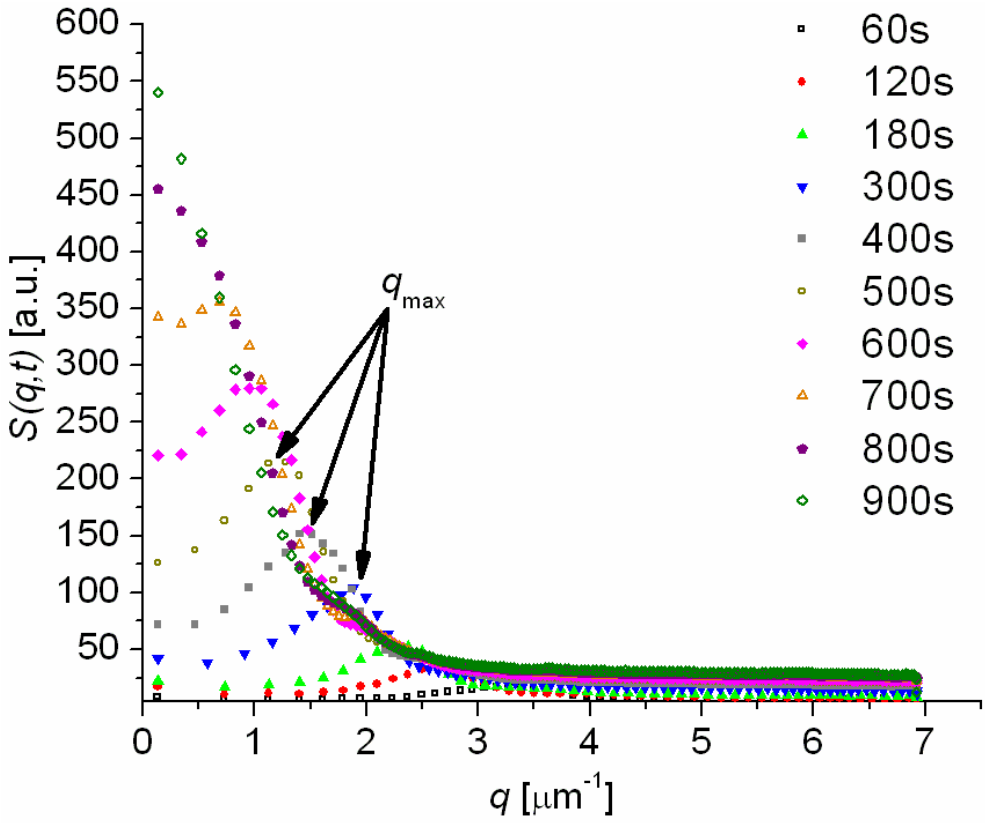

Figure 61. Time evolution of the light scattering intensity *S(q,t)* obtained for 5CB/PS 84/16 wt%. Mixture was cooled from 55 to 35.5°C in the I+I region. The dominating wavevector component (q_{max}) gives the position of the peak in the scattering intensity *S(q,t)*.

Next, I investigated the phase separation in the alternating current electric field. I used the same samples and solutions as in the measurements without electric field. I applied external electric field of intensity 0.03 to 3.3 V/μm and different frequencies from 1 Hz to 1000 Hz. The field was applied after a quench to the two-phase region, when the peak appeared in *S(q,t)*. Typically the system separated without the electric field from about 100 s to 500 s (the temperature quench, where I changed the temperature, lasted at least 30s).

Figure 62 presents a double logarithmic plot of the time evolution of q_{max} for 0.03 V/µm, 3.3 V/µm and for comparison 0 V/µm in the a) 5CB/PS 72/28 wt% cooled to 35.5 °C in the I+I region and b) 8CB/PS 75/25 wt% cooled to 44.9 °C in the I+I region.

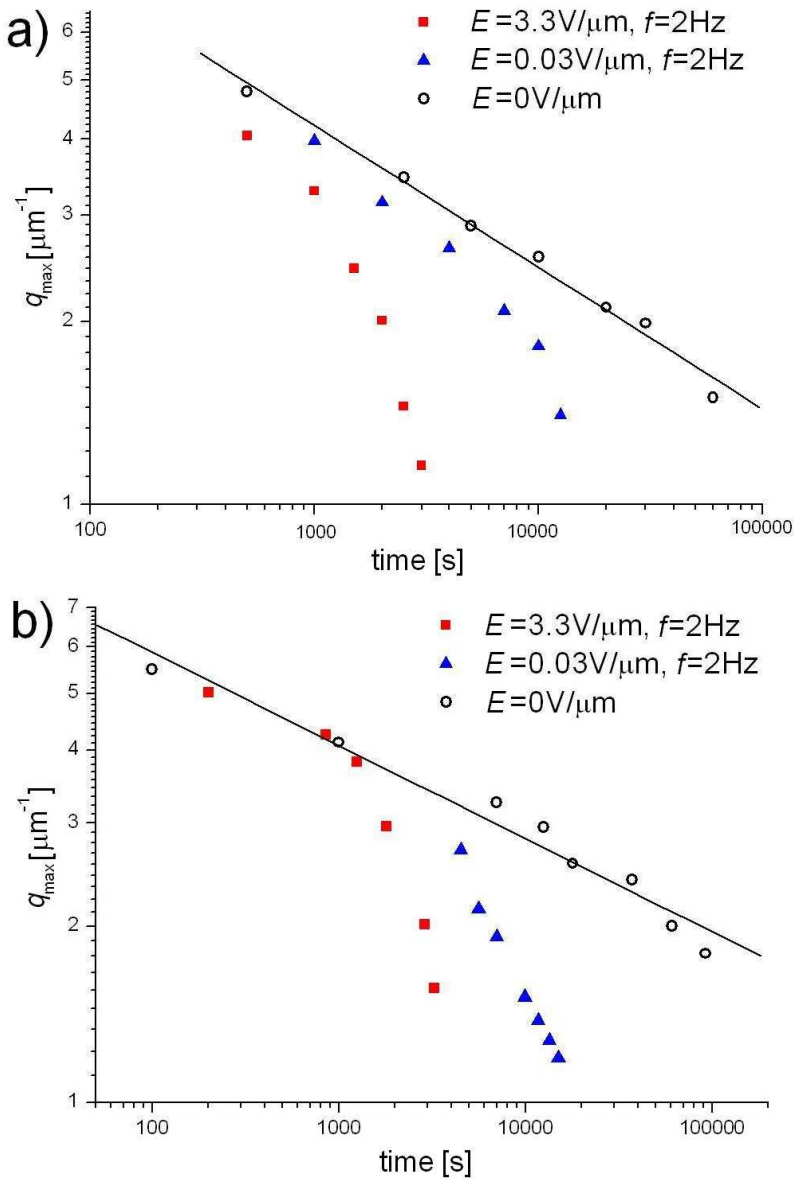

Figure 62. a) Double logarithmic plot of the time evolution of q_{max} in the 5CB/PS 72/28 wt% cooled to 35.5°C in the I+I region. Measurement without electric field is represented by circles, measurement with alternating current electric field (AC EF) of intensity 0.03 V/µm 2Hz is shown by triangles and measurement with AC EF of intensity 3.3 V/µm 2 Hz is shown by squares. **b)** Double logarithmic plot of the time evolution of q_{max} in the 8CB/PS 72/28 wt% cooled to 44.9°C in the I+I region. Measurement without electric field is represented by circles, measurement with AC EF of intensity 0.03 V/µm 2 Hz by triangles and measurement with AC EF of intensity 3.3 V/µm 2 Hz by squares.

The data shown in Figure 62 clearly indicate that alternating current electric field of low frequency definitely reduces time of phase separation in 5CB/PS mixture as well as in 8CB/PS. From Figure 62 it is also clear that the size of the domains in the electric field grows much faster than algebraically especially for high amplitude electric field. It is better visible in Figure 63 where I could fit the data for 5CB/PS and 8CB/PS in the electric field to the exponential function *L(t)~exp(bt).*

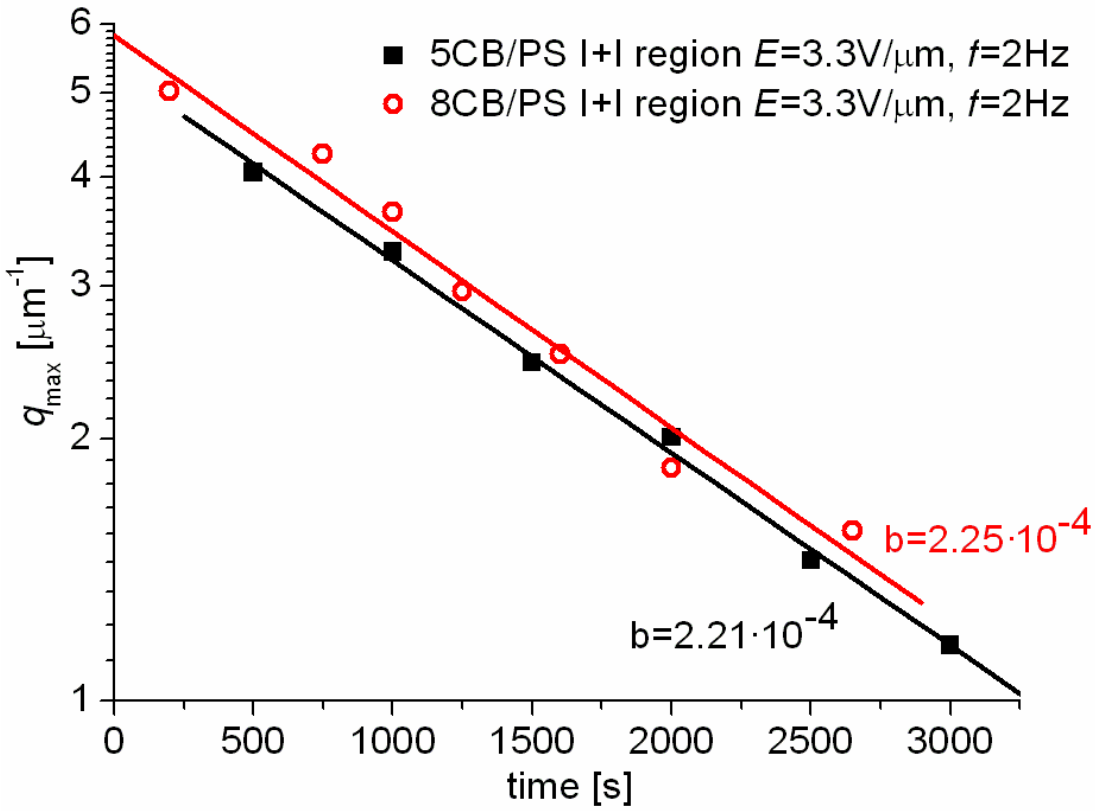

Figure 63. Logarithmic plot of the time evolution of q_{max} in the: 5CB/PS 72/28 wt% cooled to 35.5°C in the I+I region – shown by squares, 8CB/PS 72/28 wt% cooled to 44.9°C in the I+I region – shown by circles. Intensity of electric field was 3.3 V/μm and frequency 2 Hz.

All measurements done for intensity 3.3 V/μm and frequency below 30 Hz were fitted to the exponential function. Figure 64 presents dependence between frequency and coefficient *b* for intensity 3.3 V/μm for low frequencies (from 1 Hz to 20 Hz).

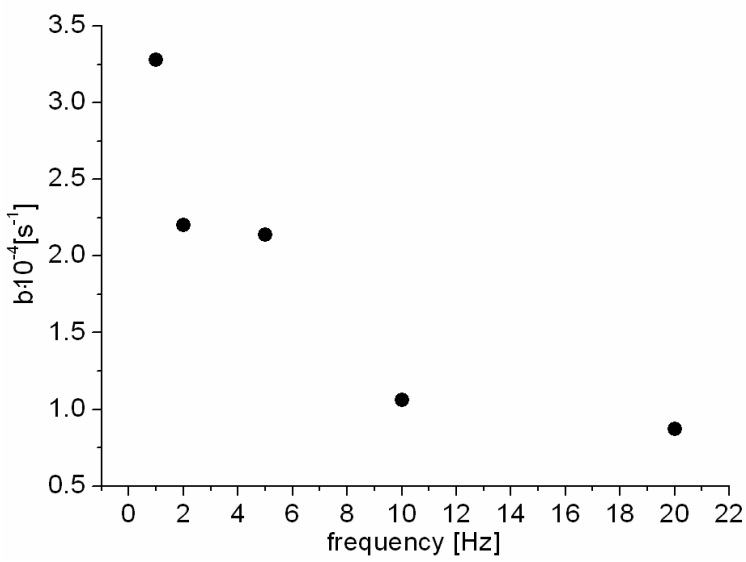

Figure 64. Dependence between frequency and coefficient b (exponential function *L(t)~exp(bt)*) for intensity 3.3 V/µm for low frequencies (from 1 Hz to 20 Hz). Coefficient b decreases with the increase in the frequency of the electric field.

The value of the exponent *b* depends on the parameters of the EF: I found *b* to decrease upon increasing the frequency of the electric fields oscillations. Next, I used external electric field of the same value (3.3 V/µm) but higher frequency (up to 1 kHz). The cross-over from the EF-accelerated to normal coarsening is clearly visible in the Figure 65 where I plot the "coarsening time" t_x as a function of the frequency of the OEF.

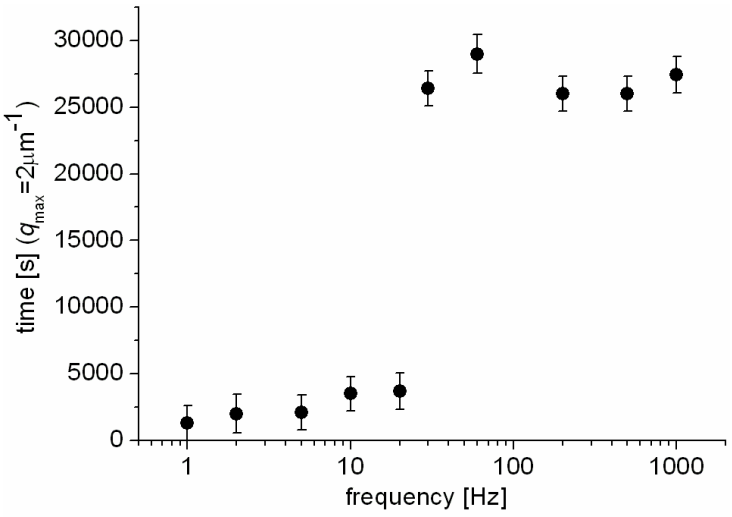

Figure 65. Dependence between frequency and time for which wave vector is 2 μm^{-1} obtained for 5CB/PS 72/28 wt%. cooled to 35.5°C in the I+I region. Threshold frequency depends on PS concentration, because PS can affect strongly the ion mobility and therefore change the threshold frequency below which the acceleration of the phase separation is observed. All measurements were done in alternating current electric field of intensity 3.3 V/µm.

I define t_x as a time at which q_{max} $(t = t_x) = 2\ \mu m^{-1}$. I find that for electric field of 3.3 V/µm and for q_{max} $(t = t_x) = 2\ \mu m^{-1}$ t_x increases abruptly between 20 and 30 Hz marking the transition from accelerated to normal coarsening. The precise definition of t_x did not affect this result. This result showed that at high frequencies there is no acceleration of phase separation. Moreover, at high frequencies the growth of the domain size is algebraic as in the absence of electric field as shown in Figure 66. This figure presents the double logarithmic plot of the time evolution of q_{max} in the 5CB/PS 72/28 wt% cooled to 35.5 °C in the I+I.

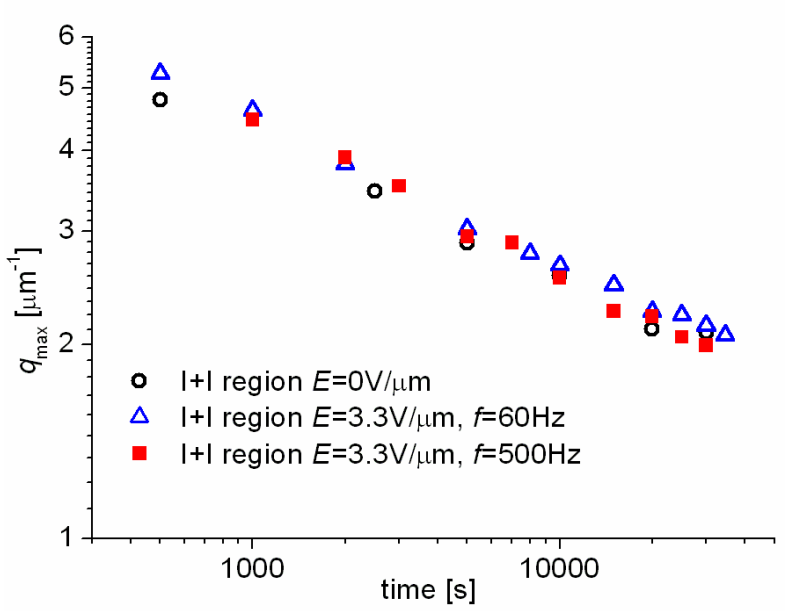

Figure 66. Double logarithmic plot of the time evolution of q_{max} in the 5CB/PS 72/28 wt% cooled to 35.5°C in the I+I region. Measurement without electric field is represented by circles, measurement with 60 Hz frequency electric field is shown by triangles and measurement with 500 Hz frequency electric field is shown by squares. Intensity of electric field 3.3 V/µm.

Finally, I performed experiments in which the low frequency oscillating electric field was turned on immediately upon the temperature quench from homogenous mixture to the phase separated I+I region.

Figure 67 shows the evolution of *L(t)* measured via optical microscopy for few different magnitudes of the electric field. I observed up to 1000 fold acceleration of the separation process.

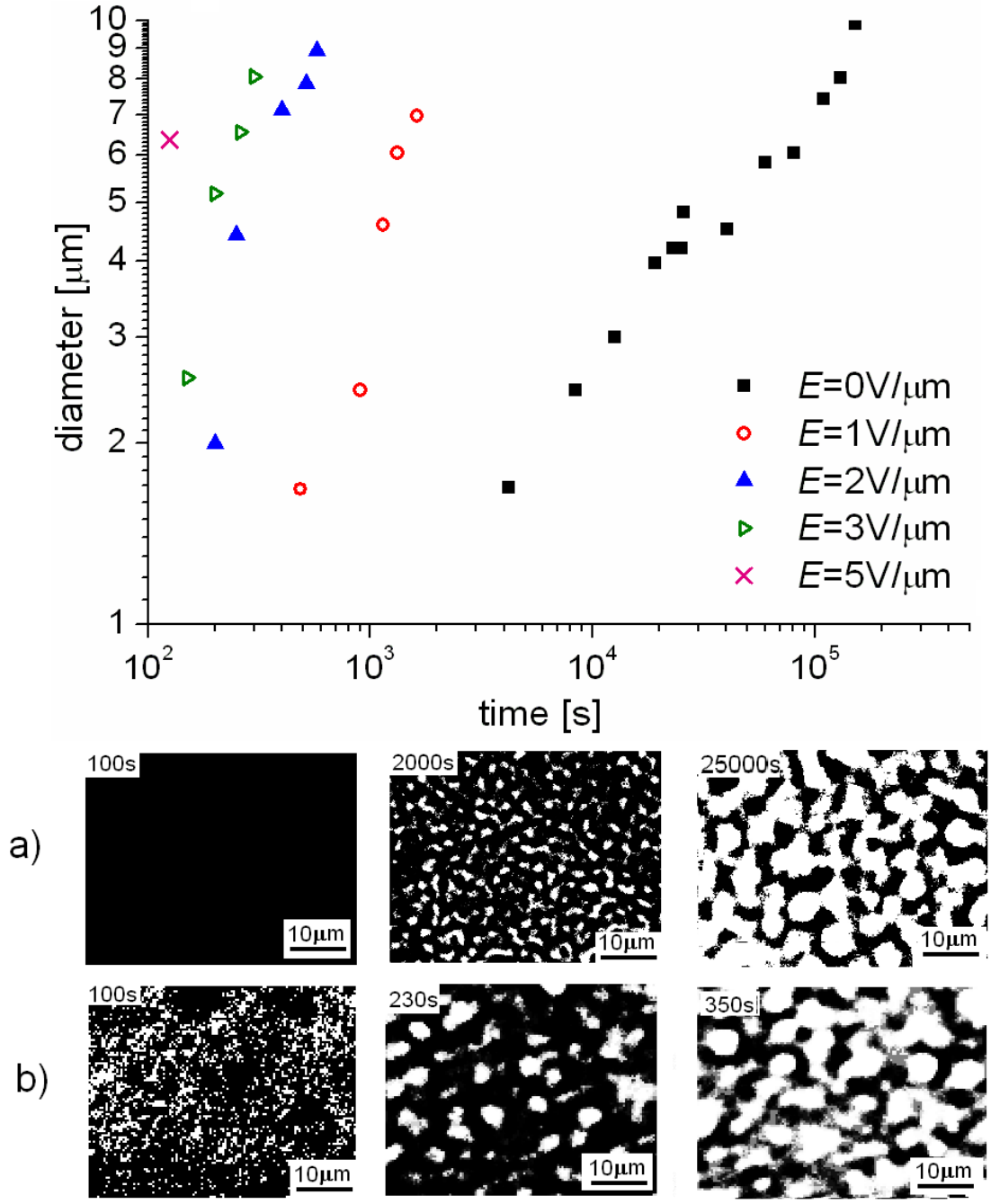

Figure 67. Average size of the domains versus time obtained for 5CB/PS=72/28 wt%. cooled to 35.5°C in the I+I region. The frequency for all measurements was set to 2 Hz. **a)** Domains without an external electric field, last micrographs recorded at *t*=25000 s. **b)** Domains in an external electric field *E*=2 V/μm, *f*=2 Hz, last micrographs recorded at *t*=350 s.

Taking into consideration all results that were presented, I suspected that ionic impurities, which inevitably contaminate liquid crystal and polymer systems, are responsible for the acceleration of the phase separation process in the LC/polymer mixtures. The ionic impurities move under the influence of the electric field to the appropriate electrodes. When they encounter the interface between LC-rich and polymer-rich domains they experience a jump in ionic conductivity. Therefore in the field they move dragging the interface with them. Such behavior should occur in any system with an interface between two materials of different ionic conductivity. In order to obtain an independent test of this hypothesis Tomasz Szymborski prepared additional experiment using pure 8CB liquid crystal with the prepared interface between this liquid crystal and air. In this experiment he optically visualized how ions drag the liquid crystal-air interface upon application of the AC electric field of low frequency. The experiment is described in detail in his Ph. D. thesis and article in Soft Matter[105]. Here, in short, I will present the most important part.

In freely suspended liquid crystal film the boundary of the meniscus charges upon decrease of the frequency of the electric field. This is the case only below a critical value (f_{CR}) which is related to the electrophoretic mobility μ of the ions in the LC and the Debye screening length λ: $f_{CR} \sim \mu E / \lambda$. For $f < f_{CR}$ the ions accumulated at the boundary of the meniscus are dragged electrophoretically beyond λ and never relax to an equilibrium distribution. Tomasz Szymborski et al. proposed[105] that the necessary conditions needed for the dynamic charge separation (dyCHASE) include a discontinuity in the conductivity at the boundary (interface) and that the changes in the polarization of the EF are slow enough to pull the ionic clouds beyond the relevant screening length in the system. In the polymer/LC mixtures that I studied in my experiments the components differ greatly in viscosity, with PS having much higher viscosity than the LC. According to the Walden rule the ionic conductivity is inversely proportional to the viscosity and therefore the LC has higher

conductivity than the polymer. During phase separation the originally homogeneous mixture divides into polymer-rich and LC-rich domains. Under the influence of electric field, the ions move relatively freely in LC but their movement is strongly hampered in the polymer-rich domains. At the interface between the domains the ions experience a sudden change in conductivity. I also observe that the acceleration of the phase separation process appears only for frequencies smaller than critical. This allows me to suggest the ions are responsible for acceleration of phase separation process.

In order to definitely prove that ions are really responsible for acceleration of phase separation process, I also prepared additional experiment. If ions are in fact responsible for the acceleration, any addition of extra ions should have visible effect on the phase separation. This experiment is described in the following section.

3.3.3.2. Polymer blends with additional ions

I have added 0.3 wt%. of organic salt (benzyltetradecyldimethylammonium chloride) into polymer blends. This polymer mixture consisted of poly(methylphenylsiloxane) (PMPS) from Sigma Aldrich Co. (M_W=2274, M_W/M_N=1.35) and polystyrene (PS) from Fluka Chemical Co. (M_W=10700, M_W/M_N=1.03). The mixture has the upper critical temperature phase diagram as shown in Figure 68a.

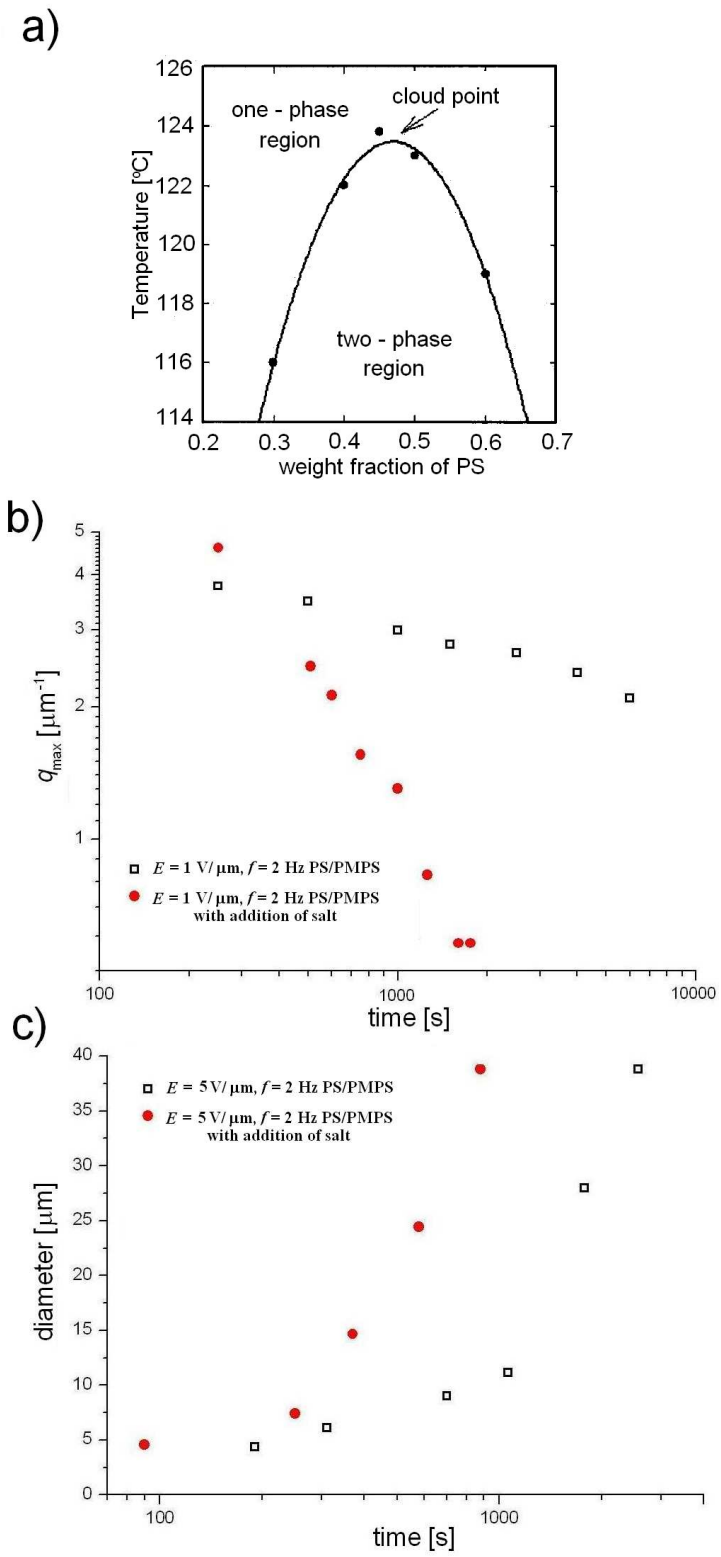

Figure 68. a) The phase diagram of PS/PMPS mixture. For more detailed information please see reference 110. **b)** Double logarithmic plot of the time evolution of q_{max} in the PS/PMPS 30/70 wt% cooled to 105°C. Measurement with 0.3 wt% of salt (benzyltetradecyldimethylammonium chloride) is represented by circles, measurement without salt is shown by squares at 1V/μm. **c)** Average size of the domains versus time obtained for PS/PMPS 30/70 wt%. cooled to 105°C at high amplitude of electric field 5 V/ μm. Measurement with 0.3 wt% of salt (benzyltetradecyldimethylammonium chloride) is represented by circles, measurement without salt is shown by squares.

The effect of acceleration of phase separation is directly connected with the addition of ions what is clearly visible in Figure 68b and Figure 68c. Figure 68b shows, that as soon as I added 0.3wt% of salt to the PS/PMPS mixture, the phase separation process goes nearly ten times faster. In my opinion, this experiment proves that the ions are responsible for acceleration of phase separation under the influence of an external electric field.

3.3.4. Summary and conclusions – application of the ion motion to phase separation in complex liquids

I applied low frequency AC electric field to the liquid crystal/polymer mixtures undergoing phase separation. I observed an acceleration of the phase separation process in this mixtures (for frequency below 30 Hz). The process was three orders of magnitude faster than in the absence of the electric field. This phenomenon is due to free ions (ionic impurities) contaminating liquid crystals and polymer. The ionic conductivity in liquid crystal is much bigger than the conductivity in polystyrene and therefore ionic impurities moving under the influence of the electric field gather at the polymer/liquid crystal interface. In the low frequency of the electric field, these ions start move to appropriate electrode, reach the interface and “drag” it. The deformation and drag of the interface enhances the transport of material to the growing domains and accelerates the phase separation process (Figure 69).

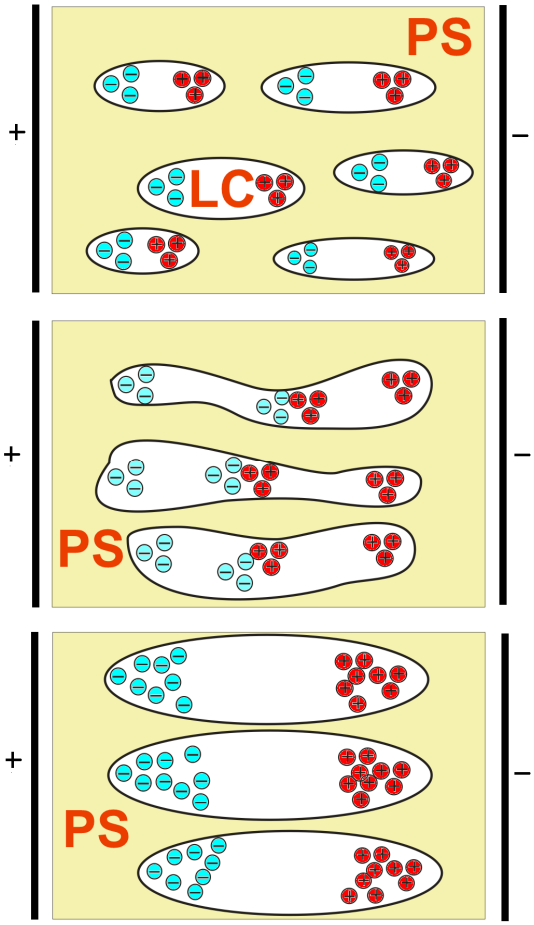

Figure 69. Visualization of the deformation of the liquid crystalline domains in the AC electric field. Dragging the interface enhances the transport of material to the growing domains and accelerates the phase separation process.

In the high frequency electric field (>30 Hz), the ions in liquid crystal cannot reach interface in the time given by the change of polarization, because it is too fast in comparison to the ion mobility. Therefore at high frequencies no acceleration of phase separation is observed. To complete measurements in external electric field I also applied direct current (DC) electric field. In DC electric field the ions should start to move to the appropriate electrode. Because of conductivity of liquid crystal is bigger than conductivity of polystyrene I expected that ionic impurities will not cross the interface and consequently will break the network and create circular droplets. To verify this theory I performed two measurements. In first one I allowed to separate my sample without an external electric field, time evolution of the light

scattering intensity obtained for this sample shows Figure 70a. My second experiment consisted of two steps: in first one I wished to separate my sample without electric field. When an evident peak appears, in second step I turn on DC electric field. Figure 70b presents this two steps experiment, which demonstrate an evident difference between Figure 70a and Figure 70b as a results of applied electric field.

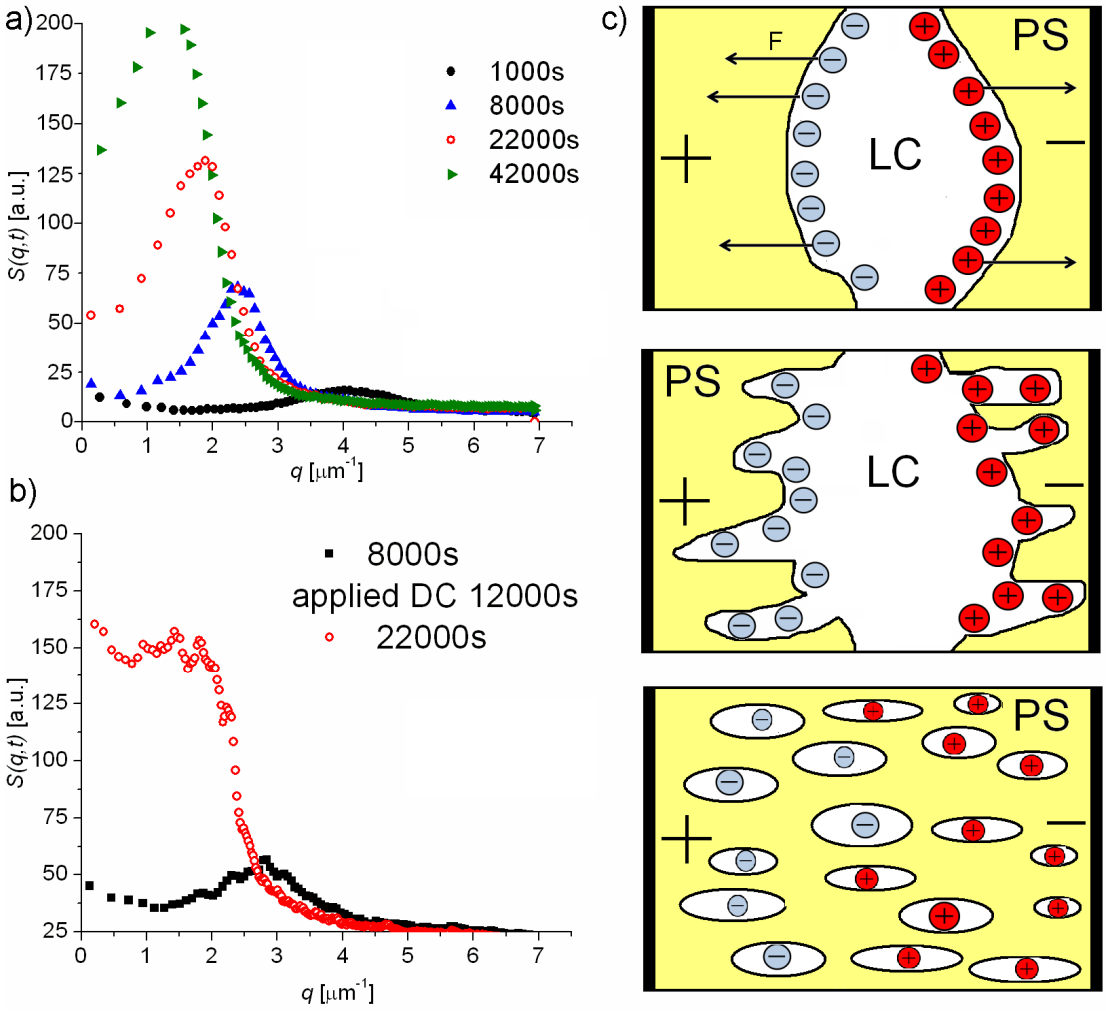

Figure 70. a) Time evolution of the light scattering intensity *S(q,t)* obtained for 5CB/PS 72/28 wt%. Thickness of sample *h* = 10μm. Mixture was cooled from 55 to 35.5^{0}C in the I+I region in the absence of electric field **b)**Time evolution of the light scattering intensity *S(q,t)* obtained for 5CB/PS 72/28 wt%. Thickness of sample *h*=10μm. Mixture was cooled from 55 to 35.5^{0}C in the I+I region. In first step I allowed to separate my sample without electric field. When an evident peak appears, in second step I turn on DC electric field and I obtained plot which shows breaking of a bicontinuous network. **c)** Visualization of breaking of a bicontinous network.

The presence of ions impurities in liquid crystals guide to ions movement to appropriate electrode when DC is applied. This movement breaks the network and cause the formation of liquid crystal droplets (Figure 70c).

As Tsori et al.[111] expected, external electric field of intensity above 2 V/μm could induce the phase separation process. In my study I did not observe any field-induced-phase separation, contrary to the theory predictions, but in agreement with experimental results obtained by Hori et al.[112] The temperature of phase transition without electric field and in the external electric field was the same, irrespective of intensity or frequency. Thus the phase diagrams presented in Figure 59 was not affected by the electric fields up to 5 V/μm.

The electric field offers a versatile tool for the modification and control over the polymer systems morphology. It seems that in many systems contaminated by the ions I can use the latter for the benefit of the formulation process for different materials. Motion of these ions in the AC electric field can change the morphology and probably also compositions of domains in non-uniform, multi-component polymer systems and also influence the whole process of their formation. This is important, since the final industrial products have mechanical, transport and electrical properties which depend on the kinetics and dynamics of the process used in their formation.

4. Conclusions

The experimental results of the Ph. D. thesis was described in three main chapters: **3.1** *Diffusion of nano-particles in polymer solutions*, **3.2** *Diffusion of plasmid DNA in polymer solutions* and **3.3** *Ions motion in liquid crystal/polymer mixtures.* The main purpose of each part was to present dynamics of nano and micro objects in complex liquids, each in a different perspective.

In the Chapter **3.1** I studied experimentally the diffusion of nanoscale probe in polymer solutions. The main conclusions of this part are as follows:

1. In polymer solutions the viscosity of nanoprobes of size R approaches the macroviscosity when R exceeds the radius of gyration of polymer, R_g. In other words, the nano to macroviscosity crossover occurs for $R \sim R_g$.

2. In the crossover regime at $R \sim R_g$ a scale dependent diffusion is observed. This phenomenon can be explained by the simplified model of diffusion with and within the depletion layer - the layer around diffusing particle depleted from polymer chains.

3. The scale dependent diffusion can be caused by the non-uniform viscosity, arising from the structure of the depletion layer, and should not be interpreted as anomalous diffusion.

In the Chapter **3.2** I analyzed the diffusion of plasmid DNA and restriction enzyme in polymer solution. The main conclusions of this part are as follows:

1. Studying processes occurring between biomolecules, we should pay attention to viscosity experienced by the biomolecules, and not only on the macroviscosity of the solution. Such viscosity experienced by the biomolecules (so called nano-viscosity) is

responsible for slowing down of the cleavage process. Large nano-viscosity of PEG 6000 decreases the diffusion coefficient of DNA and HindIII and thus reduces the frequency of encounters between DNA and HindIII. On the contrary, in PEG 8M solution, HindIII experiences low nano-viscosity, which means that it can move relatively freely in PEG 8M solution. That is why PEG 8M does not affect the cleavage of DNA, despite having the same macro-viscosity as PEG6000.

2. Analyzing processes occurring between biomolecules, we have to consider the possibilities of the presence of depletion layer. The depletion interactions between DNA also slow down the cleavage of DNA by inducing aggregation of DNA coils. When the concentration of PEG 6000 is high, DNA molecules form big aggregates due to depletion interactions, inhibiting the approach of HindIII to its target DNA. It is also possible that Hind III attach non specifically to DNA under influence of the depletion interactions.

In the Chapter **3.3** I investigated the influence of an external electric field on phase separation process. The main purpose of this subsection was to demonstrate what prospective application can have the motion of nano and micro objects in complex liquids. The main conclusions of this part are as follows:

1. The alternating current electric field of low frequency definitely reduces time of phase separation in liquid crystal/polymer mixture.

2. The motion of ionic impurities, under the alternating current electric field, is responsible for the acceleration of the phase separation process in the LC/polymer mixtures.

To sum up, presented results show how important is careful analysis of the dynamics occurring at the nano scale. It is clear that spatial variations of the viscosity as a function of a distance from the nanoparticle (arising due to the presence of the depletion layer around the particles) should always be taken into account. The presence of depletion layer can be responsible for occurrence of two – scale diffusion or can dramatically change the mechanism of processes taking place between biomolecules. Moreover, it is worth remembering that dynamics of nano and micro objects have an influence on phenomenon in the macro scale such as phase separation. Without any doubt, diffusion of nano and micro objects in complex liquids, and in particular, diffusion in crowded environment is a very important topic where understanding of the physical phenomena is far from complete. Therefore, I hope that quantitative studies presented in this Ph. D. dissertation provided a deeper insight into the physics of this complex phenomenon at the micro- and nanoscales.

5. References

[1] A. Einstein. On the motion of small particles suspended in liquids at rest required by the molecular-kinetic theory of heat. *Annalen der Physik* **1905**, *17*, 549–560.

[2] M. Smoluchowski. Zur kinetischen Theorie der Brownschen Molekularbewegung und der Suspensionen. *Annalen der Physik* **1906**, *21*, 756 – 780.

[3] M. Elimelech, J. Gregory, X. Jia, R. A. Williams. *Particle deposition & aggregation. Measurement, modelling and simulation*. Butterworth – Heinemann, USA, **1995**.

[4] M. J. Saxton. A biological interpretation of transient anomalous subdiffusion. I. Qualitative Model. Biophysical Journal **2007**, *92*, 1178 – 1191.

[5] T. Jue. *Fundamental concepts in biophysics*. Humana Press, Davis, California **2009**.

[6] N. Gal, D. Weihs. Experimental evidence of strong anomalous diffusion in living cells. *Physical Review E* **2010**, *81*, 020903.

[7] J. Klafter, I. M. Sokolov. Anomalous diffusion spreads its wings. *Physics World* **2005**, 1 – 4.

[8] A. Ochab – Marcinek, R. Hołyst. Scale-dependent diffusion of spheres in solutions of flexible and rigid polymers: mean square displacement and autocorrelation function for FCS and DLS measurements. *Soft Matter* **2011**, DOI: 10.1039/c1sm05217a.

[9] The role of Sutherland in the context of the equation relating the diffusion coefficient of small particles to the viscosity of a solvent is described in the following reviews: J. S. Rowlinson, *Notes Rec. R. Soc.* **2005**, *59*, 255 and J. Dunkel and P. Hanggi, *Phys. Rep*. **2009**, *471*, 1. Summarizing: Equation was suggested in two independent papers: by the Australian physicist William Sutherland (1859-1911) *Phil. Mag*. **1905**, S6, *9*, 781 and two months later by Albert Einstein *Ann. d. Phys*. **1905**, *17*, 549. Until the second world war the equation was called the Sutherland-Einstein equation. After the war the equation changed its name to the Stokes-Einstein equation. The Stokes name is related to the hydrodynamic drag, used in the

equation and obtained within the framework of the Navier-Stokes equations. The application of the hydrodynamic drag in the Stokes-Sutherland-Einstein equation to describe motion due to fluctuations was an assumption recognized neither by Einstein nor by Sutherland. This relation was the first example of the fluctuation-dissipation theorem.

[10] Colin A. Vincent. The motion of ions in solution under the influence of an electric field. *Journal of Chemical Education* **1976**, *53*, 490 – 493.

[11] F.F. Reuss. *Mém. Soc. Impériale Naturalistes de Moscow* **1809**, *2*, 327.

[12] V. Pattabhi, N. Gautham. *Biophysics.* Kluwer Academic Publishers, New Delhi, **2002**.

[13] R. Nagarajan. *Chapter 1: Nanoparticles: Building blocks for nanotechnology.* American Chemical Society, Washington, **2008**.

[14] C. N. R. Rao, A. Muller, A. K. Cheetham. *The Chemistry of Nanomaterials: Synthesis, Properties and Applications.* Wiley, Verlag GmbH & Co. KGaA, Weinheim, **2004**.

[15] Y. S. Lee. *Self-assembly and nanotechnology.* John Wiley & Sons, New Jersey, **2008**.

[16] E. Ruckenstein, Z. F. Li. Surface modification and functionalization through the self-assembled monolayer and graft polymerization. *Advances in Colloid and Interface Science* **2005**, *113*, 43 – 63.

[17] W.-P. Peng, Y.-C. Yang, C.-W. Lin, H.-C. Chang. Molar Mass and Molar Mass Distribution of Polystyrene Particle Size Standards. *Anal. Chem.* **2005,** *77*, 7084-7089.

[18] J. Kim, J. Kwak, Y. C. Kim, D. Kim. Preparation and size control of monodispersed surface charged polystyrene nanoparticles by reversible addition fragmentation transfer reaction. *Colloid Polym. Sci*. **2006**, *284*, 771 – 770.

[19] I. W. Hamley. *Introduction to soft matter – revised edition: synthetic and biological self – assembling materials*. John Wiley & Sons, England, **2007**.

[20] http://www.blc.arizona.edu/molecular_graphics/dna_structure/dna_tutorial.html

[21] DNA supercoil, http://en.wikipedia.org/wiki/DNA_supercoil

[22] Ionic Radius, http://np-apchemistry.wikispaces.com/chapter8

[23] Atomic and ionic radius, http://www.chemguide.co.uk/atoms/properties/atradius.html

[24] R. Kohli, K. L. Mittal. *Developments in surface contamination and cleaning.* William Andrew, Inc. New York, **2008.**

[25] D.B.A. Rep, A. F. Morpurgo, W. G. Sloof, T. M. Klapwijk. Mobile ionic impurities in organic semiconductors. *J. Appl. Phys.* **2003**, *93*, 2082 – 2090.

[26] W. M. Gelbart, A. Ben-Shaul. The "new" science of "complex fluids". *J. Phys. Chem.* **1996**, *100*, 13169 – 13189.

[27] J. L. Barrat, J. P. Hansen. *Basic concepts for simple and complex liquids.* Cambridge University Press, England, **2003**.

[28] K. Holmberg, B. Jönsson, B. Kronberg, B. Lindman. *Surfactant and polymers in aqueous solution.* John Wiley & Sons, England, **2003**.

[29] E. D. Goddard, J. V. Gruber. *Principles of polymer science and technology in cosmetics and personal care.* Marcel Dekker, Inc. New York, **1999**.

[30] K. Devanand, J. C. Selser. Asymptotic behavior and long-range interactions in aqueous solutions of poly(ethylene oxide). *Macromolecules* **1991**, *24*, 5943 – 5947.

[31] P. G. de Gennes. *The physics of liquid crystals.* Clarendon Press, Oxford, **1974**.

[32] V. N. Tsvetkov. On molecular order in the anisotropic liquid phase (Über die Molekülanordnung in der anisotrop-flüssigen Phase) *Acta Physicochimica U.R.S.S.* **1942**, *15*, 132–147.

[33] Quan Li. *Self-Organized Organic Semiconductors: From Materials to Device Applications.* John Wiley & Sons, New Yersey, **2010**.

[34] W. Schärtl. *Light Scattering from Polymer Solutions and Nanoparticle Dispersions.* Springer – Verlag Gmbh, Berlin, **2007.**

[35] L. R. Xu. *Particle Characterization: Light Scattering Methods.* Kluwer Academic Publishers, New York, **2002.**

[36] P. Atkins, J. de Paula. *Atkins' Physical Chemistry*. Oxford University Press, New York, **2006**.

[37] J. W. Strutt (Lord Rayleigh). On the light from the sky, its polarization and color. *Phil. Mag.* **1871**, *41*, 107 – 120.

[38] Light Scattering, Chapter 7, Part of lecture from Utah University, http://www.ias.ac.in/initiat/sci_ed/resources/chemistry/LightScat.pdf

[39] Molecular Expressions, http://micro.magnet.fsu.edu/primer/anatomy/introduction.html

[40] C. R. Brundle, C. A. Evans Jr., S. Wilson. *Encyclopedia of Materials Characterization.* Butterworth – Heinemann, USA, **1992**.

[41] Optical Microscopy. http://www.molphys.leidenuniv.nl/monos/students/pdf/smon02.pdf

[42] M. W. Davidson and M. Abramowitz. Optical Microscopy. http://www.olympusmicro.com/primer/opticalmicroscopy.html

[43] Nikon MicroscopyU, The source for microscopy education, Introduction to Polarized Light Microscopy, http://www.microscopyu.com/articles/polarized/polarizedintro.html

[44] R. Hołyst, A. Bielejewska, J. Szymański, A. Wilk, A. Patkowski, J. Gapiński, A. Żywociński, T. Kalwarczyk, E. Kalwarczyk, M. Tabaka, N. Ziębacz, S. A. Wieczorek. Scaling form of viscosity at all length-scales in poly(ethylene glycol) solutions studied by fluorescence correlation spectroscopy and capillary electrophoresis. *Phys. Chem. Chem. Phys*. **2009**, *11*, 9025 – 9032.

[45] J. Szymański, A. Patkowski, A. Wilk, P. Garstecki, R. Hołyst. Diffusion and Viscosity in a Crowded Environment: from Nano- to Macroscale. *J. Phys. Chem. B* **2006**, *110*, 25593 – 25597.

[46] T. Pederson. Diffusional protein transport within the nucleus: a message in the medium. *Nat. Cell Biol.* **2000**, *2*, E73 – E74.

[47] E. A. J. Reits, J. J. Neefjes. From fixed to FRAP: measuring protein mobility and activity in living cells. *Nat. Cell Biol.* 2001, *3*, E145 – E147.

[48] M. B. Elowitz, M. G. Surette, P. E. Wolf, J. B. Stock, S. Leibler. Protein mobility in the cytoplasm of Escherichia coli. *J. Bacteriol.* **1999**, *181*, 197-203.

[49] D. Langevin, F. Rondelez. Sedimentation of large colloidal particles through semidilute polymer solutions. *Polymer*, **1978**, *19*, 875-882.

[50] Y. Cheng, R. K. Prud'homme, J. L. Thomas. Diffusion of Mesoscopic Probes in Aqueous Polymer Solutions Measured by Fluorescence Recovery After Photobleaching. *Macromolecules*, **2002**, *35*, 8111 – 8121.

[51] P. G. de Gennes. *Scaling Concepts in Polymer Physics*, Cornell University Press, New York, **1979**.

[52] A. Michelman-Ribeiro, F. Horkay, R. Nossal, H. Boukari. Probe diffusion in linear Poly(Vinyl) Alcohol polymer solutions by Fluorescence Correlation Spectroscopy. *Biomacromolecules* **2007**, *8*, 1595-1600.

[53] C. N. Onyenemezu, D. Gold, M. Roman, W. G. Miller. Diffusion of polystyrene latex spheres in linear polystyrene nonaqueous solutions. *Macromolecules* **1993**, *26*, 3833-3837.

[54] K. E. Bremmell, N. Wissenden, D. E. Dunstan. Diffusing probe measurements in polyelctrolyte solutions – Deviations from Stokes-Einstein Behaviour. *Adv. Colloid Interface Sci*. **2001**, *89-90*, 141-154.

[55] T. G. Mason, D. A. Weitz. Optical Measurements of Frequency-Dependent Linear Viscoelastic Moduli of Complex Fluids. *Phys. Rev. Lett.* **1995**, *74*, 1250 – 1253.

[56] I.Y. Wong, M.L.Gardel, D.R. Reichman, Eric Weeks, M.T. Valentine, A.R. Bausch, D.A.Weitz. Anomalous Diffusion Probes Microstructure Dynamics of Entangled F-Actin Networks. *Phys. Rev. Lett.* **2004**, *92*, 178101.

[57] K. Kang, J. Gapinski, M. P. Lettinga, J. Buitenhuis, G. Meier, M. Ratajczyk, J. K. G. Dhont, A. Patkowski. Diffusion of spheres in crowded suspensions of rods. *J. Chem. Phys.* **2005**, *122*, 044905.

[58] C. W. Hoogendam, J. C. W. Peters, R. Tuinier, A. de Keizer, M. A. Cohen Stuart, B. H. Bijsterbosch. Effective Viscosity of Polymer Solutions: Relation to the Determination of the Depletion Thickness and Thickness of the Adsorbed Layer of Cellulose Derivatives. *J. Colloid Interference Sci.* **1998**, *207*, 309 – 316.

[59] T. H. Fan, R. Tuinier. Hydrodynamic interaction of two colloids in nonadsorbing polymer solutions. *Soft Matter* **2010**, *6*, 647 – 654.

[60] R. Tuinier, T. H. Fan. Scaling of nanoparticle retardation in semi-dilute polymer solutions. *Soft Matter* **2008**, *4*, 254 – 257.

[61] G. J. Fleer, A. M. Skvortsov, R. Tuinier. Mean-Field Equation for the Depletion Thickness. *Macromolecules* **2003**, *36*, 7857 – 7872.

[62] T. H. Fan, J. K. G. Dhont, R. Tuinier. Motion of a sphere through a polymer solution. *Phys. Rev. E* **2007**, *75*, 011803.

[63] T. H. Fan, B. Xie, R. Tuinier. Asymptotic analysis of tracer diffusivity in nonadsorbing polymer solutions. *Phys. Rev. E* **2007**, *76*, 051405

[64] T. Odijk. Depletion theory of protein transport in semi-dilute polymer solutions. *Biophys. J.* **2000**, *79*, 2314 – 2321.

[65] K. Devanand, J. C. Selser. Asymptotic behavior and long-range interactions in aqueous solutions of poly(ethylene oxide). *Macromolecules* **1991**, *24*, 5943 – 5947.

[66] A. C. Price, L. B. Sorensen, S. D. Kevan, J. Toner, A. Poniewierski, R. Hołyst. Coherent Soft-X-Ray Dynamic Light Scattering from Smectic- *A* Films. *Phys. Rev. Lett.* **1999**, *82*, 755 - 758.

[67] J. Szymański, A. Patkowski, J. Gapiński, A. Wilk, R. Hołyst. Movement of Proteins in an Environment Crowded by Surfactant Micelles: Anomalous versus Normal Diffusion. *J. Phys. Chem. B* **2006**, *110*, 7367 - 7373.

[68] T. Thurn-Albrecht, G. Meier, P. Muller-Buschbaum, A. Patkowski, W. Steffen, G. Grubel, D.L. Abernathy, O. Diat, M. Winter, M.G. Koch, M.T. Reetz. Structure and Dynamics of Surfactant Stabilized Aggregates of Palladium Nanoparticles under Dilute and Semidilute Conditions: Static and Dynamic X-Ray Scattering. *Phys. Rev. E* **1999**, *59*, 642 – 649.

[69] C. Li, Y. Wang, G. J. Pielak. Translational and rotational diffusion of a small globular protein under crowded conditions. *J. Phys. Chem B.* **2009**, *113*, 13390-13392.

[70] Y. Y. Kuttner, N. Kozer, E. Segal, G. Schreiber, G. Haran. Separating the Contribution of Translational and Rotational Diffusion to Protein Association. *J. Am. Chem. Soc.* **2005**, *127*, 15138-15144.

[71] M. T. Record, E. S. Courtenay, D. S. Cayley, H. J. Guttman. Responses of *E. coli* to osmotic stress: large changes in amounts of cytoplasmic solutes and water. *Trends Biochem. Sci*. **1998**, *23*, 143 – 148.

[72] G. Rivas, F. Ferrone, J. Herzfeld. Life in a crowded world: Workshop on the biological implications of macromolecular crowding. *EMBO Rep*. **2004**, *5*, 23 – 27.

[73] C. P. Brangwynne, G. H. Koenderik, F. C. MacKintosh, D. A. Weitz. Cytoplasmic diffusion: molecular motors mix it up. *J. Cell Biol.* **2008**, *183*, 582 – 587.

[74] L. Stagg, S. Q. Zhang, M. S. Cheung, P. Wittung – Stafshede. Molecular crowding enhances native structure and stability of α/β protein flavodoxin. *PNAS* **2007**, *104*, 18976 – 18981.

[75] B. R. Somalinga and R. P. Roy. Volume exclusion effect as a driving force for reverse proteolysis. *J. Biol. Chem*., **2002**, *277*, 43253 – 43261.

[76] A. P. Minton and J. Wilf. Effect of macromolecular crowding upon the structure and function of an enzyme: glyceraldehyde-3-phosphate dehydrogenase. *Biochemistry*, **1981**, *20*, 4821 – 4826.

[77] Y. Phillip, E. Sherman, G. Haran, G. Schreiber. Common Crowding Agents Have Only a Small Effect on Protein-Protein Interactions. *Biophys. J.* **2009**, *97*, 875 – 885.

[78] Theresa Phillips. *Restriction Enzymes Explained*.
http://biotech.about.com/od/proteinengineering/a/restrictenz.htm

[79] M. Napirei, H. Karsunky, B. Zevnik, H. Stephan, HG Mannherz, T. Möröy. Features of systemic lupus erythematosus in Dnase1-deficient mice. *Nat. Genet*. **2000**, *25*, 177 – 181.

[80] N. Watanabe, Y. Takasaki, C. Sato, S. Ando and I. Tanaka. Structures of restriction endonuclease HindIII in complex with its cognate DNA and divalent cations. *Acta Crystallogr., Sect. D: Biol. Crystallogr*. **2009**, *65*, 1326 – 1333.

[81] L. P. Cramer, L. J. Briggs and H. R. Dawe. Use of fluorescently labelled deoxyribonuclease I to spatially measure G-actin levels in migrating and non-migrating cells. *Cell Motil. Cytoskeleton*, **2002,** *51*, 27–38.

[82] E. H. Serpersu, D. Shortle and A. S. Mildvan. Kinetic and magnetic resonance studies of active-site mutants of staphylococcal nuclease: factors contributing to catalysis. *Biochemistry*, **1987**, *26*, 1289–1300.

[83] J. R. Wenner and V. A. Bloomfield. Crowding Effects on *Eco*RV Kinetics and Binding**.** *Biophys. J.* **1999**, *77*, 3234–3241

[84] Y. Sasaki, D. Miyoshi and N. Sugimoto. Regulation of DNA nucleases by molecular crowding. *Nucleic Acids Res*. **2007***, 35*, 4086–4093.

[85] S. B. Zimmerman and B. H. Pheiffer. Macromolecular crowding allows blunt-end ligation by DNA ligases from rat liver or Escherichia coli. *PNAS* **1983,** *80*, 5852–5856.

[86] R. D. Phair, T. Misteli. High mobility of proteins in the mammalian cell nucleus. *Nature* **2000**, *404*, 604 – 609.

[87] A. Partikian, B. Olveczky, R. Swaminathan, Y. X. Li and A. S. Verkman. Rapid Diffusion of Green Fluorescent Protein in the Mitochondrial Matrix. *J. Cell Biol*. **1998**, *140*, 821–829.

[88] A. Virij. Polymers at Interfaces and the Interactions in Colloidal Dispersions. *Pure Appl. Chem.* **1976**, *48*, 471 – 483.

[89] S. Asakura, F. Oosawa. On interaction between two bodies immersed in a solution of macromolecules. *J. Chem. Phys.* **1954**, *22*, 1255 – 1256.

[90] V. V. Vasilevskaya, A. R. Khokhlov, Y. Matsuzawa and K. Yoshikawa. Collapse of single DNA molecule in poly(ethylene glycol) solutions. *J. Chem. Phys*., **1995**, *102*, 6595–6602.

[91] M. Kojima, K. Kubo and K. Yoshikawa. Elongation/compaction of giant DNA caused by depletion interaction with a flexible polymer. *J. Chem. Phys*., **2006**, *124*, 024902.

[92] J. E. Ramos, Jr, R. de Vries and J. Ruggiero Neto. DNA Ψ-Condensation and Reentrant Decondensation: Effect of the PEG Degree of Polymerization. *J. Phys. Chem. B.* **2005**, *109*, 23661–23665.

[93] X. D. Chen, Y. Zhou, P. Qu and X. S. Zhao. Base-by-Base Dynamics in DNA Hybridization Probed by Fluorescence Correlation Spectroscopy. *J. Am. Chem. Soc*. **2008**, *130*, 16947–16952.

[94] S. Hou, N. Ziębacz, T. Kalwarczyk, T. Kamiński, S. A. Wieczorek, R. Hołyst. Influence of Nano-viscosity and Depletion Interactions on Cleavage of DNA by Enzymes in Glycerol and Poly(ethylene) Glycol Solutions: Qualitative Analysis. *Soft Matter* **2011**, *7*, 3092 – 3099.

[95] J. Seils, R. Pecora. Dynamics of a 2311 Base Pair Superhelical DNA in Dilute and Semidilute Solutions. *Macromolecules*, **1995**, *28*, 661 – 673.

[96] R. Grandori, I. Matecko, P. Mayr, N. Muller. Probing protein stabilization by glycerol using electrospray mass spectrometry. *J. Mass Spectrom*. **2001**, *36*, 918 – 922.

[97] H.-S. Kitzerow. Polymer-dispersed liquid crystals. From the nematic curvilinear aligned phase to ferroelectric films. *Liquid Cryst.* **1994**, *16*, 1 – 31.

[98] D. A. Higgins. Probing the Mesoscopic Chemical and Physical Properties of Polymer-Dispersed Liquid Crystals. *Adv. Mater*. **2000**, *12*, 251 – 264.

[99] T. J. White, L. V. Natarajan, V. P. Tondiglia, P. F. Lloyd, T. J. Bunning, C. A. Guymon**.** Holographic polymer dispersed liquid crystals (HPDLCs) containing triallyl isocyanurate monomer. *Polymer* **2007**, *48*, 5979 – 5987.

[100] L. V. Natarajan, C. K. Shepherd, D. M. Brandelik, R. L. Sutherland, S. Chandra, V. P. Tondiglia, D. Tomlin, T. J. Bunning. Switchable Holographic Polymer-Dispersed Liquid Crystal Reflection Gratings Based on Thiol−Ene Photopolymerization. *Chem. Mater*. **2003**, *15*, 2477 – 2484.

[101] L. H. Sperling. *Introduction to Physical Polymer Science*, 3rd ed.; John Wiley & Sons Inc.: New York, **2001.**

[102] G. Stroble. *The physics of polymers*. Springer, Berlin, **1996**

[103] Y. Tsori, F. Tournilhac, D. Andelman, L. Leibler. Structural Changes in Block Copolymers: Coupling of Electric Field and Mobile Ions. *Phys. Rev. Lett.* 2003, *90*, 145504-1

[104] Y. Tsori, L. Leibler. Phase-separation in ion-containing mixtures in electric fields. *PNAS* **2007**, *104*, 7348 – 7350.

[105] T. Szymborski, O. Cybulski, I. Bownik, A. Żywociski, S. A. Wieczorek, M. Fiałkowski, R. Hołyst, P. Garstecki. Dynamic charge separation in a liquid crystalline meniscus. *Soft Matter* **2009**, *5*, 2352 – 2360.

[106] M. Graca, S. A. Wieczorek, R. Hołyst. Growth of Polystyrene Domains in Isotropic, Nematic and Smectic Phase of 8CB Liquid Crystal. *Macromolecules* **2003**, *36*, 6903 – 6913.

[107] M. Graca. Ph. D. dissertation. *Spinodal decomposition in the mixtures of polymers and liquid crystals.* Institute of Physical Chemistry PAS, Warsaw, **2003**.

[108] M. Graca, S. A. Wieczorek, R. Hołyst. Polymer Domain Growth in Ordered Liquid Crystalline Matrices. *Phys. Rev. Lett.* **2003**, *90*, 115504

[109] I. Demyanchuk, S. A. Wieczorek, R. Hołyst. Phase Separation in Binary Polymer/Liquid Crystal Mixtures: Network Breaking and Domain Growth by Coalescence-induced Coalescence. *J. Phys. Chem. B* **2006**, *110*, 9869-9875.

[110] I. Demyanchuk, S. A. Wieczorek, R. Hołyst. Percolation-to-droplets transition during spinodal decomposition in polymer blends, morphology analysis. *J. Chem. Phys*. **2004**, *121*, 1141 – 1147.

[111] Y. Tsori, F. Tournilhac, L. Leibler. Demixing in simple fluids induced by electric field gradients . *Nature* **2004**, *430*, 544 – 547.

[112] H. Hori, O. Urakawa, O. Yano, Q. Tran-Cong-Miyata. Phase Separation of Binary Polymer Mixtures under an Electric Field. *Macromolecules* **2007**, *40,* 389 – 394.